Cardiac effects of NRG-1β in a doxorubicin-therapy model – focus on early molecular events and sex-differences

Inauguraldissertation

zur
Erlangung der Würde eines Doktors der Philosophie vorgelegt der Philosophisch-Naturwissenschaftlichen Fakultät der Universität Basel

von

Lilia Maryse LÉPINE

Basel, 2023

Genehmigt von der Philosophisch-Naturwissenschaftlichen Fakultät

auf Antrag von

First Supervisor: Prof. Dr. Marijke Brink
Second Supervisor: Prof. Dr. Christoph Handschin
External expert: Prof. Dr. Benoit Pourcet

Basel, den 20. September 2022

Prof. Dr. Marcel Mayor, Dekan
The Dean of Faculty

TABLE OF CONTENTS

ABBREVIATIONS

4E-BP1	4E binding protein 1
ACC	Acetyl-CoA carboxylase
ADP	Adenosine biphosphate
AMP	Adenosine monophosphate
AMPK	AMP-dependent protein kinase
ANP	Atrial natriuretic peptide
APS	Ammonium persulfate
ARVM	Adult rat ventricular myocyte
ATG	Autophagy related protein
ATP	Adenosine triphosphate
BL	Baseline
BP	Blood pressure
BSA	Bovine serum albumin
BW	Body weight
CHF	Chronic heart failure
CMs	Cardiomyocytes
CPT	Carnitine-palmitoyl transferase
CVD	Cardiovascular disease
CVW	Cardiac ventricular weight
D	Day
DMEM	Dulbecco's Modified Eagle's medium
DNA	Deoxyribonucleic acid
Dox	Doxorubicin
ECL	Enhanced chemo-luminescence
ErbB	Erythroblastic leukemia viral oncogene homolog
ERK1/2	Extracellular signal-regulated kinase ½
FAK	Focal adhesion kinase
FAO	Fatty acid oxidation
GLUT	Glucose transporter
HBSS	Hank's balanced salt solution
HF	Heart failure
HRP	Horse radish peroxidase
IP	Intraperitoneally
LC3	Microtubule-associated protein 1A/1B-light chain 3
LVAW	Left ventricular anterior wall
LVEF	Left ventricular ejection fraction
LVID	Left ventricular internal diameter
LVPW	Left ventricular posterior wall
MCII	Mitochondrial complex II
MHC	Myosin heavy chain
Mt	Mitochondria
mTORC	Mammalian target of rapamycin complex
NRG-1	Neuregulin-1ß

NRVM	Neonatal rat ventricular myocytes
Nu	Nucleus
ON	Overnight
pH	Hydrogen potential
PBS	Phosphate buffer saline
Pepst	Pepstatin A
PFA	Paraformaldehyde
PVDF	Polyvinylidenfluorid
RIPA	Radio immuno precipitation buffer
RNA	Ribonucleotide acid
ROS	Reactive oxygen species
RT	Room temperature
RT-qPCR	Reverse trasncription quantitative PCR
SDS	Sodium dodecyl sulfate
Ser	Serine
Taq	Thermus aquaticus polymerase
Top II	Topoisomerase II
TBS	Tris buffered saline
TBST	Tris buffered saline + Tween
Thr	Threonine
TL	Tibia length
Tyr	Tyrosine
ULK1	Unc-51 like autophagy activating kinase

SUMMARY

Doxorubicin (dox) is one of the most potent chemotherapeutic drugs nowadays. However, dox use in clinics is limited by its high myocardial toxicity. Recent evidence suggests that dox-induced early disturbance of metabolic pathways in cardiomyocytes conditions the later development of chronic heart failure (CHF) in patients. Interestingly, circulating levels of neuregulin-1β (NRG-1) are correlated with the development of chronic heart failure in cancer patients after dox-therapy. Moreover, inhibition of the NRG-1 co-receptor ErbB2 worsens cardiac outcomes, indicating a cardioprotective role of NRG-1 in these patients. In the present study, our aim was to 1) characterize an in vivo model of dox-induced cardiac dysfunction in male and female mice, and 2) investigate whether NRG-1 protects against dox-induced cardiotoxicity by modulating acute metabolic mechanisms, especially autophagy.

C57BL/6J male and female mice were assigned to a CTL, dox or NRG/dox group. Mice were injected intraperitoneally with vehicle or dox (4 mg/kg) at day 0, 2, 5, 8, 10, 12 yielding a cumulative dose of 24 mg/kg. NRG-1 (20 µg/kg) or vehicle (PBS) were injected 30 min before each dox injection and continued every other day until sacrifice. Heart function and architecture were measured using echocardiography at multiple timepoints before sacrifice. Body weight loss was observed in males and females, indicative of systemic toxicity. These effects were stronger in males than in females. In males, dox increased cardiac ejection fractions and left ventricular wall thickness at 2 weeks after treatment-begin and NRG-1 prevented this. In contrast, in females dox did not modulate cardiac function, however, dox decreased LV wall thickness and NRG-1 did not affect this at 3 weeks. These results were associated with increased GLUT1 and β-MHC mRNA in dox-treated males, while dox-treated females only showed an increase in β-MHC mRNA levels. Yet, NRG-1 did not modify any of these molecular responses neither in males nor in females. Our data show that dox-induced cardiac remodeling is sex-dependent: males respond with stronger cardiac compensation to dox than females at the functional and molecular level.

For our mechanistic studies, additional mice were sacrificed at day 1 after the dox injection, 1 h after NRG-1 stimulation. In males, the single dox injection was enough to decrease the cardiac LC3II/I ratios. On the other hand, female mice did not show any dox-induced cardiac modulation of the LC3II/I ratios at day 1. While NRG-1 had no effects in males, in females it significantly decreased LC3II/I and enhanced the phosphorylation of ULK1 at its inhibitory S757 site, suggesting that NRG-1 reduces autophagy in dox-treated females.

To investigate underlying mechanisms, neonatal rat ventricular myocytes (NRVM) were used as a model. NRVM were pre-treated in serum-free medium with E64D/pepstatin A inhibitors to study autophagic flux, or directly stimulated with NRG-1. After NRG-1 stimulation, NRVM were treated with dox (1 µM). At 16 h the NRVM model mimicked the molecular response observed in females at 24 h. At 1 h, NRG-1 alleviated a dox-induced increase of LC3II protein, and this was associated with increased ULK1-pS*757* as well as decreased FoxO1 nuclear location. Consistently, at 6 h, NRG/dox-treated NRVM showed decreased expression of the FoxO1 target genes LC3 and ULK1 in comparison to dox-treated cells. Furthermore, our preliminary data obtained with MTT and luciferin-based CELL TITER GLO assays showed that dox induced an increase in succinate synthetase activity, without changing ATP content at 3 h. Interestingly, this was associated with decreased mitochondrial/nuclear DNA ratios at 3 and 16 h, and NRG-1 alleviated it at 3 h.

In conclusion, our study showed that the NRG-1 treatment regimen that we used might not be suitable for males to alleviate dox-induced early cardiac autophagy disturbances. In females, evidence for NRG-1 inhibition of the autophagic pathway were uncovered upon dox-therapy and surprisingly, might be independent of the mTORC1 pathway. Our study highlighted the need to characterize sex-differences upon dox-therapy and NRG-1 preventive treatment to promote personalized medicine.

1. INTRODUCTION

1.1. CARDIAC METABOLISM IN ADULTHOOD

1.1.1. ENERGY METABOLISM IN THE HEALTHY HEART

The role of the heart is to pump blood through the body in order to ensure oxygen and nutrient distribution, inter-organ communication as well as metabolic debris elimination/removal. To ensure the heart's contractile function, large amounts of ATP need to be continuously produced, and this all day long, whatever the feeding status and subsequent nutrients availability, the occurrence of exercise activity or hormonal stimulation are [1]. For instance, the heart daily produces about 6 kg of ATP, which are by 95% produced by the mitochondrial oxidative phosphorylation. The mitochondrial phosphorylation consists in generating ATP directly through the Krebs cycle and indirectly through mitochondrial respiratory chain activity [2].

In the healthy heart, 60-90% of the mitochondrial oxidation relies on the fatty acid oxidation (FAO) which leads to acetyl-coenzyme A (acetyl-CoA) formation. 10-40% rely on pyruvate oxidation coming from glycolysis and lactate oxidation [3]. Interestingly, the heart is also able to metabolize other fuels to stimulate mitochondrial oxidation including ketone bodies or branched chain amino acids to a lower extent [4]. The last 5 percent of ATP which are not produced by mitochondrial oxidative phosphorylation is directly produced by the glycolysis reaction. The ability of the healthy heart to use so many different substrates according to their availability to produce ATP with the best yields is called metabolic flexibility [5].

Lipid metabolism

Briefly, FA are delivered to the heart either as free FA bound to albumin or as triacylglycerols (TAG) in lipoproteins by diffusion or CD36-dependent transport, respectively [6]. TAG are sequentially hydrolyzed by the adipose triglyceride lipase, the hormone-sensitive lipase, and monoacylglycerol lipase, which sequentially hydrolyze TAGs, diacylglycerols, and monoacylglycerols to liberate FA, which thereafter are acylated to form fatty acyl-CoA by the acyl-CoA synthetase [7]. Fatty acyl-CoA are addressed to the mitochondrial matrix by the L-carnitine-dependent translocation carnitine palmitoyl transferase system CPT1-CPT2.

In the mitochondrial matrix, the fatty acyl-CoA enter the FAO also called β-oxidation pathway multiple times to produce acetyl-CoA, which will enter the Krebs cycle to produce ATP in presence of oxygen. Additionally, FAO and Krebs cycle reactions lead to the production NADH

and $FADH_2$, which will afterwards contribute to the mitochondrial proton gradient by getting oxidized by the mitochondrial electron transport chain.

Glucose metabolism

In the adult heart, GLUT1 and GLUT4 transporters are responsible for glucose uptake. GLUT4 is addressed to the cell membrane upon insulin stimulation or myocardial contraction to transport glucose into the cytoplasm [8]. The glucose is then phosphorylated to G6P by hexokinases and addressed to the glycolysis pathway to form ATP, NADH and pyruvate. The obtained pyruvate is mainly transported to the mitochondrial matrix by the mitochondrial carriers 1 and 2 proteins and is converted to acetyl-CoA by the pyruvate dehydrogenase complex to enter the Krebs cycle as described above.

1.1.2. Importance of AMPK, ULK1 and LC3 in the heart

The AMP-activated protein kinase (AMPK) is a central actor in energy sensing and a modulator of energy homeostasis within the cell [9]. The activation of AMPK in cardiac stress conditions, after energy depletion, or during exercise leads to inhibition of the ATP-consuming anabolic pathways in favour of catabolic pathways known to increase ATP production (Fig. 1).

AMPK is a protein constituted of 3 subunits: the catalytic subunit α and the 2 regulatory subunits β and γ. In a situation of limited energy supply, cellular concentrations of ADP and AMP are increased, and the latter binds the AMPKγ subunit with strong affinity. This results in the allosteric activation of the AMPKα at the Thr172 site [10]. The catalytic activity of the AMPK depends on the Thr172 phosphorylated levels [11]. Upstream activators can in presence of AMP increase AMPK catalytic subunit activation by increasing its Thr172 phosphorylation. This is the case for the calmodulin kinase II which is activated by increased cytoplasmic calcium concentrations, or also for the liver kinase B1 protein. Oppositely, phosphatases can inhibit AMPK activity by decreasing the Thr172 phosphorylation.

The AMPK acts at the transcriptional and post-translational levels to maintain the energy balance. At the post-translational level, AMPK activation has been reported to enhance GLUT4 and CD36 translocation to the membrane in order to facilitate glucose and FA uptake, respectively [12-14]. Moreover, AMPK has been shown to promote on one hand the glycolysis through the activation of phosphofructokinase 2 and on the other hand to indirectly promote FAO via acetyl-CoA carboxylase (ACC) inhibition [15, 16]. Indeed, ACC plays multiple roles in lipid metabolism regulation. Firstly, when activated, ACC induces de novo lipid biogenesis. To this

end, ACCβ, (later abbreviated ACC) carboxylates acetyl-CoA to malonyl-CoA. Yet, malonyl-CoA inhibits CPT1 which is needed to transport long chain FA to the mitochondrial matrix. Therefore, by inhibiting ACC, AMPK enhances the long chain FA translocation to the mitochondria, where it could get oxidized to produce ATP.

Furthermore, AMPK enhances at the transcriptional level mitochondrial biogenesis and fatty acid oxidative metabolism via its interaction with PGC1α or PPARα [17, 18]. AMPK, in addition to inhibiting the *de novo* lipid synthesis, also inhibits the protein synthesis pathway. More precisely, AMPK modulates mTORC1 activity by inhibiting RAPTOR and activating the TSC1/TSC2. Finally, AMPK enhances autophagy by 1) alleviating the mTORC1 inhibitory phosphorylation of ULK1 at the Ser*757* site, 2) activating ULK1 through phosphorylation of its Ser317 site, and 3) inducing the transcription of autophagy genes through FoxO activation [19, 20].

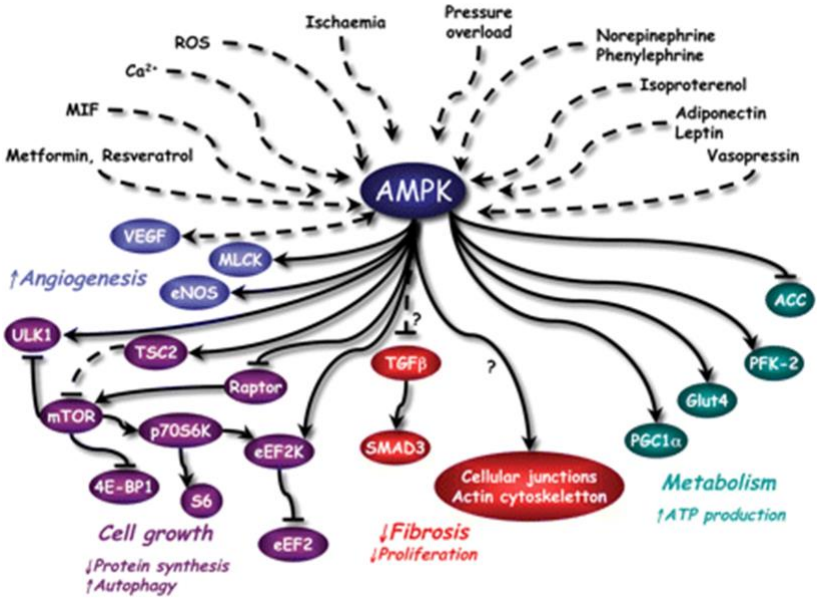

Figure 1. The cardiac AMPK is activated upon energy stress conditions, increased cellular concentrations of ROS, calcium or upstream kinases. The activation of the AMPK leads to the induction of pathways implied in ATP production such as FAO, glycolysis or autophagy, while it inhibits pathways implied in cell growth, protein synthesis and de novo lipid synthesis. Beauloye et al. 2011 [21].

Autophagy is a necessary process in all cells as it aims to ensure proper turnover of the organelles, avoid misfolded protein accumulation and keep functional and healthy cells, notably upon stress conditions to limit cell damages and stress-induced cell death [22, 23]. The autophagy pathway is therefore especially important in cardiomyocytes as in the adult heart no or limited regeneration exists [24]. Additionally, in the heart, the mitochondrial turnover and quality maintenance are of high importance to allow sufficient ATP production, avoid excessive ROS formation, and therefore promote cardiomyocytes survival. This quality control relies on a specific form of autophagy which is called mitophagy [25].

Briefly, the autophagy process can be split in 6 steps: 1) ULK1 once activated forms a complex with the protein (autophagy-related 13) ATG13, the focal adhesion kinases FIP200 and ATG101 to recruit some pieces of membrane from the endoplasmic reticulum in most of the cases, or mitochondria and Golgi to a lesser extent. 2) The ULK1 complex next phosphorylates Beclin1 which will recruit and activate the Vsp34 protein and form a second complex with the Vsp15, ATG14L to induce nucleation of the membrane and 3) contribute to the phagophore elongation by producing PI3P. Multiple proteins are then recruited during the elongation step in the lumen of the phagophore, such as the chaperone protein p62, or at the membrane such as the LC3II. The LC3II is obtained by conjugation of the cytosolic LC3I to a phosphatidyl ethanolamine by ATG7. After that, the LC3II is addressed to the phagophore by the ATG3. 4)

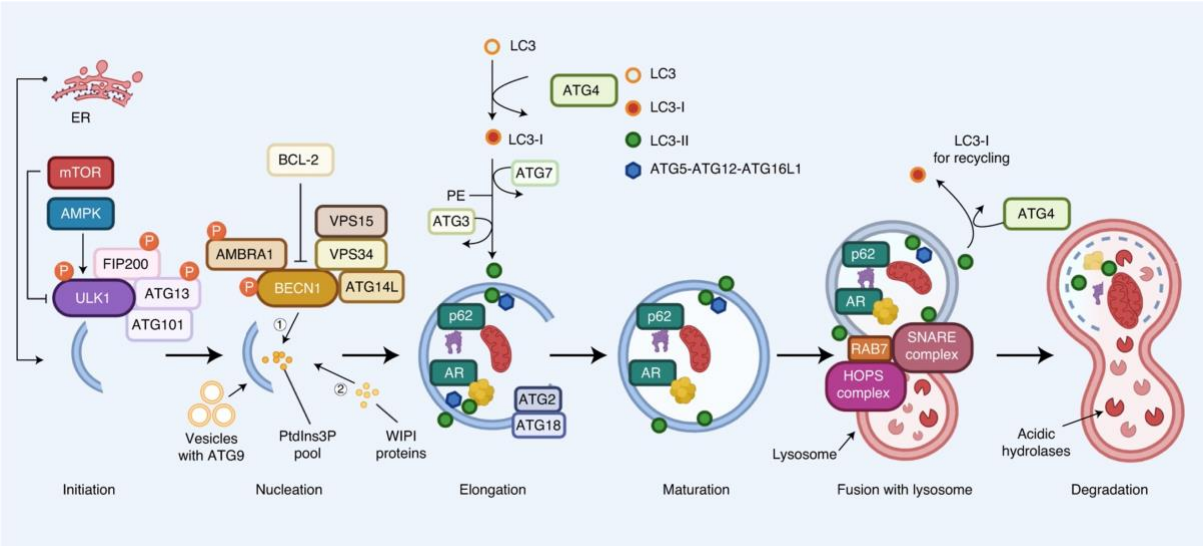

Figure 2. The autophagy process can be divided in 6 steps: 1) the initiation, 2) the nucleation and 3) the elongation of a phagophore from a piece of membrane originated from ER in most of the cases, or mitochondria/Golgi to a lower extent. This leads to the formation of the autophagosome. The autophagosome 4) matures and 5) fuses with the lysosome to form the autophagolysosome. The acid vesicular environment leads to the 6) digestion of the contents by acid hydrolases. Aman et al. 2021 [26].

The phagophore is fully matured to a complete vesicle called autophagosome. 5) The autophagosome fuses with the lysosome: the autophagolysosome contents are degraded by acid hydrolases and proteases after acidification of the vesicle by H^+ pumps. 6) The degraded products can be used again to produce proteins, or in the case of energy stress, ATP.

AMPK activation was shown to be protective in mouse models of cardiac ischemia or pressure overload-induced cardiac hypertrophy [14, 27]. Moreover, autophagy was described as a cardioprotective mechanism and its inhibition tends to be deleterious during ageing in the heart as an example [28]. On the contrary, excessive activation of the autophagic pathway could lead to cardiac atrophy [29]. Doxorubicin has been showed to increase autophagic flux in cancerous

cells, it is therefore of high importance to characterize its effects in the heart to prevent cardiotoxic events as described below [30].

1.1.3. Maladaptive cardiac metabolism and heart failure development

Heart failure has been reported to be associated with decreased metabolic flexibility: the heart becomes energy deficient due to decreased mitochondrial oxidative efficiency and decreased ATP contents [1, 31]. As a matter of fact, in proportion to the heart failure severity, the FAO is decreased and the acetyl-CoA amounts entering the Krebs cycle are reduced as well [2, 31]. To compensate for this loss in ATP contents, increased glycolysis is observed, in spite of decreased GLUT4 translocation capacity, thanks to a compensatory increase of GLUT1 expression [32]. However, the compensatory increase of glycolysis is uncoupled from the mitochondrial oxidative pathway: this compensatory increase of glycolysis is not sufficient to maintain normal ATP amounts [33]. This metabolic inflexibility leads to the cardiac contractile machinery remodeling by re-expressing neonatal contractile proteins such as the β-isoform of the myosin heavy chain, which has less efficient contractile properties (velocity) than the adult α -isoforms, but require 3 times less ATP [34].

In the beginning, this shift of metabolism and contractile machinery is needed to ensure cardiac contraction, however, when these adaptations are long-lasting, they are deleterious and induce cardiomyocyte cell death, cardiac fibrosis, decrease in contractile function and finally leads to the development of heart failure.

1.2. Doxorubicin-induced heart failure

1.2.1. Doxorubicin use in clinics and associated molecular mechanisms

Doxorubicin (dox) is one of the most potent chemotherapeutic drugs nowadays, however, because of its strong myocardial toxicity, dox use in clinics is limited [35, 36]. Dox belongs to the anthracycline family and is categorized as an antitumor antibiotic agent, meaning that dox will be efficient, regardless of the proliferative state of the cell, and would target the healthy tissues as the cancerous tissues [37]. Therefore, dox is used to treat a wide range of tumor malignancies in adult and pediatric patients (e.g. breast, gastric, ovarian cancer, or leukemia) [38, 39]. Still, as the main side effect, dox-induced cardiotoxicity has been broadly described and is definitely

dose-dependent. Over time, dosing has been optimized to reduce the dox-induced cardiotoxicity as much as possible to maintain a positive benefit-to-risk ratio. Acute cardiotoxicity has been first reported right after dox entry in clinics, and includes different complications such as arrhythmias, decrease in left ventricular function, myocarditis or hypotension and are accompanied by increased plasma cardiac stress markers including troponins and BNP. These severe acute cardiotoxic complications concern about 1% of the patients nowadays thanks to dosage refinement and they are usually reversible after an imminent stop of the dox-therapy [36, 40].

On top of this, the more challenging dox-induced cardiotoxic effect consists on the development of chronic and irreversible dilated cardiomyopathy and congestive heart failure [41], which can be diagnosed in 1.6-5% of the patients from 1 up to 30 years after the dox-therapy completion [40, 42]. Briefly, the dox-treated cancer survivors have 15 times more chances to develop congestive heart failure than their siblings, and 5 to 30% of them will suffer from diverse cardiac outcomes [35, 40, 43]. When developed this kind of heart disease is usually refractive to the common medications and has a poor prognosis [40, 44]. Currently, the strategy to prevent the development of the late stages of dox-induced CHF is very expensive for the health care systems [40, 45, 46]. Indeed, to detect dox-induced heart disease, patient's heart function and cardiac stress markers are monitored after the dox-therapy completion every 3 years by echocardiography and blood analysis. When the decreased heart function is detected in these patients, they are then given treatments they will respond to for a few years (ß-blockers, ACE inhibitors, and others [42]), however, their life quality will be strongly reduced from then. The prognosis of cancer patients is, fortunately, getting better and better over the years, but consequently, the number of dox-induced CHF patients too. Therefore, it is a high priority to understand the underlying mechanisms of dox-induced CHF development, to be able to prevent it.

Few studies have focused on defining dox-induced cardiac outcomes risk factors in the patients. For the moment, access to dox-therapy is limited for patients presenting a cardiovascular disease history [35]. Dox-induced CHF has been linked to different factors such as obesity/high-fat content, type 2 diabetes, high arterial tension, radiotherapy-treated patients, and young/elder age [35, 43]. Surprisingly, clinical trials have shown that sex is also a risk factor, depending on the patient's age at the start of the dox-therapy. Indeed, pediatric studies showed that before 12 years old no differences between males and females were observed on dox-induced cardiac outcomes, but, from 12 years old to 18 years old, females are more at risk to develop dilated CHF (rr=1.9)[35]. In adult patients, the sex differences in dox-induced CHF are less clear, as first of all, dox-induced CHF seems to depend on the cancer type, and secondly, most of the dox-treated patients suffer from breast cancer. However, the few studies

comparing sex differences on dox-induced cardiac outcomes in adult patients either identified male sex as a risk factor for cardiac hospitalization or protective effects of the female sex on the development of dox-induced left ventricle dysfunction. Further studies need to be led in clinics to validate these data, however, preclinical studies support that female sex is protective toward dox-induced CHF [47, 48]. Interestingly, the protective effect observed in female adult patients is not observed anymore when patients started their therapy after 65 years old [49].

Dox efficiency on tumor regression has been broadly studied and can be attributed to several mechanisms. The main mechanism which has been extensively described in the last decades is the ability of dox to inhibit cell growth and proliferation through genotoxicity. As a matter of fact, on the one hand, dox accumulates in the nuclear as well as the mitochondrial compartment where it inhibits DNA replication and repair processes. Indeed, after passively entering the cell, dox is shuttled either to the nucleus or to the mitochondria where it will intercalate to the DNA due to high affinity for it [37]. There dox will inhibit DNA-associated proteins such as helicases implied in DNA replication, and more importantly, the topoisomerase II (topII) which is essential for DNA replication, RNA transcription, or DNA repair processes [50]. On the other hand, dox induces ROS production through the interaction of its semiquinone group with iron, but also through its binding to the mitochondrial respiratory chain complex I protein [51]. This dox-induced ROS production subsequently leads to DNA damage induction, which cannot be repaired and is even worsened because of the topII protein inhibition. When DNA damages are important enough, the ATM/ATR pathway leads to apoptosis of the cell or senescence. Sometimes, the damaged cells could come back from senescence with more or less damages and altered contractile function and could contribute to the development of dox-induced CHF [52].

Doxorubicin also induces cellular toxicity to a larger extent. As explained above, dox interacts with iron to produce ROS. Interestingly, in patients and in vivo, the hearts from individuals who developed dox-induced heart disease were overloaded with iron, and this accumulation has been shown to happen within the cytosol, and (preferentially) in the mitochondria [53]. Also, dox has been shown to acutely lead to the release of the calcium endoplasmic reticulum stocks in the cytoplasm through alteration of RyR and SERCA expression as well as other actors of the calcium metabolism, and lead to long term calcium storage incapacity [54]. All of the non-exhaustive events described above converge to dox-induced cell death and cardiomyocytes disrupted contractility.

1.2.2. DOXORUBICIN-INDUCED DISRUPTION OF METABOLISM AS EARLY CARDIOTOXIC MECHANISM

Cardiomyocytes represent 35% of the total cardiac cell population, yet they represent 80% of the heart volume, and ensure the heart's contractile function [55]. The cardiomyocyte's contractility is highly dependent on fuel production, that's why their mitochondrial compartment is highly developed and occupies about 30% of the cell volume [56, 57]. Dox is a cationic drug, and has therefore a tropism for the mitochondrial inner membranes which are negatively charged. Besides, cardiomyocytes' mitochondria specifically present at their inner mitochondrial membrane cardiolipins, a glycerophospholipid for which dox has a strong affinity. However, this dox high affinity for cardiomyocytes mitochondria does not imply a higher accumulation of dox in the heart in comparison to any other organ nor the observed dox-induced cardiotoxicity in vivo, but it could imply a higher mitochondrial location in comparison to the other cell types [53, 54, 58, 59]. However, and non-surprisingly, genome wide association studies (GWAS) have associated variants of the dox-dependent extrusion ABC transporter proteins such as MRP1 or MRP2 with higher risks to develop dox-induced heart dysfunction as it is probably causing higher intracellular dox concentrations [60].

In vitro and in vivo, the dox-induced cardiomyocyte cell death pathway by apoptosis has been well documented and has been shown until recently to mainly rely on dox-induced DNA damage and ROS generation [51, 54]. Further studies have investigated the interaction of dox with the cytoskeleton proteins. These studies have notably highlighted dox-induced disruption of contractile protein organization, so called cardiac myofibrillar disarray and the development of myocardial abnormal contractility [61, 62].

More recent investigations have suggested that it is the early onset of dox-induced metabolic disturbances that might condition the development of later dox-induced CHF. Indeed, Torkaska and colleagues showed that dox decreases ATP/ADP ratios in the cell by uncoupling the mitochondrial respiratory chain oxidative phosphorylation and by downregulating the cell energetic sensors and effectors such as the creatine-phosphate shuttle or the AMPKα signaling pathway [63, 64]. These metabolic disturbances are accompanied by an incapacity of the cardiomyocytes to use with full efficacy lipids and glucose to produce ATP. As a matter of fact, dox has been showed to inhibit the CPT1 or to deplete the L-carnitine stores, leading to the impossibility to translocate and thus use medium and long chain FAs to the mitochondrial compartment [65]. Moreover, studies demonstrated that dox decreases glucose uptake efficiency as well as the phosphofructokinase expression, an essential and limiting enzyme of the glycolysis pathway, in neonate rat ventricular myocytes [66, 67]. These studies led some people to compare

the dox-treated hearts to diabetic cardiomyopathy models due to the development of these metabolic inflexibility features [65, 68, 69].

Besides other important pathways which are implied in the protein homeostasis and sarcomeric integrity, in particular the autophagy pathway has been shown to be dysregulated in the stressed heart and notably in dox-therapy animal models [22, 70]. As a matter of fact, on one hand several in vivo and in vitro studies have reported that dox increases LC3II protein levels, that is to say autophagosome vesicle number and autophagic process due to genotoxic effects, energy depletion and ROS production. On the other hand, dox has been shown to inhibit the autophagosome vesicle clearance by inhibiting lysosomal acidification [71, 72]. The dox-induced disturbances of the autophagic are not fully understood, however, what is sure is that autophagosome accumulation in cardiomyocytes or lack of misfolded protein clearance leads to contractile disturbances and toxicity in cardiomyocytes. Most of the studies focusing on the dox effects on the autophagic pathway are not complete as they did not characterize autophagic flux.

1.2.3. Doxorubicin studies in vivo, relevance of the dox injection protocol?

Numerous investigations have intended to uncover the mechanisms underlying doxorubicin-induced cardiotoxicity in vivo and in vitro. Most of the studies which have been published using in vivo models relied on the use of a single and high dose dox injection protocol in rodents. Therefore, these so-called dox-induced acute toxicity models are by definition irrelevant toward what is done in the clinics where dosage refinement has been extensively investigated to limit dox-induced mortality. As a matter of fact, Bian and colleagues showed that in mice 75% of mortality was observed in these kind of experimentations 15 days after the dox single injection [73]. Thus, the results obtained from these studies have to be interpreted cautiously as they are mainly reporting cardiac responses to highly toxic dox doses [71].

More relevant models relying on repeated low dose injections of dox were developed to investigate dox-induced chronic effects on cardiac function, physiology, and molecular events at later time points [74]. Most of the chronic dox models were performed in rodents, but these models are numerous and the available data are quite hard to summarize and compare [75]. Indeed, the use of numerous injection protocols yielding different cumulative doses over shorter or longer periods of time, the use of different species (rats, mice, rabbits) or strains presenting differences in their metabolic properties (C57BL/6J vs 6N mice as an example) or even the differences between the animal facilities and quality of the dox batches are factors that contribute to the heterogeneity between the pre-clinical data reported.

Surprisingly, whereas cardiovascular disease development has been reported to be sex-dependent, and unclear sex-prevalence effects have been described in the context of dox-induced cardiac toxicity in clinical studies, only few animal researchers have investigated sex-differences upon dox-treatment and therapies. These animal studies all show that dox induces more severe cardiac toxicity in male than in female animals. Interestingly, to our knowledge, only the Moulin and colleagues' study have investigated dox-induced changes in cardiac function and dimensions over time in male and female rats upon the same dox regimen [76].

1.3. NRG-1ß AND THE ERBB SYSTEM IN THE HEART

1.3.1. THE ROLE OF NRG-1ß/ERBB IN THE DEVELOPING AND ADULT HEART

The neuregulins are growth factors characterized by the presence of an EGF-like domain and are encoded by 4 individual genes (NRG1-4) [77]. NRG-1 has been shown to have 6 different subtypes, which differ by their N terminal region, EGF like domain (α, β) the presence of IgG like domain and glycation profile: more than 30 isoforms in total have been reported [78]. The NRG-1 I and II isoforms can be released to the extracellular space after metalloprotease-induced cleavage and therefore exert autocrine/paracrine activity. In the heart, mainly NRG-1 type I is expressed. Moreover, EGF like domains β have been reported to have a 10 to 100 times higher activity than the EGF like α-isoforms [79]. Therefore, in the present study we are interested in the NRG-1 type Iβ, abbreviated in this thesis as NRG-1.

The NRG-1-induced signaling relies on activation of the ErbB receptor tyrosine kinase family. Briefly, 4 ErbB receptors have been identified and are encoded by different genes. In cardiomyocytes, NRG-1 signal transduction depends on ErbB2, 3 and 4. NRG-1 can bind either to ErbB3 or ErbB4, but not to ErbB2 which has no ligand binding domain. Upon NRG-1 binding, the ErbB receptor undergoes a conformational change which leads to its hetero or homo dimerization. Transactivation of the receptor occurs and allows its full activation and subsequent downstream signaling. Yet, the ErbB3 receptor does not have a catalytic domain, therefore, to induce downstream signaling it needs to heterodimerize with cardiac ErbB2 or 4. Likewise, as ErbB2 does not have a ligand binding domain, it's signaling relies on its heterodimerization either with ErbB3 or ErbB4. Therefore, ErbB2/3, ErbB2/4, ErbB3/4 and ErbB4/4 signaling exists.

NRG-1 plays a critical role in fetal development as it is implied in cardiac trabeculation. As a matter of fact, homozygous deletion of NRG-1 leads to fetal death at day 10.5. Likewise, the deletion of either ErbB2 or ErbB4 leads similarly to fetal death at 10.5 days, suggesting that NRG-1, ErbB4 and ErbB2 are required for the normal heart morphogenesis [80-82]. Interestingly, the ablation of ErbB3 also results in embryonic lethality, this time related to defective endocardial cushion formation [83]. Moreover, NRG-1 is also implied in the process of differentiation of the embryonic stem cells into cardiomyocytes [84]. Later, in the matured heart, ErbB expression is reduced and this is believed to be one mechanism by which the heart loses its regenerative capacity [85].

The NRG-1-ErbB signaling is also required for neuronal crest migration and brain maturation, for mammary gland maturation and function, and in adulthood for lactation [86, 87].

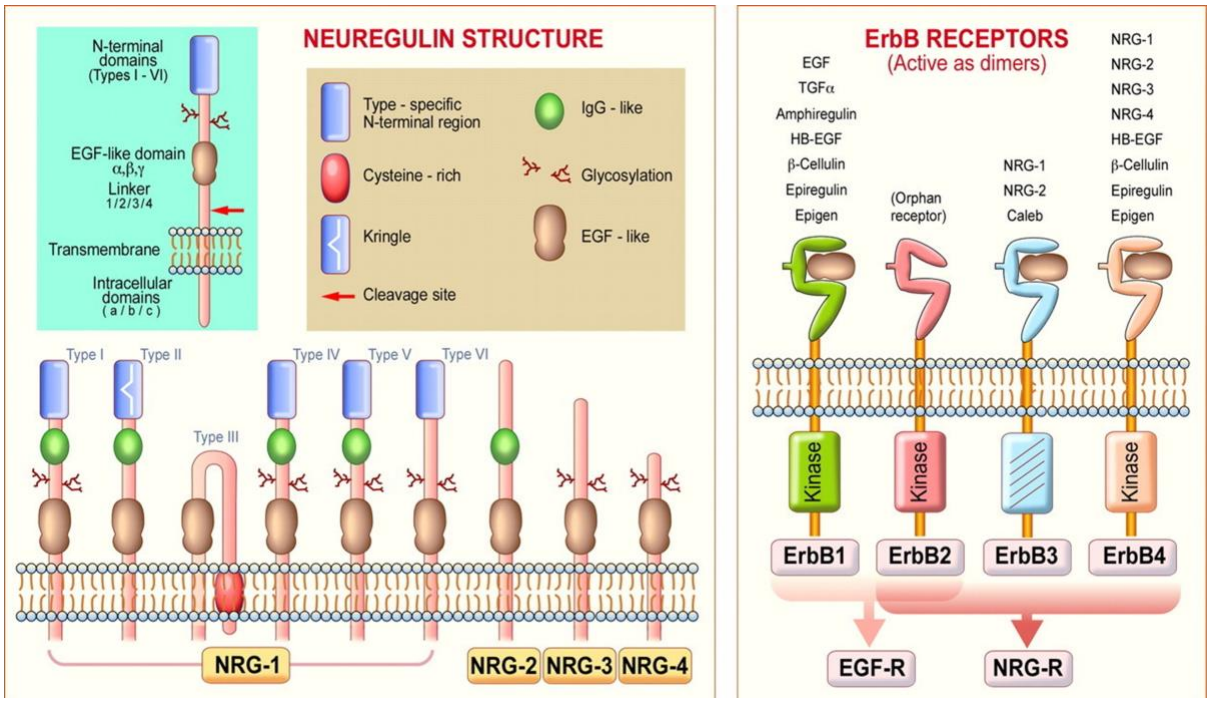

Figure 3. Schematic representation of NRG-1 classification and structure, and of ErbB receptors. Guma et al. 2010 [77].

Interestingly, ErbB1, 2 and 3 have been shown to be potential proto-oncogenes, while the role of ErbB4 in cancer is controversial, probably due to the lack of characterization of its different isoforms as described in 3.3.1.

Hence, 25% of the breast cancers are positive for ErbB2 [88]. The unexpected increased cardiotoxicity after ErbB2 inhibition on dox-treated breast cancer patients has uncovered a cardioprotective role of NRG-1-ErbB signaling in the adult heart upon cardiotoxic events.

Moreover, dox-treated patients were shown to have transiently increased plasma NRG-1 levels that were associated with the later development of chronic heart failure. The upregulation of the NRG-1-ErbB system in the context of dox-therapy was suggested to be a cardioprotective mechanism. Experimental in vivo studies supported this, as ErbB4 deletion or NRG-1 heterozygous-KO mice show increased dox-induced cardiotoxicity [89, 90]). After these initial observations, more studies have investigated the role of the NRG-1-ErbB system in different rodent models of heart disease, including ischemic models and overload-induced cardiomyopathy models, but also in models of physiological cardiac hypertrophy such as that developed during pregnancy [91-93]. These studies have highlighted the cardioprotective role of NRG-1 during acute cardiac injury and ventricular remodeling responses. It is of note that ErbB4 expression is needed to maintain cardiac homeostasis as ErbB4 deletion leads to cardiac dilation [94].

1.3.2. NRG-1 SIGNALING IN CARDIOMYOCYTES

NRG-1 has been extensively described to activate pro-survival pathways and to enhance hypertrophic responses in cardiomyocytes [95, 96]. Recent studies have also investigated the effects of NRG-1 on the autophagic response [97-100]. As a matter of fact, NRG-1 is well known for its ability to signal via PI3K/Akt, ERK1/2 and c-Src in cardiomyocytes [101]. Indeed, in adult and neonatal cardiomyocyte cultures, NRG-1 induces the PI3K/Akt pathway, which has been reported to induce pro-survival effects in different models of cardiac stress [61, 102]. Briefly, after ligand binding ErbB4 or ErbB2 activate PI3K at the membrane by phosphorylating it. PI3K then produces phosphatidyl inositol (3,4,5)-triphosphate (PIP3). PIP3 will then activate PI3K (3-phosphoinositide-dependent kinase), which in turn causes the phosphorylation of Akt on Thr308. The activated Akt will then transduce the signal by alleviating mTORC1 inhibition via TSC2 complex phosphorylation. The activated mTORC1 induces protein synthesis and other anabolic pathways and inhibits catabolic pathways as well as autophagy by increasing ULK1-pS757.

A second effector of NRG-1 signaling is ERK1/2 MAPK (extracellular signal-regulated kinase 1/2; mitogen activated protein kinase). Briefly, ErbB2 and ErbB4 activation leads to the Grb2-Sos recruitment to the membrane (Growth factor receptor-bound protein2, nucleotide exchange factor son of sevenless) [103, 104]. There, Sos activates the MAPKKK-MAPKK-MAPK cascade Ras-RAF-MEK-ERK1/2 by exchanging Ras a GDP to a GTP. ERK1/2 is known to phosphorylate and thus activate numerous transcription factors such as Myc or c-fos, and thereby causes the expression of survival and proliferative genes [105]. Moreover, while Ras activates PI3K, ERK1/2 supports mTORC1 activation by inhibiting TSC2 and activating raptor by phosphorylation [106].

Therefore, ERK1/2 activates mTORC1 and participates in the development of the NRG-1 induced cardiac hypertrophic response [107, 108].

A third well known pathway to be triggered in cardiomyocytes upon NRG-1 stimulation is the c-Src-FAK pathway (steroid receptor coactivator; focal adhesion kinase) [109]. The c-Src is directly phosphorylated by the ErbB2 receptors at Tyr215 or Tyr416. Then, the activated c-Src phosphorylates FAK at Tyr861 in cardiomyocytes [109]. This leads to formation of the focal adhesion complex, which induces myocyte to myocyte connectivity, cytoskeleton remodeling and cell survival [109-111]. As FAK is essential for the integrity and function of cardiomyocytes, multiple tyrosine kinase receptors can trigger its activation [109, 112].

Finally, few studies have investigated the effects of NRG-1 on the autophagic pathway. In skeletal muscle, Yin and colleagues showed that NRG-1 inhibits sepsis-induced autophagy in an Akt-mTOR-dependent manner [99]. Schmukler claimed that in a prostate cancer cell line, NRG-1 inhibited autophagy in an mTOR-independent manner [98]. As explained above, inhibition of dox-induced autophagy may be protective toward the development of cardiotoxicity [113, 114]. An et al. studied in neonatal rat ventricular myocytes whether NRG-1 stimulation affects dox-induced autophagy [100]. Their study suggests that NRG-1 inhibits Beclin1 and thereby the dox-induced autophagy. However, An et al. neither studied the effects of NRG-1on autophagic flux nor its in vivo effects in dox-treated animals. Thus, it has not been fully investigated whether the cardioprotective effect of NRG-1 against dox-toxicity is mediated by modulation of autophagic flux.

1.4. AIMS OF THE STUDY

This study aimed to:

1. Establish a clinically relevant model of dox-treatment using male and female mice.

2. Assess whether NRG-1 is cardioprotective in this model when injected every other day.

3. Characterize the early mechanisms whereby NRG-1β exerts its cardioprotective role in vivo and in vitro.

2. MATERIALS AND METHODS

2.1. IN VIVO METHODS

2.1.1. MOUSE HOUSING AND HANDLING, ECHOCARDIOGRAPHY AND TAIL-CUFF MEASUREMENTS

Animal background and housing

Firstly, inbred C57BL/6J wild-type male and female mice from 10 to 12 weeks (weeks) old were used to study the effects of dox on cardiac function.

Secondly, to study whether mTORC1 or mTORC2 are implicated in the NRG-1-induced effects on cardiac autophagy, 10 weeks old C57BL/6J mice positive for α-MHC-MerCreMer and carrying either 2 raptor or 2 rictor floxed alleles (α-MHC-MerCreMer/raptor$^{fl/fl}$ or α-MHC-MerCreMer/rictor$^{fl/fl}$) were compared to control mice, positive for α-MHC-MerCreMer carrying the wild-type raptor and rictor alleles. To avoid heart size and weight effects in our study, mice were distributed to the different experimental groups with the condition to get similar bodyweight averages for each group. Mice were injected with tamoxifen as described [115]. Experiments started 2 weeks after the last tamoxifen injection was given, that is to say in 13 weeks-old animals.

The mice were housed in a 12 h light/12 h dark cycle, at a temperature of 20-25°C. Ad libitum access to water and a chow diet was assured. Mice were handled by only 2 female experimenters (including the weekly cages change), and odor exposure was minimized. To avoid the stress from new environment or cage changing, mice were moved to the experimental room at least one week before the study started and no cage changing was assured within 48 h prior to each data acquisition or sacrifice.

Animals' body weight (BW) and well-being scoring were performed every second day around 1 PM, and BW values were used to prepare the injection to come 2 h later on average. It is of note that mice were assigned to the different groups with one only condition that each group had a similar body weight distribution.

Echocardiography

Transthoracic echocardiography was performed on anesthetized animal using the Vevo 2100 ultrasound system (VisualSonics, Toronto, ON Canada) equipped with a MS-550 linear-array probe working at a central frequency of 40 MHz. General anesthesia was induced in an

induction chamber with 3% isoflurane (Abbvie®) carried by air. Then the anesthetized animal was placed at supine position on a pre-warmed imaging platform and 1.5 % air carried isoflurane was used to maintain the anesthesia during the whole imaging procedure. The animal body temperature was controlled at around 37 °C with a rectal thermocouple probe. Eye gel (Lacrinorm®) was applied to prevent ocular dehydration. Subcutaneous needle probes were inserted in the mouse limbs and attached to ECG leads embedded in the imaging platform for ECG recording. Hair removal cream (Nair©) was applied on the chest to remove hairs from imaging area. 2-D guided M-mode at the mid-papillary muscle level from parasternal short-axis view was used to access the cardiac geometry and function. Left ventricular anterior (LVAW) and posterior (LVPW) wall thickness and internal dimensions (LVID) were measured at the end of systole (s) and end of diastole (d) from three cardiac cycles. Values were averaged and used to calculate the LV volumes (Vol), ejection fraction (EF) and mass ($LV\ Vol;d = (7.0 / (2.4 + LVID;d)) \times LVID;d^3$, $LV\ Vol;s = (7.0 / (2.4 + LVID;s)) \times LVID;s^3$), $LVEF\ \% = 100 \times ((LV\ Vol;d - LV\ Vol;s) / LV\ Vol;d)$, $LVmass = 1.053 \times ((LVAW;d + LVID;d + LVPW;d)^3 - LVID;d^3) \times 0.8$).

Some mice underwent tail-cuff measurements. Previous experiments performed in the laboratory showed that tail-cuff experiment-induced stress was modulating EF. Therefore, these animals underwent baseline echocardiography measurement before the tail-cuff measurements as explained in 2.1.2.

Tail-cuff measurements

To determine whether the dox-therapy modulates peripheral blood pressures, (BP) and heart rates, the non-invasive tail-cuff method was used. Animals were displayed in a restrainer, on top of the heating pad (maintained at a temperature of 37°C) integrated into the blood pressure analysis system™ BP-Series 2000 II Visitech systems. Out of the restrainer, the mouse tail was passed in a cuff followed by a pulse oximeter captor before being fixed on the support. After pressure calibration of the device, the cuff was swelled up to 20 mmHg to block the tail artery blood flow. The cuff pressure was gradually decreased in a controlled manner by the device until pulsation was detected by the captor. The higher pressure at which the artery pulsation was detected corresponds to the peripheral systolic BP.
The platform could welcome 6 animals in the meantime, and the acquisition consisted of 20 cycles of BP measurements (tail-cuff swelling/release). The 10 first cycles were considered as adaptation, and the following 10 were recorded as the daily data. To avoid handling bias, animals were trained in batches of 6 for 5 days in a row and displayed at a different spot on the platform each day. Each batch of animals underwent the BP and heart rate measurement at

the same time of the day between 9 AM and 12 AM during the animals' inactive phase, and the platform was disinfected between each batch to avoid odor exposure.

2.1.2. LONG-TERM DOXORUBICIN-THERAPY MOUSE MODEL

Mice C57BL/6J underwent a doxorubicin-therapy previously described by Milano et al. [70, 116]. This protocol aimed to yield a cumulative dose of 24mg/kg of dox (Pfizer©) with repeated intraperitoneal (IP) low dose injections at day (d) 0, 2, 5, 8, 10, 12 (dox), versus NaCl (CTL), to mimic the subacute and chronic cardiotoxicity induced by dox-therapies observed in patients. To study whether NRG-1ß pretreatment might have protective effects on the dox-induced (cardio)toxicity, a 3rd group of mice was preinjected IP with 20µg/kg rhNRG-1ß (Peprotech®, NRG/dox) while the CTL and dox groups were injected PBS as control 30 mins before the dox-injection. Heart geometry and function were assessed with echocardiography always in the mornings (between 9 AM to 12 AM) before and 14, 21, and 35 days after the dox injection. Animals were sacrificed the day after or the second day after the last echocardiography.

For the sub-group of animals underwent tail-cuff BP measurements, baseline echocardiography was performed at least 1-3 days before the 5-days tail-cuff training for baseline blood pressure measurement. The animals were allowed to recover for 2 days prior to receiving the first dose of dox. Second echocardiography and blood pressure measurement were performed at d14 and d15-20, respectively. Last echocardiography was done on d21 and the animals were sacrificed 1-2 days after.

2.1.3. SHORT-TERM DOXORUBICIN-TREATED MOUSE MODEL

To study the early metabolic modulations induced by dox and the expected preventive effect of our NRG-1β pretreatment at the molecular level, mice were injected intraperitoneally NRG-1ß 20µg/kg in the case of the NRG/dox group or PBS in dox and CTL groups 30 mins before receiving the control or dox treatment (4mg/kg). Mice were sacrificed as described in 2.1.4 and no other measurements than BW were done in these mice.

2.1.4. NRG-1 MODULATION OF THE AUTOPHAGIC PATHWAY: ROLE OF RAPTOR IN THE HEART

To study the raptor contribution in NRG-1 induced modulation of LC3II/I ratios, cardiac-specific deficient raptor mice vs their wild-type littermate controls were fasted from ZT23 and sacrificed

at ZT31 as described below. At ZT30, mice were injected either with NRG-1 (20µg/kg) or PBS control. Considering ZT0-ZT12 the active phase and ZT-13-ZT24 their resting phase.

2.1.5. SACRIFICE AND TISSUES COLLECTION

Concerning the dox long-term model, animals were fasted for 6h before sacrifice whereas in the dox short-term model animals were not. 30 mins before getting sacrificed, animals were stimulated either with PBS for the CTL and dox group, or with NRG-1β 20µg/kg for the NRG/dox.

For the sacrifice and samples collection, deep anesthesia was introduced in an induction chamber then maintained with a nose cone with 5% isoflurane carried by pure oxygen. After the complete unconsciousness was confirm by toe pinching, the chest of the animal was carefully cut open with scissors to expose a beating heart. A 27 G needle attached to a 1 ml syringe was inserted into the right ventricle quickly to collect maximum volume of blood from the heart. The blood was transferred immediately to an EDTA coated tube on the ice for later plasma collection. The heart was excited and washed briefly in ice-cold saline to stop the heart beating and remove the left-over of blood. The atria were discarded and the right ventricle was carefully separated. The weights of left ventricle and right ventricle were measured. The left ventricle was sliced into three pieces according to different purposes: the base of the heart was preserved in OCT for histology or immune-histology, the middle heart and the apex were snap-frozen in liquid nitrogen for protein and RNA respectively. Liver, kidney and gastrocnemius muscle were also collected and snap-frozen in liquid nitrogen. The tibias from both legs were collected to measure the length for the normalization of the heart weight. The whole lung and a piece of gastrocnemius muscle were collected and weighted, then they were naturally dried at room temperature for three weeks to assess the wet/dry ratios for the potential lung edema or general hydration

2.2. In vitro methods

2.2.1. Cell culture general materials

Cells were incubated at 37°C, 5% CO2 in a HERAcell 150 incubator. They were plated in 60mm Ø culture dishes purchased from Milian© All the media and media components were purchased from GIBCO when nothing else is indicated. Culture media were supplemented with L-Glutamine (2 mM), penicillin (100 units/ml), streptomycin (100µg/mL), and HEPES (25mM).

Complete medium
DMEM 1g/L D-glucose, 10% FBS, 25mM HEPES, 10µM ARAC +pyruvate

Fasting medium
DMEM 1g/L D-glucose, ACCT (0.2% bovine serum albumin, 2mM L-carnitine, 3mM creatine, 3.2mM taurine), 25mM HEPES -pyruvate

2.2.2. Isolation of neonatal rat ventricular myocytes (NRVMs)

1 to 2 days old Sprague Dawley rats were sacrificed by decapitation (d1). Hearts were dissected and atria and big vessels, enriched in fibroblasts, were discarded. The Remaining ventricles were pre-digested in a 0.05% trypsin-EDTA solution overnight (ON) at 4°C. The next day (d2), the ventricles were washed with some complete medium before getting digested in Hank's balanced salt solution (HBSS) supplemented with 0.83mg/mL collagenase type II (purchased from Worthington) under gentle agitation at 37°C for 2 to 5 mins. The supernatant containing the digested cells was collected and fresh collagenase solution was added back on the ventricles for additional digestion steps. Ventricles were digested that way 4 to 5 times. Supernatants were all collected in complete medium and finally centrifugated (500RPM, 6 mins, RT) to collect the cells. The debris were then filtered away with a strain of 100µm. To reduce the number of non-cardiomyocytes, the cellular suspension was pre-plated twice in T75 culture Flasks for 1h at 37°C (Corning®), as the non-cardiomyocyte cells from the preparation adhere quicker to the surface than cardiomyocytes. The enriched cardiomyocyte fraction was counted with a Neubauer cell, using Trypan blue to discriminate the living cells from the dead ones, and

seeded at a 2.5x10^6 cells/petri dish in complete medium. On d3, in the morning, the medium was changed to remove the dead cells.

2.2.3. NRVM TRANSFECTION

After isolation on d2, NRVM were electroporated using the Amaxa™ Rat Cardiomyocyte Neo Nucleofector™ Kit and Nucleofector II device. Briefly, 3 million cells were transfected with 6µg of either pEGFP-LC3 vector (Addgene 11546) or pEGFP-N1 using the AMAXA Neonatal Rat Cardiomyocytes Nucleofector kit according to the manufacturer's instructions. 2*10^5 cells were plated per laminin-coated glass cover-slips in complete DMEM, after a recovery step of 20 mins in RPMI supplemented with 10% FBS at 37°C.

2.2.4. NRVM CULTURE FOR AUTOPHAGY MONITORING

On d4, cells were washed 2 times with warm PBS heated at 37°C and fasting medium was added. A first stimulation step consisted of pepstatin+E64D vs vehicle or NRG-1 vs PBS. 30 minutes later, a second stimulation step consisted of NRG-1 vs PBS or dox vs DMEM. In the case of autophagic flux inhibition, a third stimulus was done 30 mins after the second one (dox vs DMEM).

Hormones and inhibitor

Stimulus	company	concentration	target
Cycloheximide	Merck	10 µg/ml	Translational machinery
Doxorubicin	LC Laboratories	1µM	/
E64d	Sigma	10 µg/ml	Cathepsins
MG-132	APExBIO	20 µM	proteasome
Pepstatin A	Sigma	10 µg/ml	cathepsins
rhNRG-1ß	R&D	10 nM	ErbB3 and ErbB4

2.3. MOLECULAR ANALYSIS

2.3.1. RNA ISOLATION

RNAse free materials and solutions were used for the whole procedure. Total RNA was extracted by the phenol/chloroform method, using the TRI-reagent solution from Sigma. In the case of cell culture, Petri dishes were washed with cold PBS (4°C), and the cells were lysed with 750µL of TRI-reagent. The lysates were collected and centrifugated to eliminate cellular debris (10 mins, 13 000RPM, 4°C), and the supernatants transferred into new microtubes. In the case of organs, a small piece of tissue (the apex for the heart) was homogenized thanks to a polytron® device in 1 ml of ice-cold TRI-reagent. The homogenates were centrifuged (10mins, 13 000RPM) and the supernatants collected. After adding 150µL (cell lysate) or 200µL(organs) of chloroform to the phenolic fraction, tubes were vortexed and incubated 5 mins at room temperature (RT) before undergoing centrifugation (10 mins, 13 000RPM, 4°C). The aqueous phase, containing the RNA, was transferred to a new microtube and 1 volume of isopropanol was added to precipitate the nucleic acids. Samples were vortexed, incubated 5 mins at RT, and centrifuged again (10mins, 13 000RPM, 4°C). Isopropanol was eliminated, and the pellets containing the RNA were washed 2 times with a solution of ethanol 70%. Residual ethanol was removed with a pipette and pellets were air-dried before getting resuspended in nuclease-free water (Promega). DNAse treatment (Invitrogen) was performed according to the manufacturer's instructions to eliminate potential genomic DNA contaminations. RNA was then aliquoted, snap-frozen in liquid nitrogen, and stored at -80°C for upcoming reverse transcription.

The RNA integrity was systematically checked by migration through a 2% agarose gel, in presence of ethidium bromide. The RNA 28s and 18s bands integrity were assessed after imaging the gel thanks to Fusion Fx (Vilber) device.

2.3.2. DNA ISOLATION

Nuclease-free materials and solutions were used during the overall procedure. Cells were collected in a PBND/proteinase K (160 µg/ml) solution and digested for 1h at 37°C. DNA was then isolated with the phenol-chloroform method as explained above, using a phenol: chloroform: isoamyl alcohol solution 25:24:1. The aqueous phase containing the DNA was collected, supplemented with 1mL of chilled isopropanol and stored for 1h at -20°C to precipitate the nucleic acid. Samples were centrifuged (10mins, 13 000RPM, 4°C). The Isopropanol was discarded, and the pellets containing the DNA were washed 3 times with a

solution of ethanol 80%. Residual ethanol was removed with a pipette and pellets were air-dried before getting resuspended in nuclease-free water. Samples were aliquoted, snap-frozen, and stored at -80°C.

2.3.3. Reverse transcription and quantitative polymerase chain reaction

RNA concentration was determined by spectrophotometry, using the NanoDrop™ device and measuring OD at 260nm. Reverse transcription of 1µg of mRNA to cDNA was performed using the High-capacity cDNA Reverse Transcription kit (appliedbiosystems) and Biometra® thermocycler. The obtained cDNAs were either stored at -20°C, or diluted right away 1/50 in nuclease-free water. Diluted cDNA was amplified by quantitative polymerase chain reaction with the GoTaq qPCR master mix kit from Promega, according to the manufacturer's instruction, to quantify the expression of the genes of interest.

For DNA samples, concentration was determined as previously described. 1µg of DNA was then pre-diluted in 20µL, and further diluted 1/20 in nuclease-free water. The diluted DNA samples underwent qPCR exactly as described above.

The following primers were purchased from Microsynth®.

Primers table

gene	organism	Forward primer	Reverse primer
ANP	Mus musculus	TGG GAC CCC TCC GAT AGA TC	TCG TGA TAG ATG AAG GCA GGA A
GLUT-1	Mus musculus	GGG CAT GTG CTT CCA GTA TGT	ACG AGG AGC ACC GTG AAG AT
ß-MHC	Mus musculus	TTG AGA ATC CAA GGC TCA GC	CTT CTC AGA CTT CCG CAG GA
POLR2A	Mus musculus	AAT CCG CAT CAT GAA CAG TG	CAG CAT GTT GGA CTC AAT GC
ACC-*β*	Rattus Norvegicus	CCA CTG GCA GCT TAG ATC CG	AGA CCA TTC AGA CAA CTG GG

COXIV-i1	Rattus Norvegicus	TTC TAC TTC GGT GTG CCT TC	CAC GCC GAT CAA CAT AAG ATG G
HPRT	Rattus Norvegicus	ATG GGA GGC CAT CAC ATT GT	ATG TAA TCC AGC AGG TCA GCA A
LC3	Rattus Norvegicus		
LONP1	Rattus Norvegicus	TCC CGG ATG TGT TTC CTC AC	CCT TCT CAG CAG CTC AAC CA
Mitochondrial D-loop	Rattus Norvegicus	GTG AAA TCA ACA ACC CGC CC	ATA GTC ACC CCC AGG ACG AA
Ndufv1	Rattus Norvegicus	CAT CCT GGA AGG GAA AGT CAC A	AGG GGC CTT GGG AAC TAA AG
PGC1α	Rattus Norvegicus	CAC CGC ACA CAT CGC AAT	ATT CGT CCC TCT TGA GCC TTT
TATA-box binding protein	Rattus Norvegicus	CAC AGG AGC CAA GAG TGA AGA AC	GCT TCT GCA CAA CTC TAG CGT ATT
ULK1	Rattus Norvegicus	CTA CGA TGG GAA GGC TGA CC	GCA CAG GTG GGG ATT TCT TG

2.3.4. Protein extraction, cytosolic/nuclear fractionation and protein assay

Protein extraction

Radio immunoprecipitation assay (RIPA) lysis buffer containing 50mM Tris pH 7.4, 150mM NaCl, 1% NP40, 0.25% sodium deoxycholate was supplemented with EDTA 5mM, SDS 0.1%, 1% protease inhibitor cocktail, 0.5% phosphatase inhibitor cocktails n°2 and n°3 purchased from Sigma, and in the case of tissue samples this lysis buffer was further supplemented with additional phosphate donors (10mM Na Glycerophosphate and 10mM Na pyrophosphate).

In the case of cell culture, cells were washed twice with ice-cold PBS and lysed with 150µL of the lysis buffer described above. Cells were scrapped and the protein lysates collected, vortexed and incubated 10 min on ice before centrifugation to remove the cellular debris

(10mins, 13 000RPM, 4°C). Supernatants were aliquoted, snap-frozen in liquid nitrogen, and stored at -80°C. In the case of tissues, a small frozen piece of the tissue of interest (half of the LV in the case of the heart) was immersed in 0.9mL of the described ice-cold lysis buffer. The tissue was homogenized with a polytron® device. The homogenates were vortexed and incubated on ice for 10 mins, and then centrifuged (15mins, 13 000 RPM, 4°C). Supernatants were aliquoted, snap-frozen in liquid nitrogen, and stored at -80°C.

Protein fractionation

Cells were washed twice in ice-cold PBS and lysed in cytosol extraction buffer (A) supplemented with protease and phosphatase inhibitors. Cells were incubated on ice for 10 mins and regularly vortexed until Trypan Blue staining showed efficient cell lysis under the microscope. Samples were centrifuged (10mins, 3 000 RPM, 4°C) and the cytosolic fraction (supernatant) was aliquoted and snap frozen. Nuclear extraction buffer B, supplemented with protease and phosphatase inhibitors, was added to resuspend the pellets, and Dounce homogenization was performed. Samples were incubated on ice for 30 mins and vortexed every 5 mins before getting centrifuged (21 000g, 20 mins, 4°C). Supernatants containing the nuclear fractions were aliquoted and snap frozen.

Buffer	**composition**
Cytosol extraction buffer A	10mM HEPES, 1.5mM MgCl2, 10mM KCl, 0.5mM DTT, 0.05% NP40, pH 7.9
Nuclear extraction buffer B	5mM HEPES, 1.5mM MgCl2, 0.2mM EDTA, 0.5mM DTT, 26% glycerol, 300mM NaCl, pH 7.9

Protein assay

Micro BCA™ protein assay from Thermoscientific© was used to quantify the protein concentration of all the samples, according to the manufacturer's instructions. The optical densitometry was read with the Synergy H1 hybrid reader (BioTek®) device.

2.3.5. Western-blotting analysis and quantification

The day preceding the electrophoresis, we poured polyacrylamide gels according to the Biorad guidelines and prepared the buffers needed for the electrophoresis and the transfer steps.

The stacking gel consists of a 125mM Tris-HCl pH6.8 solution, supplemented with 5.1% Acrylamide, 0.1% SDS, 0.1% ammonium persulfate (APS), and 0.08% TEMED

(tetramethylethylenediamine). The resolving gel consists of a 375mM Tris-HCl pH8.8 solution, supplemented with 8 to 15% Acrylamide, 0.1% SDS, 0.1% APS and 0.08% TEMED. Before the TEMED was incorporated, both solutions were air-vacuumed to favor a quick and homogenous polymerization of the gel. The resolving gel solution was poured first and covered with H2O saturated butanol (40%) for 3h to let the gel polymerize, before the butanol got discarded and the stacking gel solution poured. Electrophoresis buffer and transfer buffer are composed of 25mM Tris base, 192mM glycine, and the pH was adjusted to 8.3 by glycine addition. 0.1% SDS or 5% methanol was added to the solution to obtain the electrophoresis or the transfer buffers, respectively.

Briefly, 15 to 20µg of the protein lysates were diluted in Laemmli buffer. These proteins were then denatured by heating (5mins, 95°C) and loaded on the gel, to undergo electrophoresis (110V, 1.5h, RT) and separation by their size. Proteins were then transferred to a methanol-activated polyvinylidene difluoride (PVDF) membrane (350mA, 2h, 4°C). Protein transfer was assessed with the Ponceau Red staining of the membrane. The membrane was then rinsed in water and in tris buffer saline (TBS) supplemented with 0.01% of tween detergent (TBST), and the non-specific sites were blocked 1h in TBST supplemented with 3% bovine serum albumin (BSA). Primary antibodies diluted in TBST + 5% BSA were incubated on a rocking platform (ON, 4°C). The next day, membranes were washed 3 times with TBST, blocked 30mins in TBST 3% BSA, incubated with horseradish peroxidase (HRP)-coupled secondary antibodies in TBST 3% BSA (1h, RT). The membranes were finally washed 3 times and the signal was detected using an enhanced chemo-luminescence solution (ECL, purchased from Thermoscientific) with the Vilber fusion fx device. Quantification was done with the evolution caption edge software®, and protein normalization by using the Ponceau staining quantification to correct for loading differences.

2.3.6. Immunocytochemistry and microscopy

Cells were plated on 13 mm diameter laminin-coated glass coverslips. After treatment, cells were washed in ice-cold PBS and fixed in a 4% paraformaldehyde (PFA, Polysciences), 0.1% Triton-X solution. Samples were washed in PBS + 0.1% Tween-20, blocked in PBS + 0.1% Tween-20 + 0.1%, BSA, and incubated overnight at 4°C with primary antibodies. The next day the fixed cells were washed with PBS supplemented with 0.1% Tween-20 and incubated for 1h with secondary antibodies and DAPI. Samples were washed as above and mounted with a mounting medium on microscope slides (Superfrost™, epredia©). Pictures were acquired with Nikon Ti2 microscope.

Primary antibodies table

antibody against	company	ref. n°	dilution	Host specie & clonality
ACC	Cell Signaling	3676	1/1000	rabbit polycl.
ACC-pS79	Cell Signaling	3661	1/1000	rabbit polycl.
Akt	Cell Signaling	9272	1/4000	rabbit polycl.
Akt-pT308 (D25E6)	Cell Signaling	13038	1/1000	rabbit polycl.
AMPKα	Cell Signaling	2532	1/1000	rabbit polycl.
AMPKα-pT172	Cell Signaling	2535	1/1000	rabbit polycl.
Atg1/ULK1	Sigma	A-7481	1/1000	rabbit polycl.
Atg1/ULK1-pS757	Cell Signaling	6888	1/1000	rabbit polycl.
COX IV	Cell Signaling	4844	1/1000	rabbit polycl.
ErbB2	Santa Cruz	sc-284	1/500	rabbit polycl.
ErbB2-pY1248	Santa Cruz	sc-12352-R	1/200	rabbit polycl.
ErbB4	Santa Cruz	sc-283	1/500	rabbit polycl.
ErbB4-pY1284	Abcam	ab61059	1/500	rabbit polycl.
FoxO1	Santa Cruz	sc-11350	1/500	rabbit polycl.
FoxO1-pS319	Santa Cruz	sc-23771-R	1/500	rabbit polycl.
FoxO1-pT24	Santa Cruz	sc-16561-R	1/500	rabbit polycl.
LC3A/B	Abcam	ab58610	1/500	rabbit polycl.
Myosin, skeletal, slow	Sigma	M-8421	1/1000	mouse monocl.
p44/42 MAPK	Cell Signaling	9102	1/4000	rabbit polycl.

p44/42-pT202/Y204 MAPK	Cell Signaling	9101	1/4000	rabbit polycl.
PDK1	Cell Signaling	3062	1/1000	rabbit polycl.
Vinculin (N-19)	Santa Cruz	sc-7649	1/500	mouse monocl.

Secondary antibodies table

Secondary antibody	company	ref. n°	dilution	species reactivity
IgG-HRP conjugated	Jackson	115-035-003	1/10 000	all mouse IgG
IgG-HRP conjugated	Jackson	111-035-003	1/10 000	all rabbit IgG
Fab-Alexa 488 conjugated	Mol. Probes	A11070	1/800	all rabbit IgG
IgG-Alexa 633	Invitrogen	A21050	1/800	all mouse IgG

2.3.7. MTT ASSAY

To measure the mitochondrial dehydrogenase activity, NRVM plated in 24 wells plate were treated, and then incubated with 4,5-dimethylthiazol-2-yl)-2,5-diphenyl tetrazolium bromide (MTT) 2.5 h before the experiment ended. At the end of the experiment, the medium was discarded, acidified isopropanol was added, and gyratory shaking was performed for 10 mins to solubilize the metabolized MTT formazan crystals. The solution was transferred to ELISA plates and optical densitometry at 570 and 690nm was read with the Synergy H1 hybrid reader (BioTek®) device. MTT activity was determined according to the manufacturer's instructions (sigma CDG1 kit). To correct for cell content, a protein assay was performed in parallel treated plates, and final MTT values were corrected accordingly.

2.4. STATISTICAL ANALYSIS

Data are presented as mean ± SD. Differences in means were evaluated either with one-way ANOVA, followed by Dunnett's multiple comparison test when $n \geq 6$ or by Krustal-Wallis test when $n < 6$. All statistics was performed with GraphPad Prism 9.3.1. P-values of <0.05 were considered statistically significant and P-values between 0.05 and 0.2 were considered to show a trend.

3. RESULTS

3.1. DOXORUBICIN INDUCES CHRONIC SEX-DEPENDENT SYSTEMIC AND CARDIAC TOXICITY IN MICE, EFFECTS OF A NEW NRG-1 TREATMENT REGIMEN

3.1.1. EFFECTS OF OUR DOX-TREATMENT PROTOCOL ON BODY AND ORGAN WEIGHTS AT 3 WEEKS

This study aimed to reproduce and characterize a murine doxorubicin-therapy protocol, relevant to what is done in clinics, developed by Milano and colleagues. In the Milano et al. study, only female mice were studied [116]. In the present work, we intended to compare systemic and cardiac effects of doxorubicin-therapy in male and female mice. Secondly, we intended to characterize the potential preventive effects of a new NRG-1 regimen in this model. To this end, 10 to 12 weeks old male and female mice were assigned to 3 groups (vehicle-control (CTL), vehicle-doxorubicin (dox), and NRG-1-doxorubicin (NRG/dox), while aiming to obtain an identical average body weight for the groups at start of the experiment. Figure 4A shows the dox injection and NRG-1 treatment protocol over time. To characterize the systemic effects of the therapy in our mice, body weight was measured daily, while heart, gastrocnemius, lung weights and lung hydration indexes (wet/dry ratios) were measured at sacrifice.

Figure 4B shows that dox-treated males' body weight was reduced by 16% in comparison to the controls at 3 weeks ($p<0.0001$). Also, the muscle weight, here represented by the gastrocnemius weight, and the cardiac ventricular weight (CVW) were decreased by 16% and 27%, respectively ($p<0.01$; $p<0.0001$) in the dox-treated mice vs the CTL mice. The cardiac ventricular weight to total body weight ratio was not different between the dox-treated and the CTL group (Fig. 4B). This suggests that male mice underwent strong systemic toxicity, accompanied by a cachectic phenotype as well as cardiac toxicity at 3 weeks. Interestingly, the lung hydration index (ratio of the fresh vs dehydrated weight of the same piece of lung tissue) was increased in the dox group, indicating the development of lung edema and suggesting cardiac dysfunction. These data support that in males, dox treatment induced cardiac toxicity as the mice showed decreased ventricular weight and evidence for cardiac edema development. However, the cardiac ventricular weight/body weight ratio was not different from the CTL group, indicating that the Milano et al. protocol that we used is not inducing specifically cardiac toxicity, but overall systemic toxicity, including cardiac suffering in male mice (Fig. 4B).

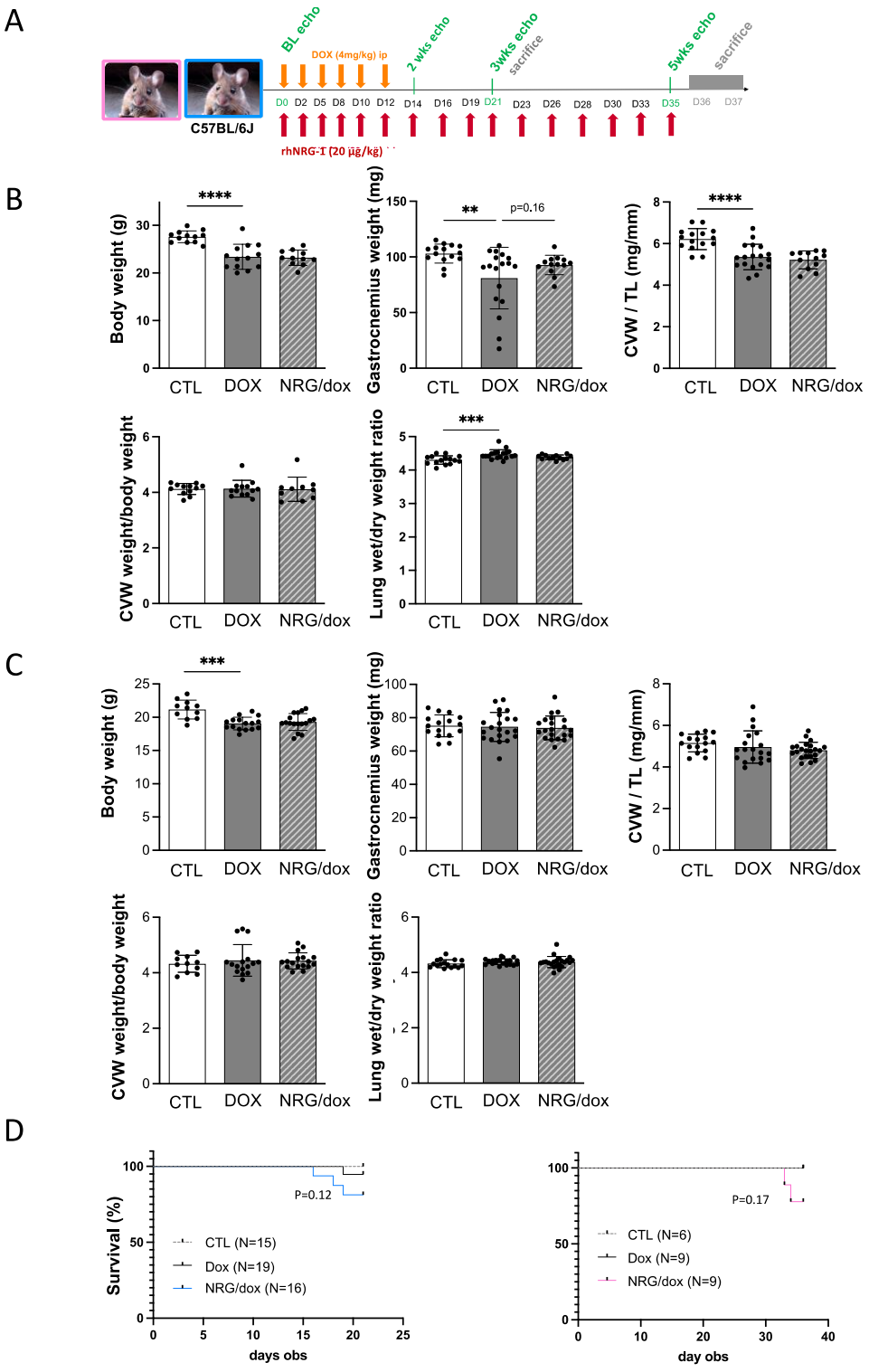

Figure 4. Effects of our dox-treatment protocol on body and organ weights at 3 weeks. (A) 10 to 12 weeks old male and female C57BL/6J mice were injected intraperitoneally every other day with doxorubicin (dox, 4 mg/kg) or the vehicle NaCl (CTL) for 12 days, yielding a cumulative dose of 24 mg/kg. 30 min before each dox injection, mice were injected saline (CTL, dox) or NRG-1 (NRG/dox, 20 µg/kg). After completion of the dox-treatments, NRG-1 injections continued 3 times/week until sacrifice. At sacrifice, we measured body weight, gastrocnemius weight, cardiac ventricular weight (CVW), tibia length and the lung edema index in males (B) and females (C). Kaplan Meier analysis for both sexes is shown in (D). Data are expressed as mean ± SD; females n=17 for CTL, n=19 for dox, n=22 for NRG/dox; males n=15 for ctl, n=19 for dox, n=16 for nrg/dox. One-way ANOVA with Dunnett's correction was performed versus the dox group. *p<0.05, **p<0.01, ***p<0.001, ****p<0.0001.

In females, dox decreased body weight by 9% in comparison to the CTL group, while no differences in gastrocnemius mass, cardiac ventricular mass, or lung wet/dry ratio were measured at sacrifice. These data suggest that females underwent dox-induced systemic toxicity but did not develop cardiac toxicity at 3 weeks (Fig. 4C).

For both males and females, no preventive effects of our NRG-1 regimen were measured on dox-induced systemic and cardiac toxicity.

Notably, the male mice suffered from mortality from week 2 onwards in the absence of NRG-treatment and even more so in the NRG/dox-treated mice, while female mice started to die later, after week 4, but only in NRG-1 pre-treated mice (Fig. 4D).

3.1.2. Dox induces changes in cardiac architecture and function in males that are partially prevented by NRG-1

Another aim of this study was to characterize over time the effects of the dox-therapy and the new NRG-1 regimen on cardiac function and architecture by echocardiography. At baseline, no differences were observed for any of the parameters between the different groups for both sexes.

In males, the time point at which we were able to detect dox-induced effects on cardiac function and architecture was 2 weeks after the treatment started, exactly 2 days after the dox-therapy was completed. Figure 5A shows that the dox-treatment increased the ejection fraction (EF) and left ventricular posterior wall thickness during systole (LVPWs, $p<0.01$; $p<0.05$). Interestingly, NRG-1 reduced the effect on the EF ($p=0.14$) and significantly inhibited the LVPWs change ($p<0.05$). Going into the same direction, dox induced a decrease in left ventricular internal diameter during diastole and systole (LVIDd $p<0.01$, LVIDs $p<0.001$). However, NRG-1 did not prevent these decreases in internal diameter (Fig. 5A). Also, while dox-treated animals did not show different LVAW during diastole (LVAWd) compared to the CTL mice, NRG/dox animals showed thinner LVAWd than the saline-treated dox animals ($p<0.05$), yielding values that were not different from the CTL group anymore. These data suggest that dox-therapy induced a compensatory response at 2 weeks in males and that this was prevented by the NRG-1 regimen.

Interestingly, at 3 weeks, these effects were not detected anymore (Table I). Briefly, the dox-treated males showed decreased LVAW during diastole and systole in comparison to the CTL group ($p<0.05$; $p=0.08$). This was associated with decreased LVIDd and LVIDs ($p<0.01$; $p=0.08$) as well as a decrease in ventricular weight. Together with unchanged ejection fractions

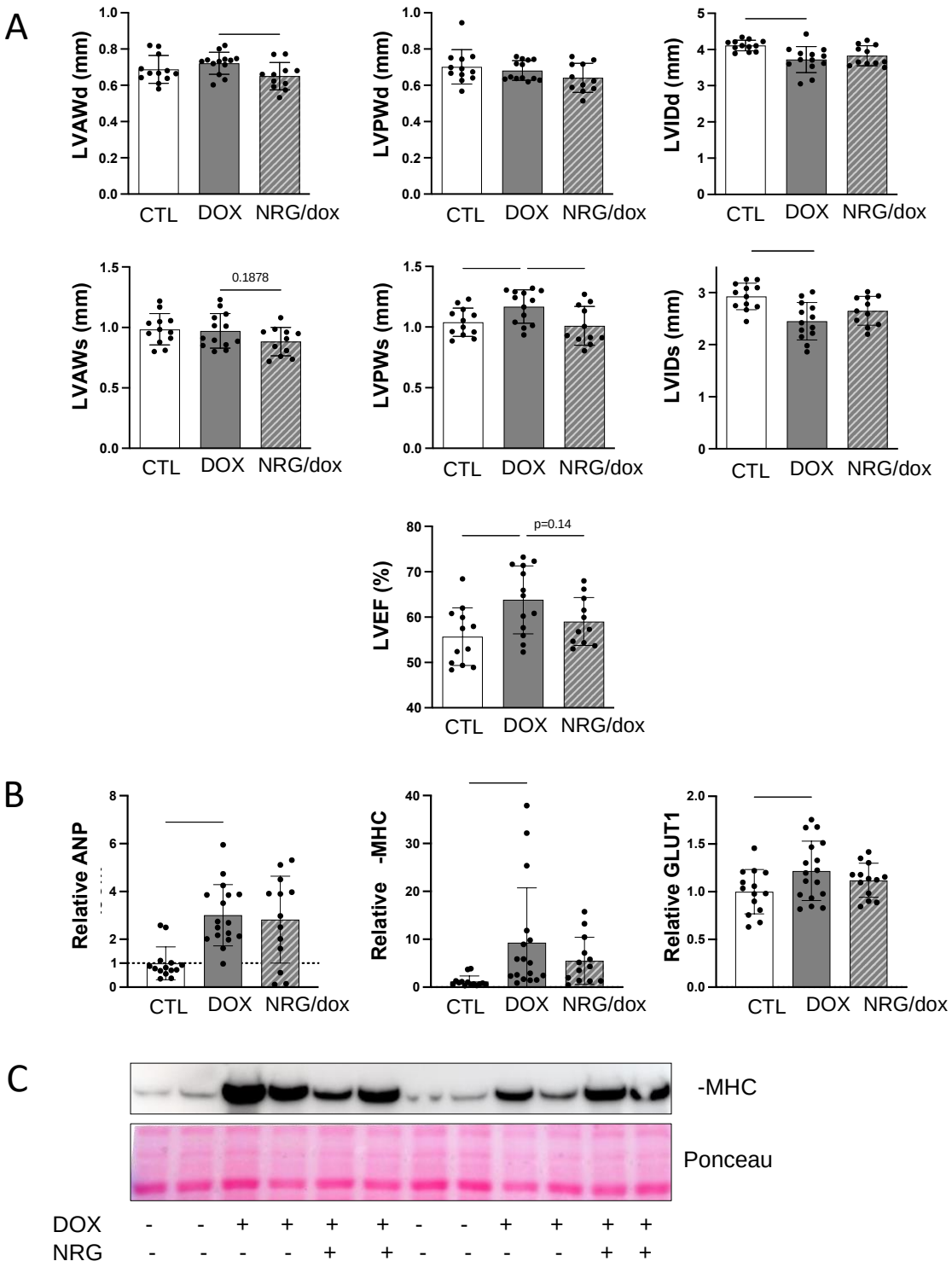

Figure 5. Dox induces compensatory changes in cardiac architecture, function and molecular profile that are partially prevented by NRG-1 in males. Echography was performed at baseline (data not shown), 2 weeks (A) and 3 weeks (see table I). Mice were sacrificed at day 22 – 23 for molecular analysis 1 h after an injection with vehicle (CTL and dox groups) or NRG-1 (NRG/dox group) (B-C). (A) echocardiography data of the left ventricular anterior wall and the left ventricle posterior wall thicknesses during diastole and systole (LVAWd, LVAWs, LVPWd, LVPWs), left ventricular internal diameter at the end of diastole and systole (LVIDd, LVIDs) and left ventricle ejection fractions (LVEF). (B) gene expression of ANP, β-MHC and GLUT1 was measured by real-time PCR, and β-MHC protein was measured by immunoblotting of total cardiac protein lysates(C). Data are expressed as mean ± SD; n=15 for CTL, n=19 for dox, n=16 for NRG/dox. One-way ANOVA with Dunnett's correction was performed versus dox. *p<0.05, **p<0.01, ***p<0.001.

and LVPWs, these data show that at 3 weeks the dox-treated male mice are not in a cardiac compensatory phase anymore.

Molecular analyses of the hearts were performed at 3 weeks when the male mice got sacrificed. Figure 5B and C show that the dox-treated animals have increased cardiac mRNA levels of ANP and β-MHC, two cardiac stress markers, in comparison to the CTL mice. GLUT-1 mRNA was also increased by dox (Fig. 5B). At the protein level, Western blotting analysis also showed increased β-MHC in the dox animals compared to controls. However, NRG-1 did not prevent any of these dox-induced molecular changes. Yet, cardiac ANP, β-MHC and GLUT-1 are known to get induced in the context of heart remodeling and compensatory responses. Therefore, the dox-related compensatory response revealed by echocardiography at 2 weeks can still be measured at a molecular level one week later. While at 2 weeks, NRG partially reverted the effects on cardiac architecture and function, at 3 weeks NRG-1 did not reverse the dox-induced molecular markers of compensation anymore. The apparent reduction of β-MHC mRNA in the NRG/dox group did not reach significance.

The dox-treated animals have lighter and smaller hearts than the control-treated animals. The body weights of the control mice did not change from baseline to the sacrifice time point, showing that our mice were not growing anymore and reached their adult and definitive heart weight. This suggests that the dox-treated males developed atrophic hearts in response to the dox-induced toxicity, and not because of a stress-induced stop of growing as it is the case in the juvenile doxorubicin-treated animal models [117, 118].

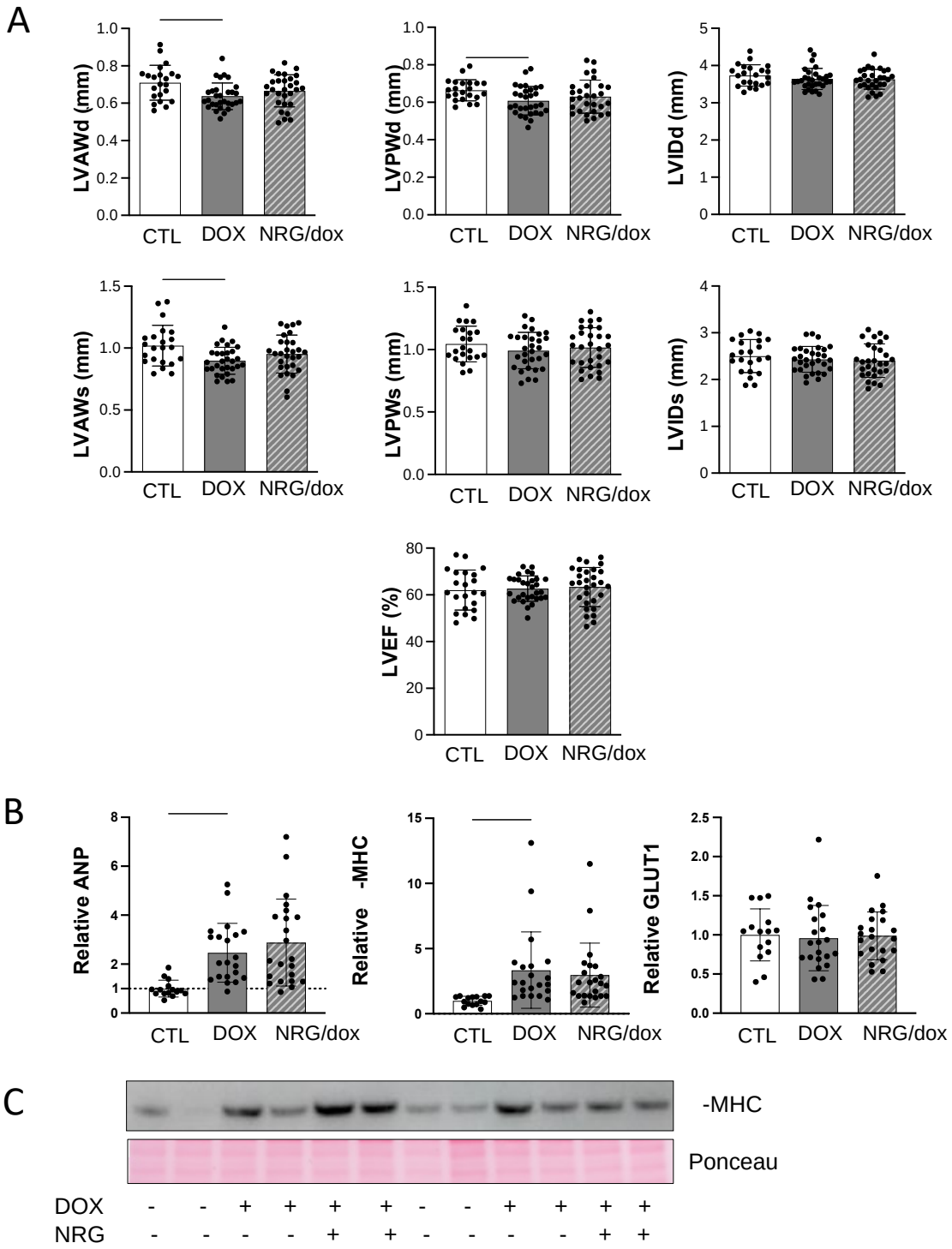

Figure 6. Dox induces slight changes in cardiac architecture and stress response in females. Transthoracic echography was performed in females at baseline, 2 weeks (data not shown), 3 weeks (A) and 5 weeks (see table II). Mice were sacrificed at day 22 – 23 for molecular analysis 1 h after an injection with vehicle (CTL and dox groups) or nrg-1 (NRG/dox group) (B-C). (A) echocardiography data of the left ventricle anterior wall and the left ventricle posterior wall thicknesses during diastole and systole (LVAWd, LVAWs, LVPWd, LVPWs), left ventricular internal diameter at the end of diastole and systole (LVIDd, LVIDs), and left ventricle ejection fractions (LVEF). (b) gene expression of ANP, β-MHC and GLUT1 was measured by real-time PCR, and β-MHC protein was measured by immunoblotting of total cardiac protein lysates. Data are expressed as mean ± SD; n=17 for CTL, n=19 for dox, n=22 for NRG/dox. One-way ANOVA with Dunnett's correction was performed versus dox. *P<0.05, **P<0.01, ***P<0.001.

3.1.3. THE CARDIAC RESPONSE TO DOX IN FEMALES DIFFERS FROM THAT IN MALES

In females, only at 3 weeks some effects of dox on cardiac architecture were detectable by echocardiography. Figure 6A shows that at 3 weeks, dox induced significant decreases of the LVAW and LVPW thicknesses during diastole ($p<0.01$; $p<0.05$) in comparison to the CTL-treated animals. The LVAW was also decreased during the contractile phase ($p<0.01$), while LVPW was not. The wall thickness changes were neither associated with dox-induced changes in cardiac function nor with LVID dimensions in females (Fig. 6A). As the dox-induced effects on cardiac architecture were mild, no effects of our NRG-1 regimen were revealed in the dox-treated females. At the molecular level, cardiac mRNA expression of ANP and β-MHC, but not that of GLUT-1, was increased in the dox group in comparison to the CTL group. As in males, NRG-1 did not prevent the dox-induced molecular stress marker expression in females (Fig. 6B and C).

The dox-induced effects revealed by echocardiography in females at 3 weeks were not observed anymore after 5 weeks, while differences in body weight could still be measured between the dox and the CTL-treated females (Table II). This suggests that the dox-treated females recovered from the dox-induced changes in cardiac dimensions, but not from dox-induced long-lasting systemic toxicity at 5 weeks.

Thus, the molecular analyses that we performed in males and females are in line with the echocardiographic assessments. In males, the dox-induced compensatory increase in EF and LVPWs was associated with ANP, β-MHC and GLUT-1 up-regulation at the mRNA level. On the other hand, in females, dox did not increase wall thickness and EF. This was accompanied by a more modest increase of β-MHC mRNA (3.3-fold) than in males (9.3-fold) and no increase of GLUT-1 mRNA levels.

TABLE I. ECHOCARDIOGRAPHIC AND PHYSIOLOGIC PARAMETERS OF MALES AT 3 WEEKS

	CTL (N=15)	**DOX (N=18)**	**NRG/DOX (N=13)**
Body weight (g)	27.9±1.39****	25.1±2.05	24.8±1.66
Ventricular weight/ tibia length (g/mm)	6.22±0.51	5.36±0.61	5.22±0.44
Heart rate (beats/min)	465±52	473±63	420±48*
LV anterior wall thickness (mm)			
diastole	0.78±0.08*	0.70±0.07	0.69±0.07
systole	1.07±0.14 (p=0.08)	0.97±0.12	0.96±0.16
LV posterior wall thickness (mm)			
diastole	0.69±0.06	0.66±0.08	0.64±0.04
systole	1.04±0.09	1.06±0.08	1.04±0.03
LV internal diameter (mm)			
diastole	3.92±0.20**	3.69±0.20	3.73±0.26
systole	2.71±0.24 (p=0.08)	2.5±0.29	2.49±0.10
Ejection fraction (%)	59.0±4.88	61.3±7.15	62.6±8.22

Three weeks after the dox-therapy was started, ultrasound analysis was performed. One to two days later, body weight was measured before sacrifice, and post mortem ventricular cardiac weight was measured and standardized to tibia length. Data are expressed as mean ± SD; n=15 for CTL, n=19 for dox, n=16 for NRG/dox. One-way ANOVA with Dunnett's correction was performed versus dox. *p<0.05, **p<0.01, ***p<0.001, ****p<0.0001.

TABLE II. ECHOCARDIOGRAPHIC AND PHYSIOLOGIC PARAMETERS OF FEMALES AT 5 WEEKS

	CTL (N=6)	**DOX (N=9)**	**NRG/DOX (N=7)**
Body weight (g)	21.23±1.2*	19.30±0.86	18.96±0.86
Ventricular weight (g)	4.85±1.32	4.96±0.78	4.80±0.39
Heart rate (beats/min)	424±51	425±39	412±58
LV anterior wall thickness (mm)			
diastole	0.62±0.04	0.59±0.07	0.58±0.04
systole	0.91±0.10	0.83±0.10	0.85±0.09
LV posterior wall thickness (mm)			
diastole	0.64±0.04	0.59±0.08	0.61±0.06
systole	0.99±0.07	0.93±0.08	1.01±0.11 (p=0.15)
LV internal diameter (mm)			
diastole	3.95±0.39*	3.62±0.17	3.74±0.20
systole	2.70±0.33	2.49±0.18	2.48±0.30
Ejection fraction (%)	60.33±6.46	60.07±3.48	63.25±6.81

Five weeks after the dox-therapy was started, ultrasound analysis was performed. One to two days later, body weight was measured before sacrifice, and post mortem ventricular cardiac weight was measured and standardized to tibia length. Data are expressed as mean ± SD; n=6 for CTL, n=9 for dox, n=7 for NRG/dox. One-way ANOVA with Dunnett's correction was performed versus dox. *$p<0.05$.

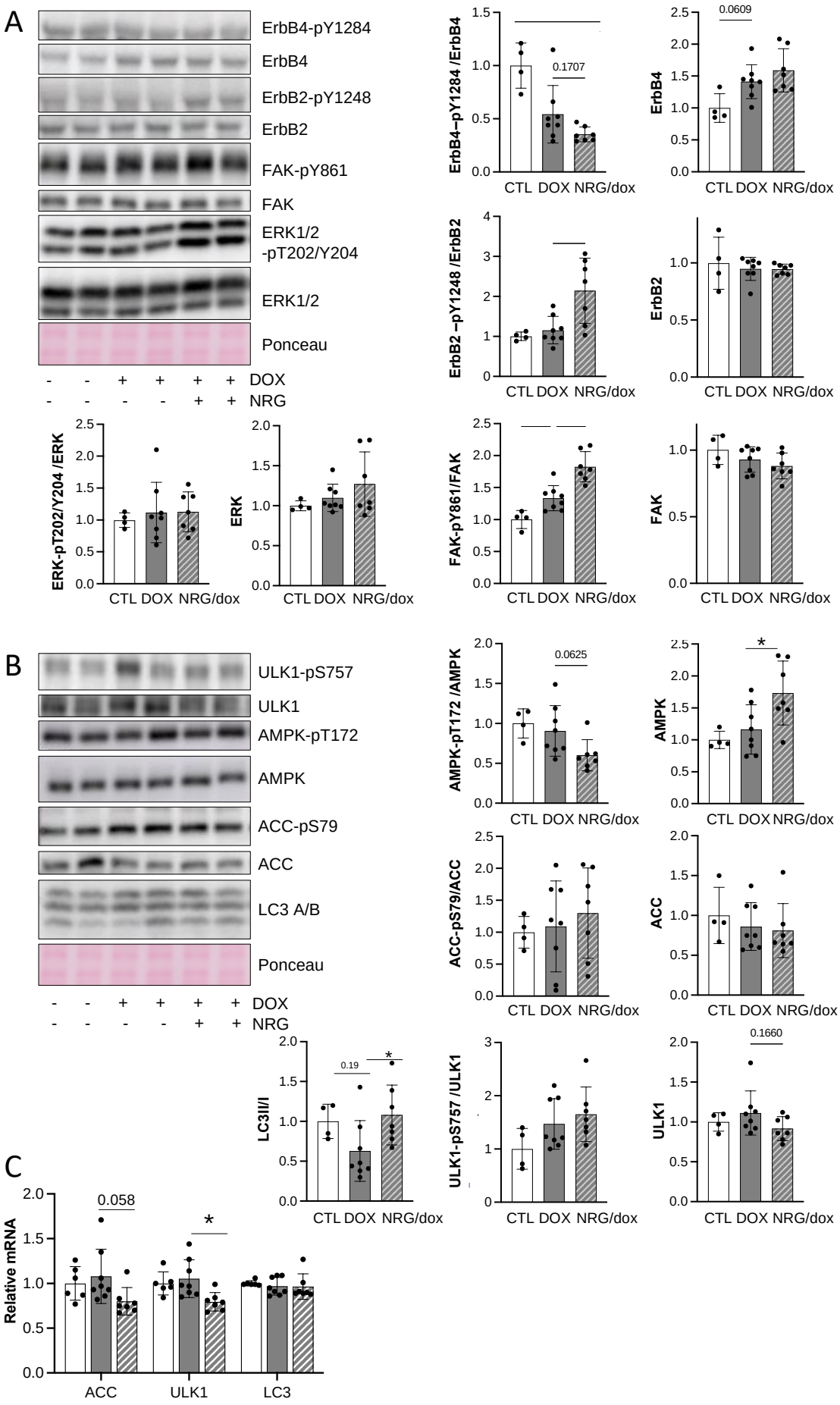
A
ErbB4-pY1284
ErbB4
ErbB2-pY1248
ErbB2
FAK-pY861
FAK
ERK1/2 -pT202/Y204
ERK1/2
Ponceau
- - + + + + DOX
- - - - + + NRG
ERK-pT202/Y204 /ERK
ERK
CTL DOX NRG/dox
ErbB4–pY1284 /ErbB4
0.1707
ErbB4
0.0609
ErbB2 –pY1248 /ErbB2
ErbB2
FAK-pY861/FAK
FAK
B
ULK1-pS757
ULK1
AMPK-pT172
AMPK
ACC-pS79
ACC
LC3 A/B
Ponceau
- - + + + + DOX
- - - - + + NRG
LC3II/I
0.19
*
AMPK-pT172 /AMPK
0.0625
ACC-pS79/ACC
ULK1-pS757 /ULK1
0.1660
C
Relative mRNA
0.058
*
ACC
ULK1
LC3

3.1.4. NRG-1 MODULATES AUTOPHAGY IN DOX-TREATED FEMALES AT 5 WEEKS

As no differences were observed anymore by echocardiography between the dox-treated group and the control group at 5 weeks in females, we wanted to determine if some protective pathways were activated at that time point in the dox-treated animals and whether the NRG-1 treatment had an effect on it. Specifically, the autophagic pathway was analyzed as it is essential for cardiac homeostasis in general.

First of all, we measured the ErbB system expression and activation in our female mice at 5 weeks to characterize the long-term dox effects on it. Secondly, to check whether it was of interest to inject mice in the long term with repeated NRG-1 injections every other day, mice were injected either with vehicle in the CTL- and dox-treated groups or with NRG-1 in the NRG/dox group at 1 h before sacrifice. The hearts were used to characterize which metabolic pathways the NRG-1 regimen could trigger in the females in the long term.

Western blot analysis showed that dox increased ErbB4 total protein levels but not the ErbB2 protein levels. The ratio of the ErbB4-pY1284/ErbB4 seemed decreased by the dox-therapy ($p=0.17$ due to high variability), while no changes in phosphorylated ErbB2 were measured at 5 weeks. These results suggest that the female mice overexpress ErbB4 as a protective mechanism to the dox-therapy, while not increasing its phosphorylated levels at 5 weeks (Fig. 7A).

Although NRG-1 stimulation did not lead to higher phosphorylated ErbB4 levels after 1 h, it increased the direct downstream FAK-pY861/FAK as well as its co-receptor ErbB2-pT1248/ErbB2 in comparison to the vehicle-treated dox mice ($p<0.001$ and $p<0.01$, respectively; Fig. 7A). Further downstream of ErbB4, ERK1/2-pT202/Y204 was not induced by the NRG-1 stimulation in comparison to the dox-treated mice stimulated with vehicle (Fig. 7A). The increased FAK phosphorylation shows that the ErbB axis can still be activated in these animals at week 5, that is to say, 3 weeks after they completed their dox-therapy.

Figure 7. NRG-1 prevents modulation of autophagy by dox in females. At 5 weeks, CTL and dox-treated mice were injected with PBS, while the NRG/dox animals were injected with NRG-1 (20 µg/kg). All mice were sacrificed 1 h later for molecular analysis. (A, B) representative immunoblots of cardiac protein extracts after incubation with antibodies specific for the proteins indicated and quantification of the bands, normalized to Ponceau. (a) shows receptor pathway activation, B shows the analysis of autophagy and metabolic regulators. (C) analysis of gene expression by quantitative real-time PCR. Data are expressed as mean ± SD; n=6 for CTL, n=9 for dox, n=7 for NRG/dox. One-way ANOVA with Dunnett's correction was performed versus dox. *$p<0.05$, **$p<0.01$, ***$p<0.001$.

We next measured the expression and activation of the adenosine monophosphate kinase α (AMPK), ACC and ULK1, as they are known to be critical in the regulation of energy homeostasis and autophagy. Figure 7B shows that dox changes neither AMPK nor ACC protein expression and phosphorylation, while the NRG-1 co-treated animals showed increased total AMPK and decreased AMPK-pT172/AMPK in comparison to the vehicle-treated dox animals ($p<0.02$; $p=0.06$; Fig. 7B). NRG-1 did not change total and phosphorylated ACC protein levels, although it induced a decrease of its mRNA expression vs the vehicle/dox-treated animals ($p<0.058$, Fig. 7C).

Dox neither changed the ULK total protein amounts nor the ULK1-pS757/ULK1 ratios ($p=0.22$) in comparison to the corresponding controls. Interestingly, the NRG-1/dox co-treated mice showed a trend toward decreased ULK1 total protein levels ($p=0.16$). ULK1 was significantly decreased at the mRNA level ($p<0.05$, Fig. 7C). However, the NRG-1-treated mice had unchanged ULK1-pS757/ULK1 ratios in comparison to the mice treated with dox alone (Fig. 7B).

Finally, we also assessed total LC3 and LC3 lipidation, related to autophagy activation, by Western blotting and LC3 mRNA levels by qPCR. Figure 7 shows that no differences were detected between the groups at the protein and mRNA levels. However, the ratio of the lipidated (vesicular)/non-lipidated (cytosolic) LC3 tended to be reduced in the dox-treated group in comparison to the CTL group ($p=0.19$). NRG-1 significantly prevented this ($p<0.05$) (Fig. 7C).

In conclusion, our observation that dox-treated females have a compensatory increase in ErbB4 expression and ErbB2/FAK phosphorylation in comparison to control mice at 5 weeks suggests that dox-mice are still triggering this cardioprotective pathway as a long-term response to the dox treatment. While the dox-treated mice do not show any clear regulation of the AMPK or the ULK1 signaling pathways, the LC3II/I tended to be decreased in comparison to the CTL-treated group. Thus, although further work is required to prove significance, our data suggest that dox may induce autophagic disturbances in the long-term. Interestingly, our observation that the NRG-1 regimen significantly increases LC3II/I in dox-treated mice suggests that it enhances autophagy. This is accompanied by increased AMPK protein levels, and decreased ULK1 and ACC expression at the mRNA but not at the protein level.

3.2. By which mechanisms does NRG-1 prevent dox-induced cardiac effects?

3.2.1. NRG-1 modulates autophagy in female hearts at 24 h after dox injection

The second main aim of this study was to determine by which mechanisms NRG-1 could exert a cardioprotective role in our mouse model. Protein analysis of cardiac tissues from the females at the 5 weeks timepoint shown in 3.1.4 highlighted a long-term inhibitory effect of dox on autophagy and a preventive role of our NRG-1 regimen on it. This led us to wonder whether the preventive effects of NRG-1 observed on dox-induced disturbances of the autophagic pathway were a result of a chronic adaptive cardiac event or whether the autophagic pathway modulation was already triggered upon the earliest dox and NRG-1 injections given in our model.

To investigate if dox disturbs the autophagic pathway in female mice and if NRG-1 could prevent it on the early stages of the treatment, we injected the females at day (d) 0 with the first dose of our protocol (CTL, dox, NRG/dox). 24 h later we injected the mice with the vehicle for the two first groups or NRG-1 in the NRG/dox group in order to characterize in which metabolic state the mice are and to test the effects of NRG-1 at this timepoint. Proteins were extracted at d 1 to make the experiment comparable with the cell culture experiments described hereafter under 3.2.3-5.

First of all, we assessed the ErbB system expression and activation in these females. Figure 8A shows that at 24 h, dox did not change the total levels of the ErbB2 and ErbB4 receptors, while it tended to increase ErbB2-pY1248 ($p=0.17$). However, dox did not affect ERK1/2 or FAK phosphorylation vs CTL. Moreover, NRG/dox-treated animals showed significant increases in ERK1/2-pT202/Y204 vs dox-treated animals. Taken together, these data show that some dox-induced cardiac ErbB2 phosphorylation can be measured 24 h after the first injection set of our protocol, but that this is not associated with phosphorylation of the downstream effectors FAK and ERK1/2. Moreover, upon dox-treatment NRG-1 stimulation might either not directly induce the downstream ERK1/2 activation via ErbB2 or that the stimulation led to the phosphorylation of the ErbB2 but somehow couldn't be measured in our experimental settings.

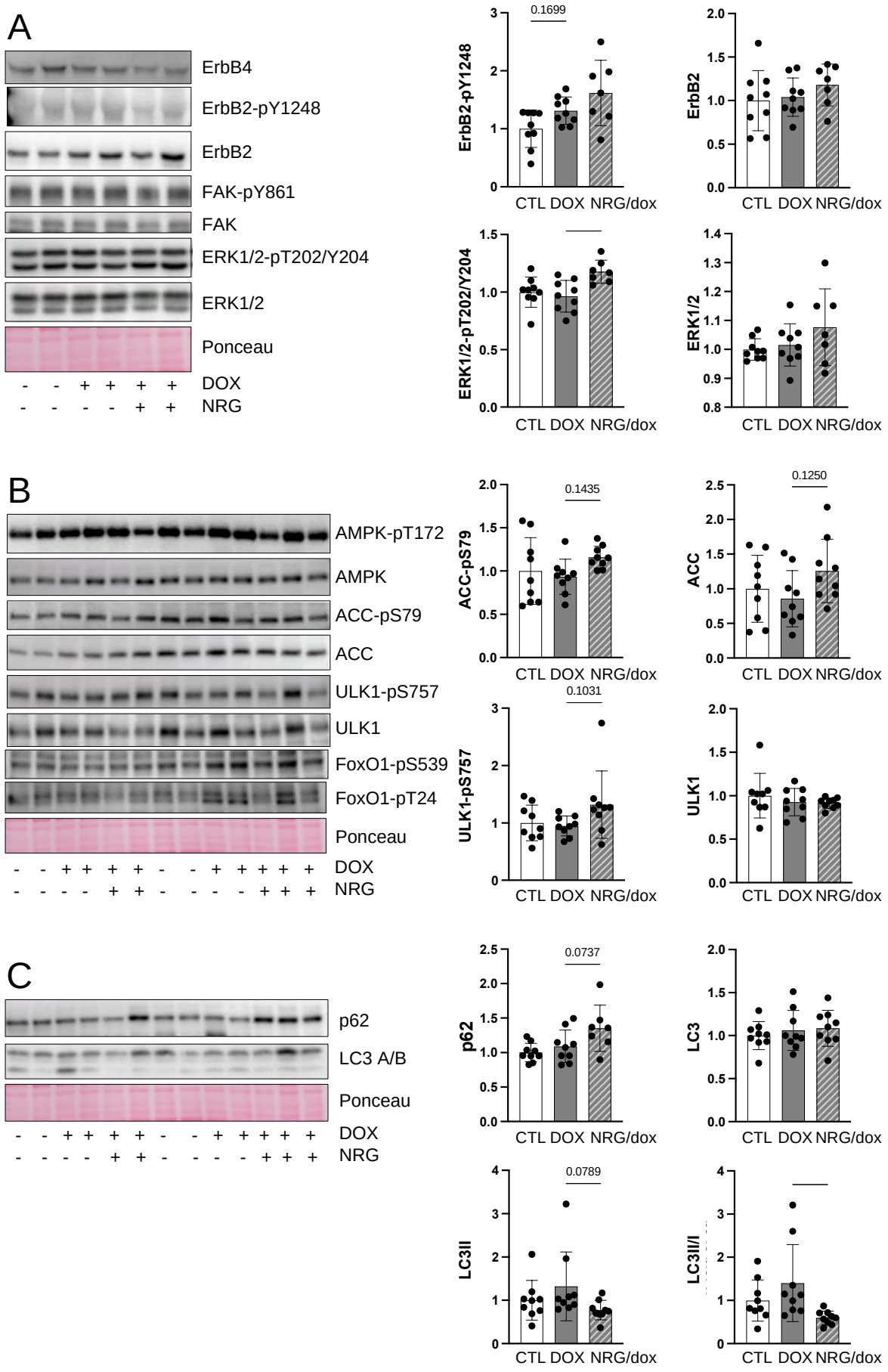
A
ErbB4
ErbB2-pY1248
ErbB2
FAK-pY861
FAK
ERK1/2-pT202/Y204
ERK1/2
Ponceau
- - + + + + DOX
- - - - + + NRG
ErbB2-pY1248
0.1699
ErbB2
CTL DOX NRG/dox
ERK1/2-pT202/Y204
ERK1/2
B
AMPK-pT172
AMPK
ACC-pS79
ACC
ULK1-pS757
ULK1
FoxO1-pS539
FoxO1-pT24
Ponceau
- - + + + + - - + + + + + DOX
- - - - + + - - - + + + NRG
ACC-pS79
0.1435
ACC
0.1250
ULK1-pS757
0.1031
ULK1
C
p62
LC3 A/B
Ponceau
- - + + + + - - + + + + + DOX
- - - - + + - - - + + + NRG
p62
0.0737
LC3
LC3II
0.0789
LC3II/I

Next, we investigated whether AMPK, ACC, ULK and FoxO1 were affected in our mouse model. Figure 8B shows that dox did not change AMPK or its downstream effector ACC compared to CTL. Similarly, dox did not change total and phosphorylated levels of ULK1 or FoxO1 in comparison to the CTL group. While no effects of NRG were measured for AMPK, the NRG/dox-treated animals showed a trend towards increased ACC total protein in comparison to the dox-treated animals ($p=0.125$). The NRG treatment of dox-injected mice also triggered an increase of ULK1-pS*757* in comparison to the saline/dox group ($p=0.1$). On the other hand, NRG-1 did not modulate phosphorylated FoxO1 levels (Fig. 8B).

Given the small effect of NRG-1 on phosphorylated ULK1, a regulator of autophagy, we also measured the expression of LC3 and p62, two hallmark proteins of the autophagic process (Fig. 8C). While dox did not change LC3 total protein levels, LC3II/I ratios or p62 protein levels vs CTL, the NRG/dox-treated group showed a significant decrease of the LC3II/I ratios and a tendency for increased p62 protein levels (Fig. 8C). These data show that NRG-1 decreases the amount of autophagosomes in the female hearts and p62 increased levels suggest increased amounts of lysosomes. Further analyses with autophagic flux inhibitors should be used to determine whether the autophagic flux was blocked or increased by the NRG-1.

To summarize, at 24 h dox did not change AMPK, ACC, ULK1 and LC3II/I vs CTL. Our data also show that NRG-1 reduces autophagosomes and leads to lysosome accumulation in the hearts of dox-treated females. Consistently, the effects of NRG-1 were associated with slightly increased ULK1-pS*757*, which is known to inhibit the autophagy initiation step [26].

Figure 8. NRG-1 increases ULK1-pS*757* and reduces LC3II/I ratios in females at 24 h. Female mice were injected with vehicle or NRG-1 (20 µg/kg) 30 min before receiving control- or dox-treatment (4 mg/kg). 24 h later, the mice were injected intraperitoneally with vehicle (CTL, dox) or NRG-1 (NRG/dox) and sacrificed 1 h later. (A-C) cardiac lysates were analyzed by immunoblotting using antibodies against phosphorylated and total proteins as indicated. (A) shows receptor pathway activation. (B) shows the analysis of metabolic and autophagy regulators. (C) shows two key markers of autophagy. Protein expression was standardized to the corresponding Ponceau-stained bands. Data are expressed as mean ± SD; n=6 for CTL, n=9 for dox, n=7 for NRG/dox. One-way ANOVA with Dunnett's correction was performed versus dox. *$p<0.05$, **$p<0.01$.

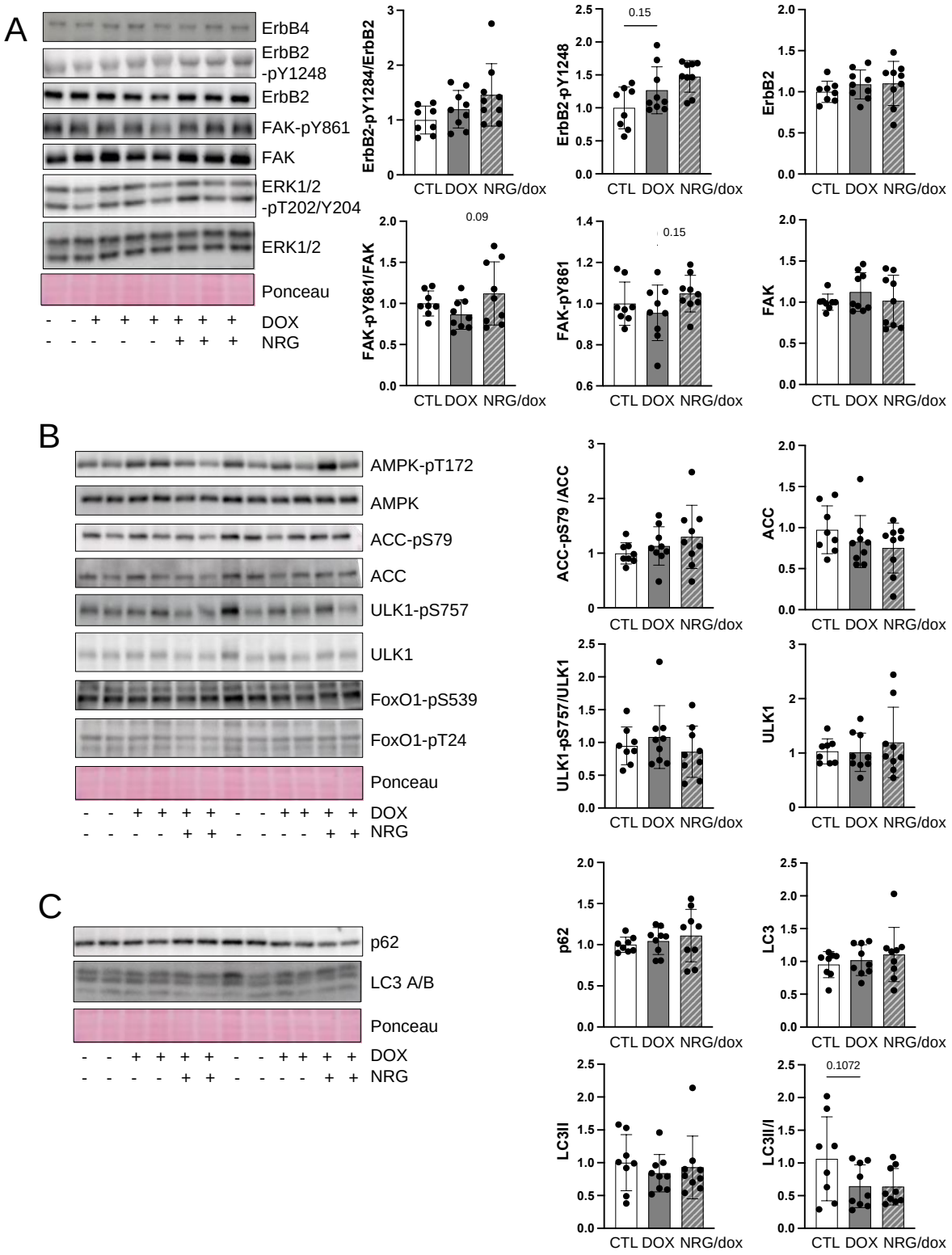

Figure 9. Dox decreases LC3II/I at 24 h in males, NRG-1 does not prevent this. Male mice were injected with vehicle or NRG-1 (20 µg/kg) 30 min before receiving control or dox-treatment (4 mg/kg). 24 h later, mice were injected intraperitoneally with vehicle (CTL, dox) or NRG-1 (NRG/dox) and sacrificed 1 h later. (A-C) cardiac lysates were analyzed by immunoblotting using antibodies against phosphorylated and total proteins as indicated. (A) shows receptor pathway activation. (B) shows the analysis of metabolic and autophagy regulators. (C) shows two key markers of autophagy. Protein expression was standardized to the corresponding Ponceau-stained bands. Data are expressed as mean ± SD; n=6 for CTL, n=9 for dox, n=7 for NRG/dox. One-way ANOVA with Dunnett's correction was performed versus dox. *p<0.05, **p<0.01.

3.2.2. DOX DECREASES LC3II/I IN MALES AT 24 H AND NRG-1 DOES NOT CHANGE THIS

As our data presented in chapter 3.2.1 show that NRG-1 has effects on Erk1/2 and autophagy at 24 h, after the first dox injection in females, we wanted to study whether these pathways are also modulated in males. Male mice underwent the same experimental protocol as the females in chapter 3.2.1. Briefly, at d 0 male mice were given the first injection (CTL, dox, NRG/dox) and 24 h later the CTL and the dox-treated group were injected with saline, while the NRG/dox-treated group was re-stimulated with NRG-1. Animals were sacrificed 1 h after the injection.

Firstly, Figure 9A shows that no differences in ErbB4 or ErbB2 total proteins were measured between the different groups at 24 h. While no effects on ErbB2-pY1248 were observed in NRG/dox treated mice in comparison to the dox treated mice, the FAK-pY861/FAK tended to be increased ($p=0.09$). Interestingly, dox by itself tended to increase phosphorylated levels of ErbB2 ($p=0.15$), but not those of FAK and ERK in comparison to CTL in males. These data show that as in females, dox-treated males show tendency for increased ErbB2 phosphorylated levels but not its downstream effectors vs CTL, while NRG/dox treated animals only have increased downstream FAK effector phosphorylation in comparison to the dox-treated animals.

As in the case of females, this set of data suggests that in males, at 24 h, the NRG-1 stimulation either did not induce the cardiac ErbB2 phosphorylation, and the increased FAK-pY861/FAK were not triggered by the cardiac ErbB2 activation, or our experimental protocol was not optimized (notably on the stimulation timing) to detect NRG-1 induced cardiac ErbB2 phosphorylation.

Figure 9B shows that neither the AMPK–ACC axis nor the ULK1-pS757 phosphorylated levels were changed in the dox-treated males, similar to what we observed in females. Surprisingly, NRG-treated male mice did not show any regulation of the total and phosphorylated levels of the proteins reported above to be regulated by NRG-1 in female mice. Moreover, no modulation of the total and phosphorylated FoxO neither by the dox nor by NRG/dox treatment were detected.

Finally, analysis of the LC3 and p62 proteins showed that dox tended to decrease the LC3II/I ratio ($p=0.11$) but not of the total LC3 nor p62 proteins in comparison to the CTL-treated males at 24 h, and the NRG-1 regimen did not prevent it (Fig. 9C).

All of these data show that in males dox did not trigger the AMPK-ACC pathway nor the ULK1-pS757 pathway at 24 h after its first injection. However, contrary to females, dox-treated males show slightly decreased LC3II/I while p62 expression levels remained unchanged in comparison to the CTL-treated males. Moreover, NRG-1 did not prevent the dox-induced

modulation of any of the markers we identified in chapter 3.2.1 for females. Thus, dox induces sex-specific cardiac functional and architectural modulation in the long term, but also at the molecular level at the beginning of the treatment. Therefore, this suggests that sex differences have to be considered for future research focusing on dox-induced cardiotoxic events but also NRG-1 effects as therapeutics.

Sex-differences were also observed in the response of our mice after NRG-1 stimulation, and this raises the question as to whether a NRG-1 regimen would be similarly beneficial for both sexes? In our model, the NRG-1 inhibition of the autophagic process through the ULK-1-pS757 was only observed in females, the potential protective mechanisms triggered by NRG-1 in males are still to be investigated.

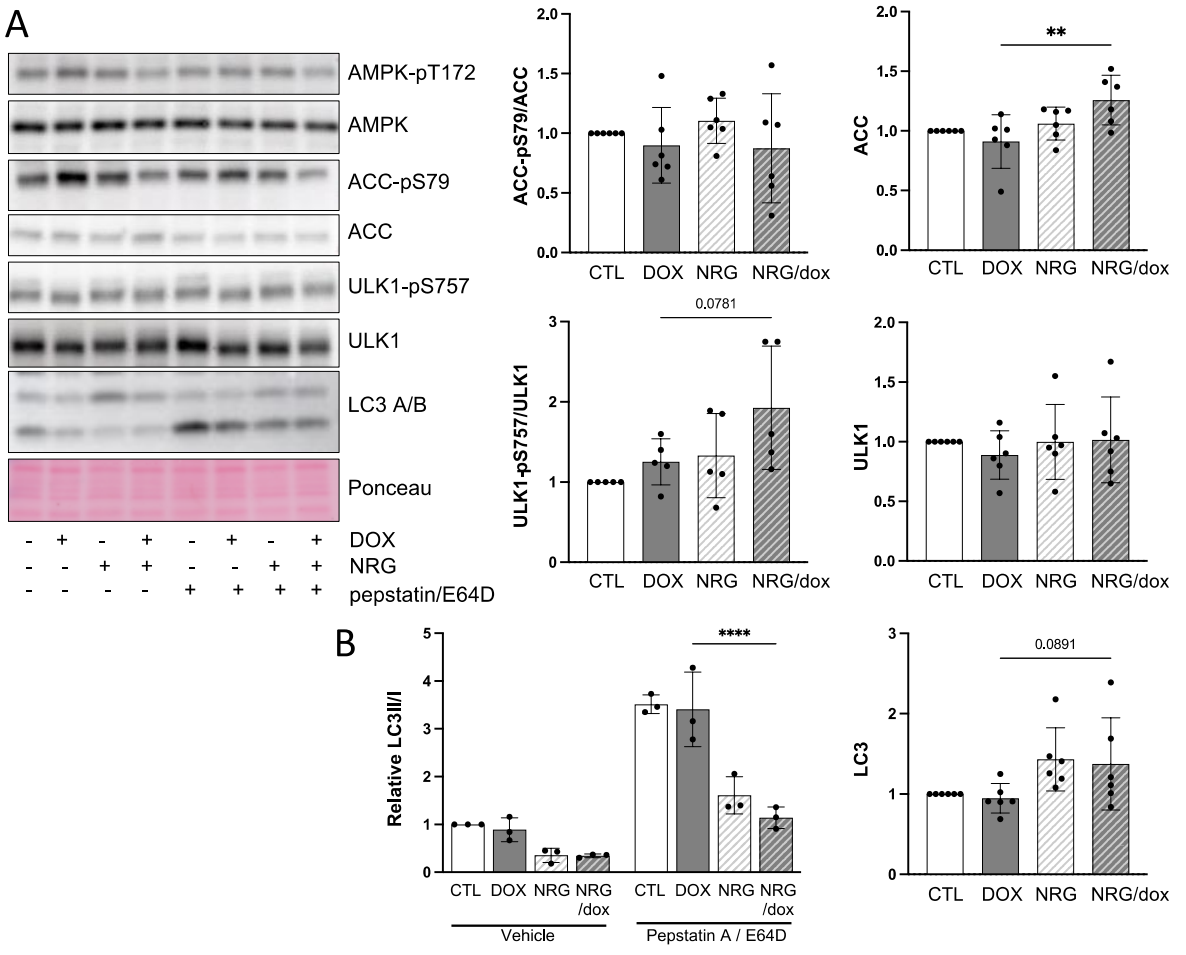

Figure 10. Neonatal rat ventricular myocytes mimic the cardiac response to NRG-1 in females. In serum-free/low glucose medium, NRG-1- (10 ng/ml, 30 min) or vehicle-treated neonatal rat ventricular myocytes (NRVM) were exposed to dox (1 µm) for 16 h in presence or absence of autophagic flux inhibitors (pepstatin A and E64D). Western blot analysis was performed with antibodies as indicated. Data are expressed as mean ± SD; One-way ANOVA with Dunnett's correction statistical analysis was performed versus dox for the experiments without inhibitors n=6 data. Krustal-Wallis analysis was performed versus dox for the experiments with inhibitors, n=3. *p<0.05, **p<0.01, ***p<0.001, ****p<0001.

3.2.3. NEONATAL RAT VENTRICULAR MYOCYTES MIMIC THE CARDIAC RESPONSE TO NRG-1 OBSERVED IN FEMALES AT 24 H

To study in further detail the mechanisms whereby dox changes cardiac metabolic and autophagic pathways and how NRG-1 prevents the effects described in 3.2.1, we used a neonatal rat ventricular myocyte (NRVM) culture model. As we aimed to measure autophagy modulation, NRVM were incubated in serum- and pyruvate-free medium containing 1 g/L glucose. This medium has been characterized in our laboratory to favorize autophagy detection. Cells were first incubated with the autophagic inhibitors E64D and pepstatin A (pepst) or vehicle (DMSO). 30 min later, cells were stimulated with NRG-1 or saline, and 30 min later a 3rd incubation step with dox or PBS was done. Proteins were collected after 16 h of treatment.

Figure 10A shows that after 16 h, dox did not change phosphorylated or total AMPK, ACC, ULK1 or LC3 protein. However, NRG-1/dox-treated cells showed higher ACC total protein levels ($p<0.01$) and decreased LC3II/I ($p=0.014$) in comparison to the dox-treated cells. Moreover, NRG/dox-treated cells tend to have higher ULK1-pS*757* than the dox-treated cells ($p=0.09$). These results are consistent with the analysis that we performed in females 24 h after their first injection: no effects of dox were observed vs CTL, and NRG1 decreased the LC3II/I and tended to increase the total ACC protein levels compared to the dox-treated animals. These data suggest that our cell culture model is mimicking the females' response to our NRG treatment at 24 h. Our observation that in vitro, the ULK1 phosphorylated levels are still increased at 16 h after stimulation, suggests that the inhibition of the autophagic process by ULK could be a long-lasting effect of NRG-1.

Another reason to use the NRVM model was to characterize the autophagic flux by pharmacologic inhibition. Figure 10B shows that the pepst treatment induced an increase of the LC3II/I in CTL conditions. This confirms the efficiency of the pepst to inhibit the autophago(lyso)some degradation. The pepst increased the LC3II/I in dox-treated cells in a similar manner as in the CTL condition, suggesting that dox does not modulate the autophagic flux at 16 h in NRVM. NRG-1 decreased the LC3II/I to a similar extent in the absence or presence of dox, suggesting that NRG-1 decreases autophagic flux in both cases. This effect on flux is indeed confirmed because in the presence of pepst, both NRG- and NRG/dox-treated cells showed an increase in LC3II/I compared to the corresponding vehicle conditions. These data also indicate that some autophagic flux is still ongoing after NRG/CTL and NRG/dox treatment. Similar to what we found in its absence, in presence of pepst, LC3II/I was significantly lower in NRG- and NRG/dox-treated cells in comparison to CTL and dox-treated cells, respectively. These data suggest that NRG-1 stimulation inhibits the early autophagic steps in the presence and in the absence of dox at 16 h.

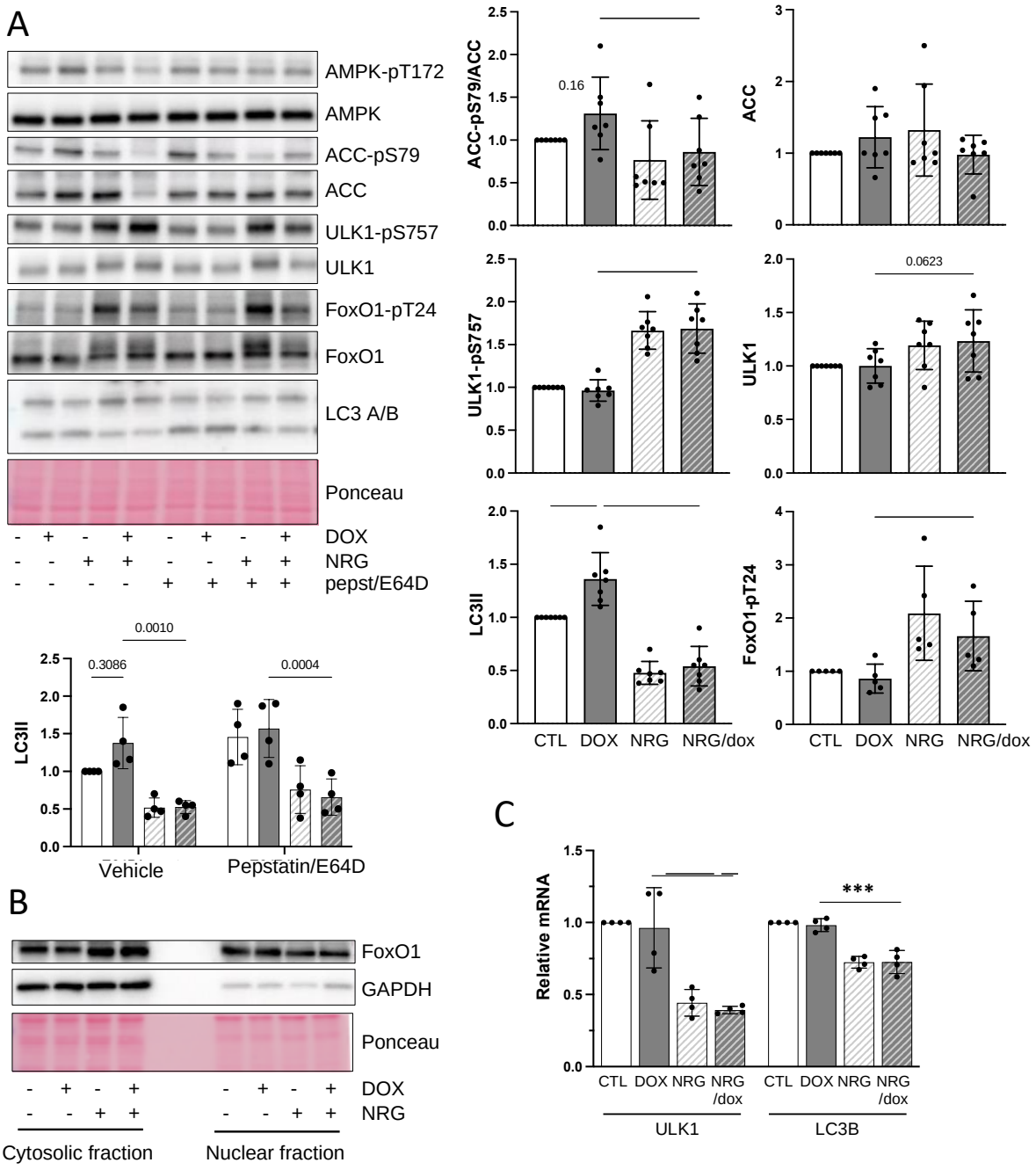

Figure 11. The effects of dox on autophagy at 1 h are prevented by NRG-1. Role of FoxO1. NRVM were pre-incubated for 30 min with the autophagic flux inhibitors pepstatin A and E64D or DMSO before being treated with NRG-1 (10 ng/ml) or PBS. 30 minutes later, the cells were treated with dox (1 μm) or DMEM. Cell lysates were collected 1 h after the NRG-1 stimulation (A), while nuclear protein fraction and RNA were collected at 6 h (B-C). (A-B) Western blot analysis was performed with antibodies as indicated. (C) analysis of gene expression by quantitative real-time PCR. Data are expressed as mean ± SD; One-way ANOVA test with Dunnett's correction was performed versus dox in (A) n=7. Krustal-Wallis analysis was performed versus dox for the experiment (C), n=4. *p<0.05, **p<0.01, ***p<0.001, ****p<0001.

3.2.4. NRG-1 MAY MODULATE AUTOPHAGY BY INHIBITING FOXO1-INDUCED EXPRESSION OF AUTOPHAGY GENES

As our protein analysis showed similarities in the regulation of ACC, ULK1-pS757 and LC3II/I for NRVM in vitro and for female mice in vivo, we decided to study early metabolic responses to NRG-1 and dox in NRVM at 1 h.

Figure 11A shows that at 1 h, dox increased the LC3II protein levels vs CTL and that NRG-1 prevented this increase ($p<0.01$; $p<0.0001$). Furthermore, data show a clear decrease of the LC3II by NRG and NRG/dox in comparison to CTL and dox-treated cells, respectively, both in the presence and the absence of pepst. After pharmacological inhibition with pepst, the differences between CTL and dox were not revealed anymore, which could be due to high variability. Therefore, some more repetitions of these experiments should be performed before drawing any conclusion. Yet, no effects of dox were observed on the LC3II/I ratio (data not shown). These data show that the decrease of autophagic flux by NRG-1 observed at 16 h can already be measured at 1 h and is a very early event.

Furthermore, dox tended to increase ACC-pS79/ACC vs CTL ($p=0.16$), while NRG caused a significant reduction compared to dox alone ($p<0.05$). This was not associated with any detectable effects on AMPK phosphorylation (not shown). In addition to preventing the dox-induced ACC-pS79/ACC and LC3II increase, NRG/dox-treated NRVM showed an increase of ULK1-pS757/ULK1 (an mTORC1 target site) and phosphorylated FoxO1-pT24 levels in comparison to the dox-treated NRVM at 1 h. The NRG-induced increase of FoxO1-pT24 was associated with an increase in the cytosolic and a decrease in the nuclear protein amounts of FoxO1 (Fig. 11B). This was the case in the absence as well as presence of dox.

It has been reported that when FoxO1 is phosphorylated at the T24 site, it is retained in the cytoplasm, which prevents its transcriptional activity [19]. This is why we proceeded to measure the expression of some FoxO1 target genes at the mRNA level at 6 h. Figure 11C shows that NRG- and NRG/dox-treated samples have significantly decreased mRNA expression of ULK1 and LC3B in comparison to CTL and dox-treated NRVM, respectively.

In conclusion, our data suggest that NRG-1 decreases nuclear location of FoxO1 by increasing its phosphorylation at the T24 site and that this leads to decreased expression of the FoxO1 target genes LC3 and ULK1 at 6 h. Interestingly, these effects are associated at the functional level with an NRG-1-induced decrease in autophagic flux and suggests a complex and orchestrated mechanism to coordinate the NRG-1 induced autophagic modulation at the protein and transcriptional levels.

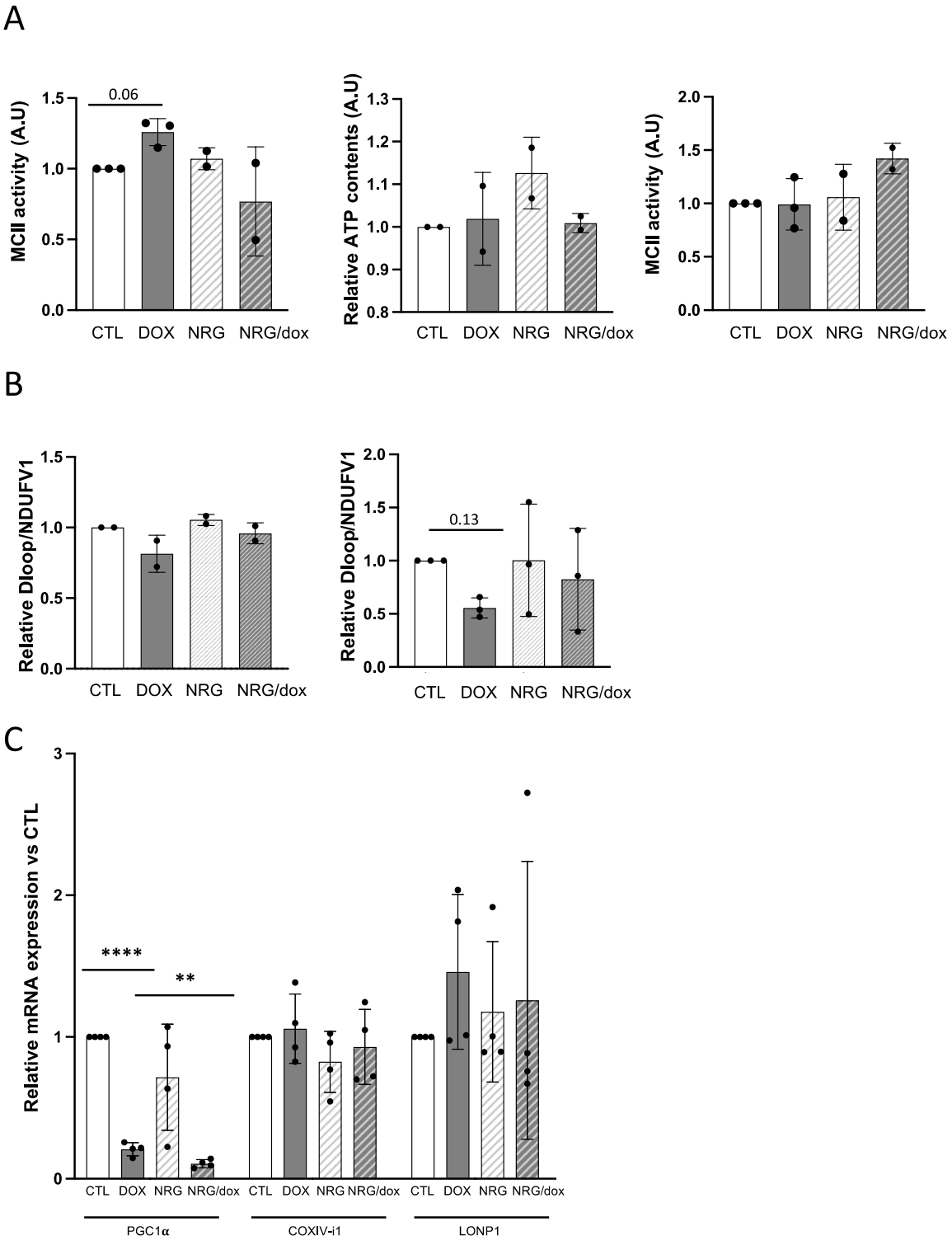

Figure 12. Effects of dox on the mitochondrial compartment and activity. NRVM were incubated in a serum-free and low glucose medium and immediately stimulated with NRG-1 (10 ng/ml) or vehicle. 30 min later, cells were treated with dox (1 µm) versus DMEM. (A) ATP contents were measured at 3 h using cell titer glo, while metabolic activity and mitochondrial contents were measured using the MTT method and quantification of the ratio between mitochondrial and nuclear DNA amounts at 3 and 16 h (A-B). (C) gene expression of mitochondrial genes and ACC was measured by real-time PCR. Data are expressed as mean ± SD; n=2-4; Krustal-Wallis analysis was performed versus dox. *P<0.05, **P<0.01, ***P<0.001, ****P<0001.

3.2.5. EFFECTS OF DOX ON MITOCHONDRIAL CONTENT AND ACTIVITY

Dox has been reported to induce mitochondrial dysfunction and decrease cellular ATP content [63, 119]. We aimed to assess whether in our NRVM model the mitochondrial compartment was affected by dox and if so, whether NRG-1 changed this, as several studies suggest that NRG-1 might induce mitochondrial biogenesis [120, 121].

To this end, we measured the mitochondrial complex II (MCII) activity at two different timepoints, using an MTT assay. We also measured ATP cellular contents at 3 h, using the cell titer glo® kit. The presented values were standardized for protein content.

Figure 12A shows that at 3 h, dox induced a modest increase of MCII activity (25%, p=0.06) in comparison to the CTL-treated cells. In one experiment, cellular ATP was increased and in the other experiment it was decreased, so more experiments are needed to draw the conclusion that the observed increase in MCII activity is correlated with higher ATP content. Furthermore, NRG-1 stimulation prevented the dox-induced increase in MCII activity at 3 h in 2 independent experiments, suggesting that NRG-1 prevents the dox-induced succinate dehydrogenase activity. NRG-1 by itself did not change MCII activity, however, NRG-1-treated NRVM contained 20% more ATP than the CTL-treated NRVM in two independent experiments. At the later timepoint of 16 h, no effects of dox were measured on MCII activity anymore, however, in two experiments NRG-1/dox-treated NRVM showed enhanced MCII activity in comparison to the dox-treated NRVM.

The next step was to characterize the effects of dox and NRG-1 on the mitochondrial content at 3 and 16 h. Figure 12B shows that dox induced a decrease in the ratio of mitochondrial to nuclear DNA content (mt/nu DNA) at 3 and 16 h in comparison to the CTL. While at 3 h NRG/dox had higher mt/nu DNA than dox-treated cells in two 2 independent experiments, at 16 h variability was much higher and did not allow any conclusion about the effects of NRG-1 in CTL- or dox-treated NRVMs.

Taken together, our preliminary data show that dox treatment of NRVM causes a decrease in mitochondrial content at 3 and 16 h, and that this appears prevented at 3 h by the NRG-1 pre-treatment. Yet, because of high variability, more experiments are needed to draw conclusions on the preventive effect of NRG-1 on dox-induced decrease in mitochondrial contents.

Since we detected a dox-induced decrease in mitochondrial contents at 16 h, we proceeded to analyze at 6 h the mRNA levels of PGC1α, a regulator of mitochondrial biogenesis, cytochrome c oxidase subunit IV-i1 (COXIVi1), a subunit of the mitochondrial complex IV, and LONP1, a mitochondrial protease implied in mitochondrial quality control and known to regulate COXIVi1

at the protein level. Consistent with the decrease in mitochondrial content (Fig. 12B), Figure 12C shows that dox induces an 80% decrease of PGC1α mRNA expression vs CTL ($p<0.0001$). NRG-1 decreased PGC1α expression even further in comparison to the dox-treated samples ($p<0.01$). On the other hand, no transcriptional regulation of the COXIVi1 or LONP1 was measured at 6 h. Our observation that the dox-induced decrease in mitochondrial content at 16 h is associated with a decrease of PGC1α mRNA at 6 h suggests that dox reduces mitochondrial biogenesis.

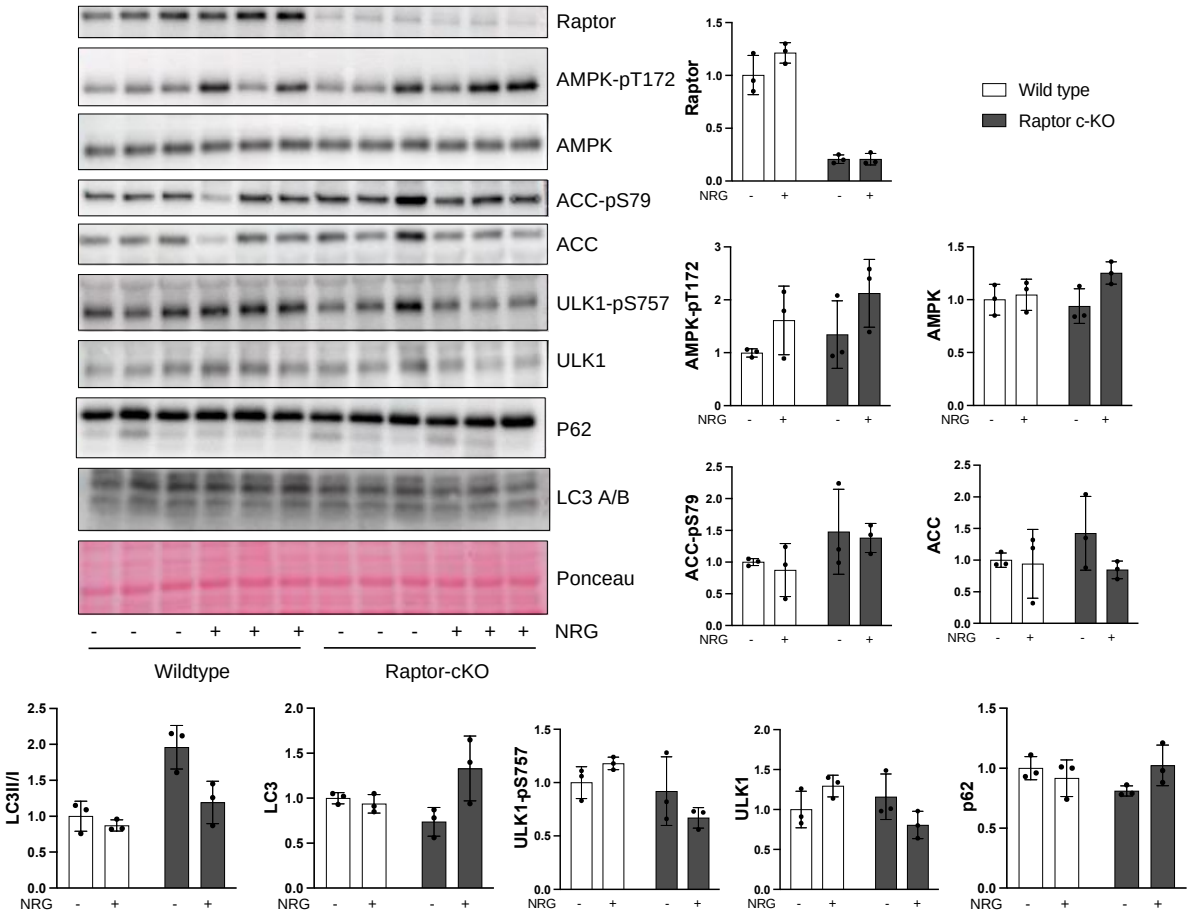

Figure 13. Effects of NRG-1 stimulation and cardiac raptor ablation on the autophagic pathway. Raptor deletion was induced in ***α***-MHC-MerCreMer/raptor$^{fl/fl}$ mice at the age of 10 weeks by intraperitoneal injection of tamoxifen for 5 consecutive days. Controls consisted of mice homozygous for the wild type raptor gene (α-MHC-MerCreMer/raptor$^{wt/wt}$), injected with tamoxifen. At 13 weeks of age, mice were fasted for 8 h from 1 h before the lights switched on (ZT23). At ZT30, mice were injected intraperitoneally with NRG-1(20µg/kg) versus PBS, and sacrificed at ZT31. Cardiac lysates were analyzed by Western blot. Protein expression was quantified and standardized to the related ponceau-stained membrane. Data are expressed relative to the PBS-injected wildtype as mean ± SD; N=3. Krustal-Wallis analysis was performed versus dox. *p<0.05, **p<0.01, ***p<0.001, ****p<0001

3.3. PRELIMINARY DATA OF SIDE PROJECTS

3.3.1. NRG-1-INDUCED CARDIAC DECREASES IN LC3II/I ARE MTORC1-INDEPENDENT

ULK1 is known to be phosphorylated at its S757 site by mTORC1. To investigate whether mTORC1 has a role in the NRG-1-induced increase of ULK1-pS757 and autophagy inhibition, we generated female mice carrying raptor-specific deletion in cardiomyocytes (raptor-cKO) and their littermate controls (ctr) as described in the methods section. Briefly, C57BL/6J female mice positive for α-MHC-MerCreMer and carrying either 2 raptor floxed alleles (α-MHC-MerCreMer/raptor$^{fl/fl}$) or 2 wildtype raptor alleles were injected with tamoxifen as described [115]. 2 weeks after the last tamoxifen injection, mice were fasted for 8 h from ZT23 to ZT31, that is to say from 1 h before the end of the active phase to 7 h after their resting phase started. 1 h before sacrifice, at ZT30, mice were either injected with NRG-1 or with vehicle. Cardiac protein lysates were analyzed by Western blotting (Fig. 13).

Figure 13 shows that the raptor-cKO mice have reduced cardiac raptor expression by 81% in comparison to the ctr mice, thus validating the raptor deletion in our model. Interestingly, the raptor deletion was associated with increases in AMPK-pT172, ACC and ULK1 of 34%, 42% and 16%, respectively, suggesting a compensatory response. Raptor deletion was also associated with increased LC3II/I (by 2-fold), as well as decreased p62 (19%) and decreased LC3 total protein (26%), suggesting that raptor-cKO mice have increased activity of the AMPK-ACC and autophagy pathways in comparison to the ctr mice.

In ctr mice, NRG-1stimulation induced increased ULK1-pS757 phosphorylated and total protein levels (by 18 and 29%, respectively), and surprisingly, this was associated with 57% increased AMPK-pT172/AMPK ratios, but not with any ACC-pS79/ACC modulation vs vehicle ctr mice. Also, as expected, NRG-1 decreased LC3II/I ratios while p62 protein levels were slightly decreased. These data suggest that in ctr mice, NRG-1 inhibited autophagy and this was associated with increased ULK1-pS757 levels.

In the raptor-cKO mice we first of all observed that after NRG-1 stimulation ULK1-pS757 was not increased anymore, and that the total ULK1 protein levels were even decreased by 30% vs vehicle-injected raptor-cKO mice. These data support that the NRG-1-induced increases in total and phosphorylated ULK1 in WT mice are mTORC1-dependent. Secondly, in the raptor-cKO mice, NRG-1 stimulation increased AMPK-pT172/AMPK by 21%, while ACC total protein levels were decreased by 40% in comparison to the vehicle-injected raptor-cKO mice. Finally NRG-

1-stimulated mice showed increased p62 protein levels, increased LC3 as well as decreased LC3II/I ratio by 27%, 40% and 40%, respectively.

Thus, although the NRG-1-induced increases in ULK1 are mediated by mTORC1, NRG-1 still inhibits the strong increase in LC3II/I after mTORC1 inactivation, indicating that NRG-1 can reduce autophagy independently of mTORC1. Further support for mTORC1-independent autophagy regulation by NRG-1 comes from the observation that NRG-1 increases LC3II total protein in the raptor-cKO mice.

More experiments should be performed to increase the number of animals and validate these data. Moreover, autophagic flux inhibitors could be used in vivo or in vitro to investigate if and how NRG-1 modulates autophagy, and at which stage in the context of the raptor deletion. Our hypothesis was that NRG-1 was inhibiting autophagy initiation by inducing ULK1-pS757 via mTORC1. The mechanisms by which NRG-1 modulates autophagy are still unclear, and are probably either dependent on the feeding conditions, or on the cell type. Indeed, NRG-1 has been shown to decrease autophagy in a mTORC1-independent manner in PCNA prostate cell line, while Yin et al. showed that in skeletal muscle, this autophagy inhibition was dependent on the Akt/mTORC1 pathway [98, 99].

Interestingly, in this experiment, mice showed NRG-1-induced AMPK-pT172, which had never been observed in our previous experiments. Repeating this experiment to increase the number of animals seems crucial to draw further conclusions. Moreover, in this experiment, the cages were changed to avoid fecal feeding, and the fasting lasted for 8 h instead of 6 h, these conditions maybe more stressful for the animals, or led to a more efficient fasting and therefore might have favorized NRG-1 induced AMPK pathway activation.

3.3.2. ERBB4 ISOFORMS IN THE HEART

As described earlier, ErbB4 is the only member of the ErbB family to have different isoforms. ErbB4 isoforms have been first characterized by Elenius and colleagues in 1997 [122]. As shown in Figure 14, 4 isoforms of ErbB4 have been described in healthy tissues. The presence or the absence of a TACE and γ-secretase site confers ErbB4 the property to be cleavable (JM-a) or not (JM-b). Likewise, the presence or the absence of a 16 amino acid sequence gives ErbB4 the property to activate the PI3K-Akt pathway (cyt-1) or not (cyt-2).

Further analysis by Veikkolainen et al. has revealed that in human adult heart tissue, the non-cleavable isoform JM-b represents a bit more than 60% of the total ErbB4 isoforms. Moreover, 80% of the cardiac ErbB4 receptors are the cyt-1 isoform, meaning that they are able to activate the PI3K-Akt pathway in the heart [123, 124]. However, the heart includes numerous cell types, and Icli et al. report that adult rat ventricular myocytes are all expressing the non-cleavable JM-b isoform and express cyt-1 and cyt-2 isoforms in a 80%/20% ratio [125].

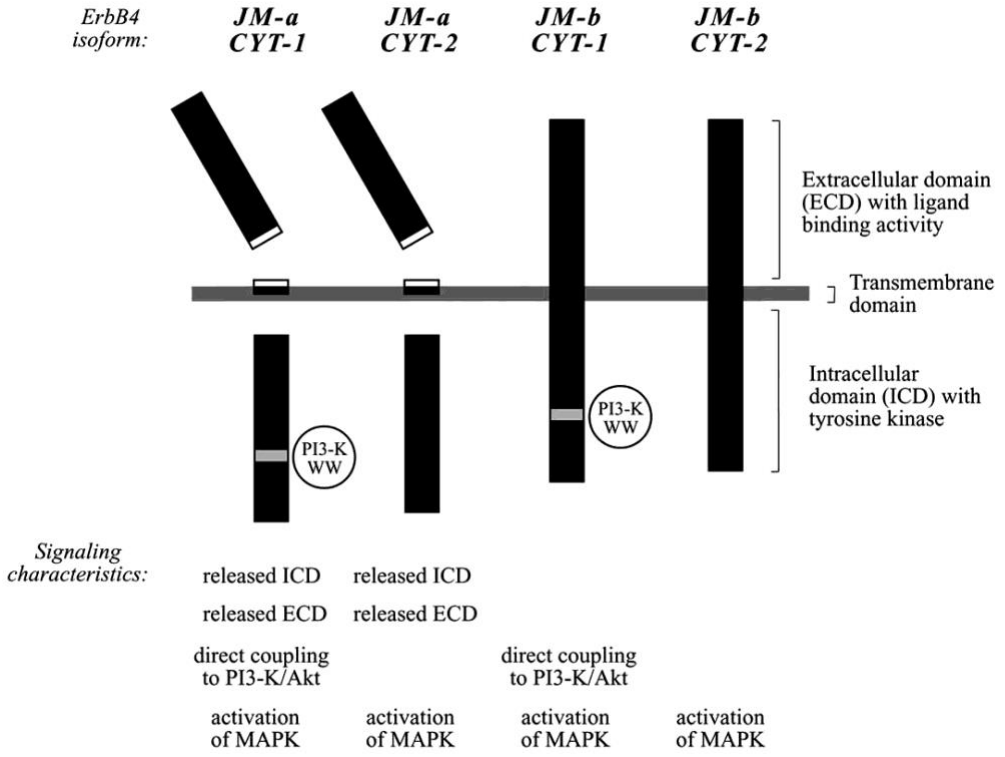

Figure 14. Schematic presentation of the ErbB4 isoforms. The ErbB4 receptor has 2 alternative splicing sites, the first one is the juxta-membranal site, which confers the ability of the receptor to get cleaved or not (JM-a, JM-b). The second site consist on the translation of a 16 amino acids site containing a WW rich sequence and PI3K binding site, or not (cyt1, cyt-2). Paatero et al. 2008 [126].

It is known that ErbB4 expression strongly decreases during the heart maturation process, however, no studies focused on characterizing ErbB4 isoform expression in the matured vs non-matured heart, whereas numerous studies either use adult rat ventricular myocytes/adult

animals, or NRVM/neonates [127]. Moreover, while our dox-therapy model relied on the use of adult mice, our mechanistic studies relied on a non-matured rat cardiomyocyte model (NRVM). It was therefore to us a very important matter to be aware whether the ErbB4 isoforms were similar in neonatal or aged rats. To this end, we sacrificed rats at 1, 8 or 26 days after birth, and the left ventricle, which mainly contains cardiomyocytes, was collected for RNA extraction. Then, ratios of the obtained cDNA amounts were calculated to check the prevalence of the JM-b/JM-a and the cyt-2/cyt-1 at the different timepoints.

Figure 15 shows that the total ErbB4 receptor expression was decreased by 57% from d 1 to d 26. Interestingly, the ErbB4 JM-b/JM-a ratio increased by 4-fold from d 1 to d 26. In parallel, the cyt-2/cyt-1 ratio was not modulated between the different conditions. These data suggest that at d 1, ErbB4 is mainly a JM-a subtype, while at d 26, in the matured heart, ErbB4 is mainly JM-b. Concerning the cyt isoforms, no striking differences were measured between d 1 and 26, suggesting that there is no switch toward one or the other cyt isoform from non-matured to matured cardiac tissue. To characterize more quantitatively the JM-b/JM-a and cyt-2/cyt-1 expression, primers have been designed to amplify the entire JM or cyt region, and migration of the PCR products should be performed.

Our data show a JM isoform switch during maturation of the rat hearts. Therefore, characterization in our cultures of the potential cleavage of the ErbB4-JM-a should be investigated. In 2021, Wang et al. addressed the same question as we did, and his results were comparable [128]. The next step would be to characterize for each cardiac cell type which ErbB4 isoforms are expressed to have a better understanding of the ErbB4 biology in the heart. Moreover, it would be of interest to determine whether under stress conditions, cardiac remodeling changes the expression of the ErbB4 isoforms in the cardiomyocytes or not.

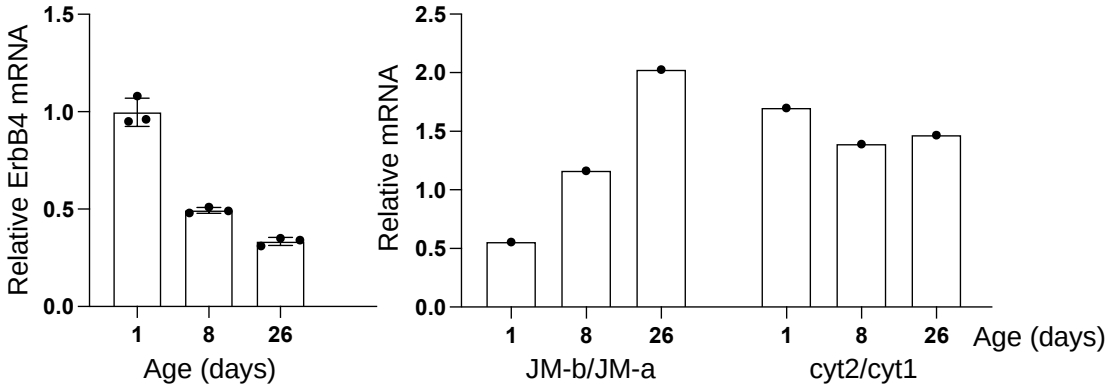

Figure 12. Characterization of the ErbB4 isoforms in hearts of rats at 1 to 26 days after birth. ErbB4 has 4 isoforms. They differ in their Juxta-membrane domain, which can be cleaved or not (JM-a vs. JM-b) and in their cytosolic tail, which can contain a PI3K binding domain or not (CYT-1 vs. CYT-2). Rat hearts are not fully matured at birth. Therefore, hearts were collected from of 1, 8 and 26 days-old rats and the mRNA expression of the ErbB4 isoforms was compared over time by real time PCR.

4. DISCUSSION

Doxorubicin-induced CHF has been extensively reported, yet, the mechanisms and risk factors behind its development are not fully understood and are still to be investigated [51, 52, 129]. Regrettably, breast cancer patients included in clinical trials combining dox and ErbB2-targeted immunotherapy showed increased prevalence to develop dox-induced cardiotoxic side effects [130]. Therefore, the cardiac NRG-1-ErbB2 axis was highlighted as a new potential therapeutic target in the prevention of cardiotoxicity after dox-therapy [131].

What stroke us at the start of this project was that in the available literature, most of the studies on dox-induced CHF in vivo are analyzing short term models injected with single or multiple highly toxic doses of dox [132, 133]. Only few studies established relevant dox-therapy protocols aiming to reduce mouse mortality by injecting the animals repeatedly with low doses of dox, and following the animals' cardiac changes and survival to later timepoints than 1 week [70, 74, 116]. Surprisingly, while sex-differences are very well-known to exist in the context of cardiovascular disease, they remain unclear in the context of dox-induced cardiotoxicity. Only Ventura-Clapier and colleagues compared male and female rats in response to a dox-therapy model on the long term [58, 76].

Several studies have investigated whether NRG-1 protects against dox-induced cardiotoxicity, mostly using short-term in vivo experiments or in vitro experiments [73, 100, 134]. Only few studies aimed to characterize the cardioprotective effects of NRG-1-ErbB2 in a long term in vivo model [74, 90]. Our study therefore aimed to characterize in a long-term doxorubicin-therapy mouse model whether a new NRG-1 regimen could exert protective effects against dox-induced cardiac and systemic toxicity, and to investigate which mechanisms could be implied in male and female mice.

4.1. DOXORUBICIN AND NRG-1-TREATED MICE DEVELOP SEX-SPECIFIC PHYSIOLOGICAL AND MOLECULAR CHANGES OVER TIME

4.1.1. MALES ARE MORE SENSITIVE TO DOX-INDUCED TOXICITY THAN FEMALES

Systemic and cardiac toxicity. Dox-therapy is used in clinics to treat a wide range of tumors [35]. While the prevalence to develop dox-induced CHF is estimated to be 5% in patients, each cancer type is characterized by unique survival rates, metastasis potential, relapse, and last but

not least sex prevalence. The heterogeneity between the different tumor types and patient features contributes to the difficulty to identify the risk factors associated with the cardiac outcomes and CHF. Meiners et al. have summarized the difficulties encountered to constitute cohort of patients enabling to study the role of sex as a factor of risk or protection in dox-induced cardiomyopathy [35]. To the best of our knowledge, only Moulin and colleagues have rigorously investigated sex-differences in a long term dox-therapy model in rats [76].

Consistent with Moulin's observations, our dox-therapy induced higher toxicity in males than in females: only males showed cardiac atrophy and lung edema. Furthermore, the males had a more severe cachectic phenotype at 3 weeks, as they underwent higher body weight loss than the females.

Cardiac architecture and function. While Moulin et al. showed that dox induced a stronger decrease in ejection fractions in male than in female rats, our echocardiography measurements revealed on the one hand dox-induced compensatory increases in ejection fraction and thickness of the left ventricular posterior wall during systole in males at 2 weeks, and on the other hand a decrease of total wall thickness with no changes in cardiac function at 3 weeks in the females. Interestingly, in males this compensatory response at 2 weeks was accompanied by increased expression of β-MHC and GLUT1, two well-known markers of cardiac compensatory responses [135, 136]. The difference between the Moulin study and our own work with respect to the dox-induced changes in males could be either species dependent, or simply dose dependent [76]. Concerning the effects of dox in females, the different studies mainly show slight dox-induced changes of LVEF or wall thickness. Milano et al. from whom we copied the dox-therapy protocol, showed a dox-induced decrease in ejection fraction which lasted up to 6 weeks. At week 6, histology analysis showed a dox-induced decrease of the LV and RV free wall thickness, but no additional echocardiographic data were presented, suggesting that no changes in wall thickness were measured at 3 weeks [116]. Similarly, Jay et al. measured in their long term mouse model that dox induced a decrease in fractional shortening which was not accompanied by wall thickness changes [74]. In contrast, in female rats much milder effects of dox have been described by Moulin and colleagues, as only a slight decrease in ejection fractions was measured at 8 weeks [76].

To partially conclude about our dox-therapy model, few studies have characterized dox-induced chronic cardiac responses in males. While females have been more studied, the variety of dox-therapy protocols described in the literature, as well as the differences between the species and mouse strains, make the comparison of studies hard to interpret. Consistent with Moulin et al., we showed that male mice undergo a stronger systemic toxicity than females as

well as cardiac atrophy. Moulin and colleagues have described dox-induced decreases in ejection fractions in male rats, while we showed increased ejection fractions with our protocol in male mice. This difference of cardiac function can be explained by the fact that in our experiments, male mice were in a cardiac compensatory phase at 2 weeks, while Moulin et al. measured decreased ejection fractions at a later time point when compensation was not occurring anymore and cardiac dilation could be measured [76]. Altogether, our data seem to be also in line with what has been observed in clinical studies: Meiners et al. reported that according to human studies, male sex was either deleterious or female sex was protective toward dox-induced cardiac toxicity [35].

The effects observed in our mice were transient. While no compensatory cardiac effects were measured anymore at 3 weeks in males, high body weight losses and mortality were observed. According to animal well fare guidelines we were not allowed to follow the males for any longer. These data suggest that our dox-therapy protocol might not have been optimal for male mice and a dosage refinement should be considered. Concerning the females, no cardiac effects were revealed by transthoracic echography at 5 weeks. Since some animals from the NRG/dox group started to die, we chose to stop the experiment before the analysis of the echocardiography data were done. It is of note that Milano et al. showed in female C57BL/6J that dox induced a decrease in LVEF at 3 and 6 weeks. While in our own experiments slight effects of dox on cardiac wall thickness were measured at 3 weeks, they were not observed anymore at 5 weeks, suggesting that we might have needed to monitor the mice longer to reach a state of dox-induced cardiac dilation.

4.1.2. Did NRG-1 prevent the dox-induced toxicity in males?

Male mice have previously been used to study the protective effects of NRG-1 on dox-induced acute cardiac toxicity [74, 134]. As explained earlier, studies of acute dox-induced toxicity usually rely on the use of highly toxic and clinically irrelevant doses in the range of 20 mg/kg. As a matter of fact, Bian and colleagues showed that the injection of a dose of 15 mg/kg dox in male mice led to 86% of mortality in males after 2 weeks [73]. Therefore, our study is the first to characterize the effects of NRG-1 on cardiac parameters in a model of dox-therapy that mimics the dox protocols used for patients. Moreover, this is the first time that a new once-every-other-day NRG-1 regimen was tested in both male and female mice.

Firstly, our data show that the NRG-1 regimen did not prevent the overall dox-induced toxicity in males, namely the loss of body weight, cardiac atrophy and the development of lung edema. Still, the NRG-1 regimen tended to prevent the development of a cachectic phenotype in the

males at 3 weeks. Interestingly, the trend of our NRG-1regimen to prevent cachexia is in line with the Yin study in skeletal muscle or the Galindo study in which it has been reported that GGF2, the full length NRG-1β peptide analogue, induces anti-atrophic gene expression and prevents atrophic gene expression in intercostal muscles in a model of heart failure in swans [99, 137]. Altogether these data suggest that NRG-1 might indeed have an anti-atrophic effect in skeletal muscle, and should encourage more studies to characterize these properties. Secondly, our results point toward a protective role of NRG-1 during the dox-induced compensatory cardiac response at the functional and architectural level at 2 weeks. Indeed, NRG-1 prevented dox-induced increases in ejection fraction and LVPW during systole at 2 weeks. However, no differences between the NRG/dox and dox-treated animals were measured for GLUT1 and β-MHC at the mRNA or protein level at 3 weeks. Consistently, at 3 weeks echocardiography did not reveal any significant differences in ejection fraction or wall thickness, suggesting the end of the compensatory phase in the dox-treated males. Still, at 3 weeks, the NRG/dox group showed lower heart rates than the dox group, hence we couldn't fully conclude on the NRG-1 regimen absence of effects on cardiac function at that timepoint, as ejection fractions and heart rates are inversely correlated [138].

Finally, Kaplan-Meier analysis revealed a trend for increased mortality in the NRG/dox group. The number of animals in our study was not high enough to draw a final conclusion about any effect of the NRG-1regimen on mortality. However, as this is the first time that NRG-1 has been tested in a long-term model of dox-therapy, further investigations have to be performed to determine the benefit/risk balance of our NRG-1 regimen versus that of alternative NRG-1 treatment regimens used in the context of dox-therapy. Few studies have highlighted the possible deleterious effects of NRG-1 in the context of its use as a curative drug. Zurek et al. showed in a rat model of myocardial infarct that rhNRG-1 treatment induced an increase in ejection fractions as well as cardiac hypertrophy in a dose-dependent manner. This was associated at the highest doses with myocardial contractile disturbances, which were uncovered using myocardial strain measurements [95]. In our model no hypertrophic response was associated with the use of our NRG-1 regimen and we can therefore conclude that NRG-1 did not trigger any maladaptive cardiac hypertrophic response. However, strain analysis of our echography measurements might be of interest to investigate treatment-induced changes of myocardial contractility. Furthermore, clinical trials with GGF2 had to be stopped because of the development of hepatic side effects. For this reason, we might want to analyze the collected livers in the future [139].

4.1.3. In females, NRG-1 prevents dox-induced autophagy

More data are available on females than males concerning dox-therapy in pre-clinical models. Two studies have focused on the preventive effects of NRG-1 during dox-therapy aiming to follow up on the animals for more than 2 weeks [73,74]. While both Jay et al. and Bian et al. did not show any cardioprotective effects of NRG-1 in female mice, Bian et al. showed increased survival rates in the NRG/dox-treated mice vs the dox-treated mice, revealing a protective effect of NRG-1 on dox-induced mortality in their female model [73,74]. Consistent with these two studies, no preventive effects of our NRG-1 regimen on cardiac architecture and function were observed in females in our study at 5 weeks.

It is known that disturbances in protein homeostasis promote heart dysfunction and disease development and several studies have shown that dox-therapy is associated with impaired autophagy. Nevertheless, no studies have investigated the role of NRG-1 in dox-induced autophagy changes in female mice [28,41].

Our data show that our NRG-1 regimen had a preventive effect on dox-induced decreases in LC3II/I in females at 5 weeks. Furthermore, NRG-1/dox-treated mice showed significantly increased AMPK total protein levels in comparison to the dox-treated mice. This suggests that NRG-1 might regulate or enhance the AMPK pathway activation in the context of dox-induced chronic cardiotoxicity, while in other models such as myocardial infarction, early activation of the AMPK had been showed to be NRG-1-independent. Our study did not characterize in which features the autophagic flux was modulated by dox in our model or not, and further experiments with autophagy inhibitors would be required to do so.

Interestingly, only one long-term in vivo study, relying on the use of repeated low doses of dox, showed increased cardiac LC3II/I ratios in mice [140,141]. While most of the in vivo short-term and in vitro studies also indicated that dox increased cardiac LC3II/I or LC3II, few studies highlighted dox-induced decreases in LC3II [71, 113, 114, 133, 141, 142]. Nevertheless, whether or not LC3II is increased or decreased by dox, the different studies agree on the beneficial effects of reversing dox-induced LC3II/I modulation. While some studies induced physiologically (starvation, exercise) the autophagic process before dox-injection [114, 133, 143], others intended to block it pharmacologically, for example with rapamycin [144]. In all of these studies, the prevention of the dox-induced changes in autophagy was beneficial toward dox-induced cell death and cardiac dysfunction, be it in vivo or in vitro.

Our results show that NRG-1 prevented the dox-induced decrease in LC3II/I. It is of note that some studies have highlighted the property of NRG-1 to inhibit the autophagy pathway in different organs and cell types [97-100]. NRG-1 might exert long term cardioprotective features

through the modulation of the autophagic pathway, by increasing AMPK expression as a compensatory mechanism.

4.2. DOXORUBICIN AND NRG-1 INDUCE EARLY SEX-SPECIFIC MOLECULAR RESPONSES

4.2.1. DOX CHANGES THE AUTOPHAGY PATHWAY IN MALE, BUT NOT IN FEMALE MICE AT 24 H

As described in 4.1.3, dox-therapy in females decreased LC3II/I at 5 weeks and this was reverted by the NRG-1 treatment regimen. These data suggest that NRG-1 prevents dox-induced protein homeostasis disturbances occurring after long-term treatment. Interestingly, NRG-1 increased cardiac AMPK total protein in dox-treated mice, suggesting that NRG-1 increases the activity of the AMPK as a compensatory and protective mechanism [145].

Another aim of this study was to determine by which early mechanisms NRG-1 protects against dox-induced toxicity in male and female mice, and especially the autophagy pathway and its upstream regulators. Thus, we analyzed which metabolic pathways were modulated at 24 h after the first dox injection of our protocol and tested whether NRG-1 changed the effects.

Firstly, our data show that dox treatment tends to decrease LC3II/I in males but not in females, suggesting that cardiac autophagy might be disturbed already 24 h after the first injection of our protocol in males. On the other hand, no changes in the upstream regulators of autophagy AMPK-ACC, ULK1 and FoxO1 were detected in either gender. In contrast to our own finding, studies by Li et al. (female mice, day 3, 4 mg/kg) or Kawagushi et al. (rats, day 5, 10 mg/kg) show that dox increases LC3II. Consistently, Dutta et al. showed increased LC3II at 24 h after a single injection of 10 mg/kg in rats [70,114,146]. As for the effects of NRG-1, the NRG/dox-treated males were not different from the dox-treated saline-controls at the signaling and LC3II/I levels. However, the NRG/dox-treated female mice had increased cardiac ACC and ULK1-pS757 levels. Moreover, in females we provide some first evidence for decreased autophagic flux as the LC3II/I was decreased and p62 protein amounts were increased. These data show a clear sex-effect of our NRG-1 regimen on dox-induced early toxicity and raises the following questions: are the molecular mechanisms underlying dox-induced cardiotoxicity comparable in male and female patients? Would both of them benefit from NRG-1 treatment? Does it make sense to have common therapies?

Secondly, in males and in females, dox-treated animals tended to have increased ErbB2-pY1248, suggesting that dox-treatment induces the endogenous NRG-1-ErbB2 cardioprotective axis at 24 h, and neither ErbB4 nor ErbB2 were downregulated by dox in contrast to the Horie et al. study which showed that in male mice ErbB4 receptor started to get decreased from 12 h up to day 5 after a 20 mg/kg dox injection [127, 134]. The results described by Horie et al. probably reflect the receptor downregulation in response to a highly toxic dox dosage. However, our study could not reveal any ErbB activation after NRG-1 stimulation of dox-treated mice. Indeed, no differences in phosphorylated ErbB2 levels neither in males nor in females in comparison to the dox-treated animals was detected. The lack of an effect of NRG-1 could be explained as follows. 1) NRG stimulation couldn't cause any additional effects on the ErbB2 activation already induced by dox. 2) The animals were sacrificed 1 h after the stimulation, which might be too late to observe receptor phosphorylation, which is a transient event. 3) We used total protein extracts, which does not allow us to determine if the receptor was at the cellular membrane or internalized.

Downstream of the receptors, the NRG/dox females showed increased phosphorylated ERK1/2, whereas the NRG/dox males showed a trend towards increased FAK-pY861 in comparison to the sex-matched dox-treated groups. Previous experiments in our laboratory showed that the FAK-pY861could be induced by the NRG-1-ErbB4-src pathway, however, it could also be induced by other stimuli such as VEGF [112]. Furthermore, the ERK1/2 phosphorylation is not a specific readout for ErbB activation neither. We also have to keep in mind that the NRG-1 injection leads to systemic ErbB stimulation, notably in metabolic organs such as the liver or skeletal muscle. 1 h after the NRG-1 stimulation it is not excluded that our analysis might reflect indirect effects of the NRG-1 stimulation on the heart.

4.2.2. NRVM DO MIMIC FEMALE'S CARDIAC MOLECULAR RESPONSE TO DOX AND NRG-1

One question which emerged from the field of cardio-oncology is whether the dox-induced early metabolic disturbances, few minutes or hs after the dox injection, are conditioning the cardiac toxicity in patients [129]. We aimed to characterize this early response with focus on autophagy, using an NRVM model cultured in a medium optimized to detect autophagy changes. At 16 h, our model mimicked the females' response observed at 24 h described in 4.2.1. That is to say, almost no effects of the dox-treatment by itself, but decreased LC3II/I ratios associated with increased ULK1-pS757 and increased ACC total protein. The use of autophagic flux inhibitors allowed us to conclude that the NRG-1 induced decrease in LC3II/I is the consequence of NRG-1-dependent inhibition of autophagic flux, at the initiation step, probably by increasing phosphorylation of ULK1 at S757, which is known to be inhibitory [26].

Interestingly, An et al. showed in a NRVM model at 18 h that dox induced an increase of LC3II protein contents, and NRG/dox prevented it by bringing the LC3II protein levels similar to the ctl conditions by modulating Beclin1, another key actor of the autophagy process initiation [100]. Likewise, most of the other studies were able to reveal LC3II or LC3II/I modulation by dox at timepoints similar to 16 h [71, 100, 113]. These differences in cell responses might be due to cell culture conditions. Indeed, we use a serum free medium depleted in pyruvate containing 1 g/L glucose in order to optimize the autophagic induction. Moreover, as our mice are injected in the late afternoon, this would have mimicked the nutritional state of our mice when they receive their treatments. On the contrary, most of the published studies used serum containing media for their cell culture experiments, and these studies showed in numerus cell culture models dox-induced increase in LC3II at 12 h or later. [71, 100, 113, 147]. Interestingly, using H9C2 in serum free conditions, Bartlett et al. showed a transient increase of LC3II at 2 h and its later decrease vs ctl at 24 h. The variety of cell culture models and medium composition are probably affecting the measured dox effects.

Still, the molecular analysis of our NRVM at 16 h and female cardiac lysates at 24 h showed similar results thus suggesting that we might use this in vitro model to analyze early metabolic pathways changes.

4.2.3. NRG-1 PREVENTS DOX-INDUCED LC3II, AT 1 H, AND INHIBITS THE FOXO1 TRANSCRIPTIONAL ACTIVITY.

The use of our NRVM model allowed us to show that dox induces increased levels of LC3II already 30 min after its addition to cells, highlighting that this dox-induced stress response is an

acute event. Yet, few of the available studies investigated the effect of dox on the autophagic flux and only settled on the LC3 protein expression and lipidation [148].

Still, our data show that the NRG-1-induced inhibition of the autophagic flux and the NRG-1-induced increase of ULK1-pS757 can already be observed at 1 h, in presence or absence of dox treatment. This indicates that NRG-1 prevents the early dox-induced increase in LC3II, and it could be by this mechanism that NRG-1 exerts cardioprotective effects toward dox. At 1 h, the NRG/dox treated cells showed increased FoxO1-pT24 phosphorylated levels and cytoplasmic location/exclusion, whereas at 6 h, decreased mRNA expression of LC3 and ULK1, 2 FoxO1 target genes, was observed. These data suggest that in addition to inhibiting autophagy initiation, NRG-1 inhibits the expression of autophagy related genes by sequestrating FoxO1 in the cytoplasm in our NRVM model. The NRG/dox effects couldn't be observed in cardiac lysates of male or female mice at 24 h. This difference could be due to sacrifice timing issue, or to neonate vs adult models. Still, Ennequin et al. previously showed that NRG-1β2a stimulation could trigger FoxO1-pS256 phosphorylation, which has the same function as the pT24, in murine liver [19, 149].

4.2.4. Dox decreases mitochondrial content and induces compensatory succinate dehydrogenase activity at 3 h in NRVM

On one hand, dox is known to have mitochondrial tropism. It binds to the mitochondrial complex I of the mitochondrial respiratory chain and contributes to decreased production of ATP in the cell. Moreover, dox has also been showed by Schlattner and colleagues to disturb the cellular energy buffer and transport system based on creatine Cr and phosphocreatine PCr [52, 150]. Numerous studies have described dox-induced decreases in mitochondrial content and quality, notably associated with dox-induced mitophagy disturbances [151]. On the other hand, NRG-1 is a growth factor known to enhance glucose uptake in skeletal muscle and cardiac myocytes. NRG-1 also has been shown to improve complex-II mediated mitochondrial respiration in mouse gastrocnemius [77, 120, 152]. Furthermore, controversial studies suggest that NRG-1 might induce mitochondrial biogenesis [120, 121]. Therefore, we addressed the question: does dox change mitochondrial content and function in our NRVM model and if so, does NRG-1 prevent this?

Our results show that at 3 h, dox decreased the mitochondrial content and induced a compensatory increase in mitochondrial complex II activity with preserved total ATP amounts, while the NRG/dox were not different from the control conditions. This suggesting that at 3 h, NRG-1 prevents mitochondrial loss of mass and compensatory respiratory response of NRVM to dox treatment. At 16 h, the dox-induced compensatory increase of succinate dehydrogenase

was not observed anymore, and the loss of mitochondrial mass was stronger than at 3 h. NRG-1 effects on dox induced mitochondrial contents at 16 h couldn't be confirmed as more experiments are needed due to high variability.

However, at 6 h NRG-1 did not prevent dox-induced decreases in PGC-1α mRNA levels, suggesting that if NRG-1 prevents dox-induced loss of mitochondrial mass it might not be through upregulation of the genes related to mitochondrial biogenesis. Yet, PGC-1α and other biogenesis actors have to be quantified at the protein level to draw any conclusion on NRG-1 induced biogenesis effects. Based on these data, it would be of interest to study whether NRG-1 prevents mitochondrial compartment loss at 3 h by modulating mitophagy, as NRG-1 has been shown to modulate the autophagic pathway in numerus studies and in our present work [97-100].

4.2.5. Outlook for IGF and NRG-1 cross talk?

IGF-I is known to have cardioprotective properties in the context of heart failure and cardiotoxicity [153]. The more the IGF-I receptor (IGF-IR) is activated, the more the protective mechanisms are activated due to stress. Interestingly, when we analyzed IGF-IR phosphorylation in the 3 weeks animals. The IGF-IR-phosphorylation was correlated with the effects of dox. When we ranked the animals, the highest phosphorylation rates were in the dox groups, while the intermediate ranks were mostly attributed to the nrg/dox group. These data suggest that NRG-1 was protective toward dox-induced cardiotoxicity.

This is of note, because previous experiments in our laboratory have revealed an additive effect of the NRG-1 in IGF-I or insulin-stimulated NRVMs. Also, in astrocytes, IGF and NRG-1 co-treatment have been shown to increase mitochondrial biogenesis [121]. Moreover, we have to keep in mind that dox-treated mice do secrete endogenous NRG-1. Some more characterization of potential cross talk of NRG-1and IGF in the context of heart disease might be considered in future studies.

5. CONCLUSIONS AND PERSPECTIVES

This study characterized for the first time the effects of a new non-daily NRG-1 regimen in a dox-treatment protocol on long term cardiac modulations in male and female mice. Thereby, we showed in vivo that dox has a higher toxicity in males than in females, consistent with the literature. While dox induced cardiac compensatory response in males, females underwent much milder cardiac toxicity event. Our major finding there was the preventive effects of the NRG-1 treatment on the male's compensatory response, revealed by ultrasound. Surprisingly, evidences for mortality related to the NRG-1 therapy were measured in both sex, and further experiments would be required to define whether our NRG-1 regimen was deleterious on the mice survival upon dox-treatment.

Secondly, we aimed to uncover by which mechanisms the NRG-1 could exert cardioprotective effects with a special focus on the autophagic pathway. We showed for the first time that 24 h after a single injection of our protocol, dox strongly decreased the LC3II/I in males while it did not in females. NRG-1 restimulation did not induce any effect in males, while in females NRG-1 did decrease LC3II/I ratios vs dox. These results highlighted sex-difference in response to dox at the molecular levels at 24 h. Similarly, NRG-1 only had effects in females at that time point. These data suggest that more investigations of sex-related response to NRG-1 should be investigated to address NRG-1 as a preventive treatment with the best benefit-to-risk balance as possible.

Finally, the use of NRVM model allowed us to point the mechanisms whereby NRG-1 could have a protective effect in cardiomyocytes at 1 h toward dox-induced autophagy disturbance. In this cell culture model, NRG-1 prevented dox-induced autophagy by blocking the autophagic flux at the initiation step. This was associated with the inhibition of the ULK1 protein. Moreover, for the first time our data show that NRG-1 prevented FoxO1 transcriptional activity by sequestering it in the cytoplasm. Therefore, decrease of the ULK1 and LC3B gene expression was observed at 6 h. Finally, preliminary data showed that NRG-1 prevented dox-induced decrease in mitochondrial contents, it would be of interest to investigate whether it was due to a decrease in mitochondrial clearance, or an amelioration of the mitochondrial function by sea horse experiments as an example.

In the future it would be of interest to evaluate ex vivo, in an adult system the observations we did in NRVM. Characterizing in further details the sex-differences of NRG-1 single injections and regimens on cardiac molecular events would be of highest interests and allow to ensure personalized-medicine treatments. Finally, in the laboratory, the establishment of a mice model

of xenograft breast tumor would also of interest. In the future we plan to treat the mice with dox, and it would be of high interest to assess 1) if the NRG-1 has protective effects toward dox-induced cardiac toxicity in this model, and 2) the effects of NRG-1 on the tumor regression.

6. ACKNOWLEDGEMENTS

First of all, I want to thank Prof. Marijke Brink to have allowed me to participate in this great and exciting scientific adventure. To have taken time to answer my questions helped me to better understand unexpected results, and therefore to have taught me so much about cardiac physiology and research in general. I have learned a lot, and I am really thankful for this.

I want to particularly thank Christian Morandi for his technical support with the Western blot mystical art and other molecular analyses, but also for the nice advices concerning Swiss cultural to do. I also wish to thank Lifen Xu for performing the echocardiography analysis and furthermore for her help and valuable discussions about the experiments related to my project, or other scientific topics, and all these hours we spent to take care of the animals downstairs, which were rewarded with our tea-time-lunches filled with so much cultural exchanges. I thank Meryem Alioui for doing some of the RT-qPCR analysis and Vivienne Grüterich for her contributions to the final cell culture experiments.

I also wish to thank all the other former or current members of the lab: Philippe, Gian, Hagena, Matthias, Tanja, Benedikt, Parisa. I wish to thank them all for their entertaining mood, the happy ambiance brought to the lab and also all these cultural exchanges which occurred for these 4 last years it was a great pleasure to work with you all, and enjoy our famous TGIFs (one day who knows I might be able to speak German with you?).

I also wish to thank the "French connection" and other marvelous people I have been able to meet here in Basel notably by taking part in the PhD club committee, thank you all for the great time there and all our scientific or less scientific discussions (would you know the joke of the yellow Dwarf….). Many thanks to my "co-PhDs" Adelin, Hailey, Cecile, Anna, Lulu, Madhuri particularly, and all the others.

Moreover, I want to thank Prof. Dario Diviani, Prof. Christoph Handschin, and Prof. Benoit Pourcet to have benevolently supervised my PhD project, as well as Prof. Susan Treves to have accepted to chair my examination.

Finally, I wish to especially thank my partner to have been so supportive and patient, sometimes with the finest jokes ever to cheer me up the days I was needing it.

7. REFERENCES

1. Neubauer S. The failing heart--an engine out of fuel. *N Engl J Med*. 2007;356:1140-51.

2. Lopaschuk GD, Karwi QG, Tian R, Wende AR and Abel ED. Cardiac Energy Metabolism in Heart Failure. *Circ Res*. 2021;128:1487-1513.

3. Stanley WC, Recchia FA and Lopaschuk GD. Myocardial substrate metabolism in the normal and failing heart. *Physiol Rev*. 2005;85:1093-129.

4. Karwi QG and Lopaschuk GD. Branched-Chain Amino Acid Metabolism in the Failing Heart. *Cardiovascular Drugs and Therapy*. 2022:1-8.

5. Taegtmeyer H, Golfman L, Sharma S, Razeghi P and van Arsdall M. Linking gene expression to function: metabolic flexibility in the normal and diseased heart. *Ann N Y Acad Sci*. 2004;1015:202-13.

6. Kuang M, Febbraio M, Wagg C, Lopaschuk GD and Dyck JR. Fatty acid translocase/CD36 deficiency does not energetically or functionally compromise hearts before or after ischemia. *Circulation*. 2004;109:1550-7.

7. Schulze PC, Drosatos K and Goldberg IJ. Lipid Use and Misuse by the Heart. *Circ Res*. 2016;118:1736-51.

8. Luiken JJ, Glatz JF and Neumann D. Cardiac contraction-induced GLUT4 translocation requires dual signaling input. *Trends Endocrinol Metab*. 2015;26:404-10.

9. Hardie DG, Carling D and Carlson M. The AMP-activated/SNF1 protein kinase subfamily: metabolic sensors of the eukaryotic cell? *Annu Rev Biochem*. 1998;67:821-55.

10. Xiao B, Heath R, Saiu P, Leiper FC, Leone P, Jing C, Walker PA, Haire L, Eccleston JF, Davis CT, Martin SR, Carling D and Gamblin SJ. Structural basis for AMP binding to mammalian AMP-activated protein kinase. *Nature*. 2007;449:496-500.

11. Hawley SA, Davison M, Woods A, Davies SP, Beri RK, Carling D and Hardie DG. Characterization of the AMP-activated protein kinase kinase from rat liver and identification of threonine 172 as the major site at which it phosphorylates AMP-activated protein kinase. *J Biol Chem*. 1996;271:27879-87.

12. Luiken JJ, Coort SL, Willems J, Coumans WA, Bonen A, van der Vusse GJ and Glatz JF. Contraction-induced fatty acid translocase/CD36 translocation in rat cardiac myocytes is mediated through AMP-activated protein kinase signaling. *Diabetes*. 2003;52:1627-34.

13. Russel M. Current status of genetic discoveries in cluster headache. *Ital J Neurol Sci*. 1999;20:S7-9.

14. Russell III RR, Bergeron R, Shulman GI and Young LH. Translocation of myocardial GLUT-4 and increased glucose uptake through activation of AMPK by AICAR. *American Journal of Physiology-Heart and Circulatory Physiology*. 1999;277:H643-H649.

15. Marsin AS, Bertrand L, Rider MH, Deprez J, Beauloye C, Vincent MF, Van den Berghe G, Carling D and Hue L. Phosphorylation and activation of heart PFK-2 by AMPK has a role in the stimulation of glycolysis during ischaemia. *Curr Biol*. 2000;10:1247-55.

16. Park H, Kaushik VK, Constant S, Prentki M, Przybytkowski E, Ruderman NB and Saha AK. Coordinate regulation of malonyl-CoA decarboxylase, sn-glycerol-3-phosphate acyltransferase, and acetyl-CoA carboxylase by AMP-activated protein kinase in rat tissues in response to exercise. *J Biol Chem*. 2002;277:32571-7.

17. Hardie DG and Sakamoto K. AMPK: a key sensor of fuel and energy status in skeletal muscle. *Physiology (Bethesda)*. 2006;21:48-60.

18. Ratman D, Mylka V, Bougarne N, Pawlak M, Caron S, Hennuyer N, Paumelle R, De Cauwer L, Thommis J, Rider MH, Libert C, Lievens S, Tavernier J, Staels B and De Bosscher K. Chromatin recruitment of activated AMPK drives fasting response genes co-controlled by GR and PPARalpha. *Nucleic Acids Res*. 2016;44:10539-10553.

19. Cheng Z. The FoxO-Autophagy Axis in Health and Disease. *Trends Endocrinol Metab*. 2019;30:658-671.

20. Shin H-JR, Kim H, Oh S, Lee J-G, Kee M, Ko H-J, Kweon M-N, Won K-J and Baek SH. AMPK–SKP2–CARM1 signalling cascade in transcriptional regulation of autophagy. *Nature*. 2016;534:553-557.

21. Beauloye C, Bertrand L, Horman S and Hue L. AMPK activation, a preventive therapeutic target in the transition from cardiac injury to heart failure. *Cardiovascular Research*. 2011;90:224-233.

22. Taneike M, Yamaguchi O, Nakai A, Hikoso S, Takeda T, Mizote I, Oka T, Tamai T, Oyabu J, Murakawa T, Nishida K, Shimizu T, Hori M, Komuro I, Takuji Shirasawa TS, Mizushima N and Otsu K. Inhibition of autophagy in the heart induces age-related cardiomyopathy. *Autophagy*. 2010;6:600-606.

23. Wang ZV and Hill JA. Protein quality control and metabolism: bidirectional control in the heart. *Cell Metab*. 2015;21:215-226.

24. Haubner BJ, Adamowicz-Brice M, Khadayate S, Tiefenthaler V, Metzler B, Aitman T and Penninger JM. Complete cardiac regeneration in a mouse model of myocardial infarction. *Aging (Albany NY)*. 2012;4:966-77.

25. Koleini N and Kardami E. Autophagy and mitophagy in the context of doxorubicin-induced cardiotoxicity. *Oncotarget*. 2017;8:46663.

26. Aman Y, Schmauck-Medina T, Hansen M, Morimoto RI, Simon AK, Bjedov I, Palikaras K, Simonsen A, Johansen T, Tavernarakis N, Rubinsztein DC, Partridge L, Kroemer G, Labbadia J and Fang EF. Autophagy in healthy aging and disease. *Nat Aging*. 2021;1:634-650.

27. Liao Y, Takashima S, Maeda N, Ouchi N, Komamura K, Shimomura I, Hori M, Matsuzawa Y, Funahashi T and Kitakaze M. Exacerbation of heart failure in adiponectin-deficient mice due to impaired regulation of AMPK and glucose metabolism. *Cardiovasc Res*. 2005;67:705-13.

28. Abdellatif M, Sedej S, Carmona-Gutierrez D, Madeo F and Kroemer G. Autophagy in Cardiovascular Aging. *Circulation Research*. 2018;123:803-824.

29. Cao DJ, Jiang N, Blagg A, Johnstone JL, Gondalia R, Oh M, Luo X, Yang KC, Shelton JM, Rothermel BA, Gillette TG, Dorn GW and Hill JA. Mechanical unloading activates FoxO3 to trigger Bnip3-dependent cardiomyocyte atrophy. *J Am Heart Assoc*. 2013;2:e000016.

30. Chen C, Lu L, Yan S, Yi H, Yao H, Wu D, He G, Tao X and Deng X. Autophagy and doxorubicin resistance in cancer. *Anticancer Drugs*. 2018;29:1-9.

31. Zhang L, Jaswal JS, Ussher JR, Sankaralingam S, Wagg C, Zaugg M and Lopaschuk GD. Cardiac insulin-resistance and decreased mitochondrial energy production precede the development of systolic heart failure after pressure-overload hypertrophy. *Circ Heart Fail*. 2013;6:1039-48.

32. Tian R, Musi N, D'Agostino J, Hirshman MF and Goodyear LJ. Increased adenosine monophosphate–activated protein kinase activity in rat hearts with pressure-overload hypertrophy. *Circulation*. 2001;104:1664-1669.

33. Diakos NA, Navankasattusas S, Abel ED, Rutter J, McCreath L, Ferrin P, McKellar SH, Miller DV, Park SY, Richardson RS, Deberardinis R, Cox JE, Kfoury AG, Selzman CH, Stehlik J, Fang JC, Li DY and Drakos SG. Evidence of Glycolysis Up-Regulation and Pyruvate Mitochondrial Oxidation Mismatch During Mechanical Unloading of the Failing Human Heart: Implications for Cardiac Reloading and Conditioning. *JACC Basic Transl Sci*. 2016;1:432-444.

34. Gupta MP. Factors controlling cardiac myosin-isoform shift during hypertrophy and heart failure. *J Mol Cell Cardiol*. 2007;43:388-403.

35. Meiners B, Shenoy C and Zordoky BN. Clinical and preclinical evidence of sex-related differences in anthracycline-induced cardiotoxicity. *Biology of sex differences*. 2018;9:38.

36. 1 - Discovery and Development of Doxorubicin. *Medicinal Chemistry*. 1981;17:1-47.

37. Tacar O and Dass CR. Doxorubicin-induced death in tumour cells and cardiomyocytes: is autophagy the key to improving future clinical outcomes? *J Pharm Pharmacol*. 2013;65:1577-89.

38. Thorn CF, Oshiro C, Marsh S, Hernandez-Boussard T, McLeod H, Klein TE and Altman RB. Doxorubicin pathways: pharmacodynamics and adverse effects. *Pharmacogenetics and genomics*. 2011;21:440.

39. Singal PK and Iliskovic N. Doxorubicin-induced cardiomyopathy. *N Engl J Med*. 1998;339:900-5.

40. Danúbia Silva dos S and Regina Coeli dos Santos G. Doxorubicin-Induced Cardiotoxicity: From Mechanisms to Development of Efficient Therapy. 2018.

41. Bartlett JJ, Trivedi PC and Pulinilkunnil T. Autophagic dysregulation in doxorubicin cardiomyopathy. *Journal of molecular and cellular cardiology*. 2017;104:1-8.

42. Rui Adão CM-R, Diana Santos-Ribeiro, Pedro Mendes-Ferreira1, Adelino F. Leite-Moreira and Carmen Brás-Silva. *Cardiotoxicity of Cancer Chemotherapy–Recent Developments*. Frontiers in Drug Design & Discovery; 2015.

43. Raj S, Franco VI and Lipshultz SE. Anthracycline-induced cardiotoxicity: a review of pathophysiology, diagnosis, and treatment. *Curr Treat Options Cardiovasc Med*. 2014;16:315.

44. Takemura G and Fujiwara H. Doxorubicin-induced cardiomyopathy from the cardiotoxic mechanisms to management. *Prog Cardiovasc Dis*. 2007;49:330-52.

45. Jain D, Russell RR, Schwartz RG, Panjrath GS and Aronow W. Cardiac Complications of Cancer Therapy: Pathophysiology, Identification, Prevention, Treatment, and Future Directions. *Curr Cardiol Rep*. 2017;19:36.

46. Voigt J, Sasha John M, Taylor A, Krucoff M, Reynolds MR and Michael Gibson C. A reevaluation of the costs of heart failure and its implications for allocation of health resources in the United States. *Clin Cardiol*. 2014;37:312-21.

47. Lenneman CG and Sawyer DB. Cardio-Oncology: An Update on Cardiotoxicity of Cancer-Related Treatment. *Circ Res*. 2016;118:1008-20.

48. Lipshultz SE, Lipsitz SR, Mone SM, Goorin AM, Sallan SE, Sanders SP, Orav EJ, Gelber RD and Colan SD. Female sex and higher drug dose as risk factors for late cardiotoxic effects of doxorubicin therapy for childhood cancer. *N Engl J Med*. 1995;332:1738-43.

49. Hershman DL, McBride RB, Eisenberger A, Tsai WY, Grann VR and Jacobson JS. Doxorubicin, cardiac risk factors, and cardiac toxicity in elderly patients with diffuse B-cell non-Hodgkin's lymphoma. *J Clin Oncol*. 2008;26:3159-65.

50. Fornari FA, Randolph JK, Yalowich JC, Ritke MK and Gewirtz DA. Interference by doxorubicin with DNA unwinding in MCF-7 breast tumor cells. *Mol Pharmacol*. 1994;45:649-56.

51. Carvalho FS, Burgeiro A, Garcia R, Moreno AJ, Carvalho RA and Oliveira PJ. Doxorubicin-induced cardiotoxicity: from bioenergetic failure and cell death to cardiomyopathy. *Med Res Rev*. 2014;34:106-35.

52. Cappetta D, Rossi F, Piegari E, Quaini F, Berrino L, Urbanek K and De Angelis A. Doxorubicin targets multiple players: A new view of an old problem. *Pharmacol Res*. 2018;127:4-14.

53. Ichikawa Y, Ghanefar M, Bayeva M, Wu R, Khechaduri A, Prasad SVN, Mutharasan RK, Naik TJ and Ardehali H. Cardiotoxicity of doxorubicin is mediated through mitochondrial iron accumulation. *The Journal of clinical investigation*. 2014;124:617-630.

54. Mitry MA and Edwards JG. Doxorubicin induced heart failure: Phenotype and molecular mechanisms. *Int J Cardiol Heart Vasc*. 2016;10:17-24.

55. Zhou P and Pu WT. Recounting Cardiac Cellular Composition. *Circ Res*. 2016;118:368-70.

56. Page E and McCallister LP. Quantitative electron microscopic description of heart muscle cells. Application to normal, hypertrophied and thyroxin-stimulated hearts. *Am J Cardiol*. 1973;31:172-81.

57. Ventura-Clapier R, Garnier A and Veksler V. Energy metabolism in heart failure. *J Physiol*. 2004;555:1-13.

58. Moulin M, Solgadi A, Veksler V, Garnier A, Ventura-Clapier R and Chaminade P. Sex-specific cardiac cardiolipin remodelling after doxorubicin treatment. *Biol Sex Differ*. 2015;6:20.

59. Sun XP, Wan LL, Yang QJ, Huo Y, Han YL and Guo C. Scutellarin protects against doxorubicin-induced acute cardiotoxicity and regulates its accumulation in the heart. *Arch Pharm Res*. 2017;40:875-883.

60. Couture L, Nash JA and Turgeon J. Role of ATP-binding cassette transporters in drug distribution to the heart and protection from toxic compounds. *Heart and metabolism*. 2007;35:16-21.

61. Sawyer DB, Zuppinger C, Miller TA, Eppenberger HM and Suter TM. Modulation of anthracycline-induced myofibrillar disarray in rat ventricular myocytes by neuregulin-1β and anti-erbB2: potential mechanism for trastuzumab-induced cardiotoxicity. *Circulation*. 2002;105:1551-1554.

62. Lim CC, Zuppinger C, Guo X, Kuster GM, Helmes M, Eppenberger HM, Suter TM, Liao R and Sawyer DB. Anthracyclines induce calpain-dependent titin proteolysis and necrosis in cardiomyocytes. *Journal of Biological Chemistry*. 2004;279:8290-8299.

63. Tokarska-Schlattner M, Zaugg M, da Silva R, Lucchinetti E, Schaub MC, Wallimann T and Schlattner U. Acute toxicity of doxorubicin on isolated perfused heart: response of kinases regulating energy supply. *Am J Physiol Heart Circ Physiol*. 2005;289:H37-47.

64. Tokarska-Schlattner M, Wallimann T and Schlattner U. Alterations in myocardial energy metabolism induced by the anti-cancer drug doxorubicin. *C R Biol*. 2006;329:657-68.

65. Abdel-aleem S, el-Merzabani MM, Sayed-Ahmed M, Taylor DA and Lowe JE. Acute and chronic effects of adriamycin on fatty acid oxidation in isolated cardiac myocytes. *J Mol Cell Cardiol*. 1997;29:789-97.

66. Hrelia S, Fiorentini D, Maraldi T, Angeloni C, Bordoni A, Biagi PL and Hakim G. Doxorubicin induces early lipid peroxidation associated with changes in glucose transport in cultured cardiomyocytes. *Biochimica et Biophysica Acta (BBA)-Biomembranes*. 2002;1567:150-156.

67. Jeyaseelan R, Poizat C, Wu H-Y and Kedes L. Molecular Mechanisms of Doxorubicin-induced Cardiomyopathy: SELECTIVE SUPPRESSION OF REISKE IRON-SULFUR PROTEIN, ADP/ATP TRANSLOCASE, AND PHOSPHOFRUCTOKINASE GENES IS ASSOCIATED WITH ATP DEPLETION IN RAT CARDIOMYOCYTES *. *Journal of Biological Chemistry*. 1997;272:5828-5832.

68. Renu K, V GA, P BT and Arunachalam S. Molecular mechanism of doxorubicin-induced cardiomyopathy - An update. *Eur J Pharmacol*. 2018;818:241-253.

69. Arunachalam S, Pichiah PT and Achiraman S. Doxorubicin treatment inhibits PPARγ and may induce lipotoxicity by mimicking a type 2 diabetes-like condition in rodent models. *FEBS letters*. 2013;587:105-110.

70. Li M, Sala V, De Santis MC, Cimino J, Cappello P, Pianca N, Di Bona A, Margaria JP, Martini M and Lazzarini E. Phosphoinositide 3-kinase gamma inhibition protects from anthracycline cardiotoxicity and reduces tumor growth. *Circulation*. 2018;138:696-711.

71. Dimitrakis P, Romay-Ogando M-I, Timolati F, Suter TM and Zuppinger C. Effects of doxorubicin cancer therapy on autophagy and the ubiquitin-proteasome system in long-term cultured adult rat cardiomyocytes. *Cell and tissue research*. 2012;350:361-372.

72. Li DL, Wang ZV, Ding G, Tan W, Luo X, Criollo A, Xie M, Jiang N, May H and Kyrychenko V. Doxorubicin blocks cardiomyocyte autophagic flux by inhibiting lysosome acidification. *Circulation*. 2016;133:1668-1687.

73. Bian Y, Silver M, Onufrak J, Ho KK, Marchionni MA, Kang PM, Goukassian DA, Carrozza J, Morgan JP and Yan X. Neuregulin1 Improved Cardiac Function in Doxorubicin-Treated Mice with Cardiomyocyte-Specific over expression of a Dominant-Negative PI3Kp110Î±. *Journal of Cardiovascular Diseases & Diagnosis*. 2013;2013.

74. Jay SM, Murthy AC, Hawkins JF, Wortzel JR, Steinhauser ML, Alvarez LM, Gannon J, Macrae CA, Griffith LG and Lee RT. An engineered bivalent neuregulin protects against doxorubicin-induced cardiotoxicity with reduced proneoplastic potential. *Circulation*. 2013;128:152-161.

75. Podyacheva EY, Kushnareva EA, Karpov AA and Toropova YG. Analysis of Models of Doxorubicin-Induced Cardiomyopathy in Rats and Mice. A Modern View From the Perspective of the Pathophysiologist and the Clinician. *Front Pharmacol*. 2021;12:670479.

76. Moulin M, Piquereau J, Mateo P, Fortin D, Rucker-Martin C, Gressette M, Lefebvre F, Gresikova M, Solgadi A, Veksler V, Garnier A and Ventura-Clapier R. Sexual dimorphism of doxorubicin-mediated cardiotoxicity: potential role of energy metabolism remodeling. *Circ Heart Fail*. 2015;8:98-108.

77. Gumà A, Martínez-Redondo V, López-Soldado I, Cantó C and Zorzano A. Emerging role of neuregulin as a modulator of muscle metabolism. *American Journal of Physiology-Endocrinology and Metabolism*. 2010;298:E742-E750.

78. Cote GM, Miller TA, Lebrasseur NK, Kuramochi Y and Sawyer DB. Neuregulin-1alpha and beta isoform expression in cardiac microvascular endothelial cells and function in cardiac myocytes in vitro. *Exp Cell Res*. 2005;311:135-46.

79. Falls DL. Neuregulins: functions, forms, and signaling strategies. *The EGF Receptor Family*. 2003:15-31.

80. Lee KF, Simon H, Chen H, Bates B, Hung MC and Hauser C. Requirement for neuregulin receptor erbB2 in neural and cardiac development. *Nature*. 1995;378:394-8.

81. Meyer D and Birchmeier C. Multiple essential functions of neuregulin in development. *Nature*. 1995;378:386-90.

82. Liu X, Hwang H, Cao L, Buckland M, Cunningham A, Chen J, Chien KR, Graham RM and Zhou M. Domain-specific gene disruption reveals critical regulation of neuregulin signaling by its cytoplasmic tail. *Proc Natl Acad Sci U S A*. 1998;95:13024-9.

83. Erickson SL, O'Shea KS, Ghaboosi N, Loverro L, Frantz G, Bauer M, Lu LH and Moore MW. ErbB3 is required for normal cerebellar and cardiac development: a comparison with ErbB2-and heregulin-deficient mice. *Development*. 1997;124:4999-5011.

84. Wang Z, Xu G, Wu Y, Guan Y, Cui L, Lei X, Zhang J, Mou L, Sun B and Dai Q. Neuregulin-1 enhances differentiation of cardiomyocytes from embryonic stem cells. *Med Biol Eng Comput*. 2009;47:41-8.

85. D'Uva G, Aharonov A, Lauriola M, Kain D, Yahalom-Ronen Y, Carvalho S, Weisinger K, Bassat E, Rajchman D and Yifa O. ERBB2 triggers mammalian heart regeneration by promoting cardiomyocyte dedifferentiation and proliferation. *Nature cell biology*. 2015;17:627-638.

86. Golding JP, Trainor P, Krumlauf R and Gassmann M. Defects in pathfinding by cranial neural crest cells in mice lacking the neuregulin receptor ErbB4. *Nat Cell Biol*. 2000;2:103-9.

87. Forster N, Saladi SV, van Bragt M, Sfondouris ME, Jones FE, Li Z and Ellisen LW. Basal cell signaling by p63 controls luminal progenitor function and lactation via NRG1. *Dev Cell*. 2014;28:147-60.

88. Dean-Colomb W and Esteva FJ. Her2-positive breast cancer: herceptin and beyond. *European Journal of Cancer*. 2008;44:2806-2812.

89. Vasti C, Witt H, Said M, Sorroche P, Garcia-Rivello H, Ruiz-Noppinger P and Hertig CM. Doxorubicin and NRG-1/erbB4-Deficiency Affect Gene Expression Profile: Involving Protein Homeostasis in Mouse. *ISRN Cardiol*. 2012;2012:745185.

90. Liu FF, Stone JR, Schuldt AJ, Okoshi K, Okoshi MP, Nakayama M, Ho KK, Manning WJ, Marchionni MA, Lorell BH, Morgan JP and Yan X. Heterozygous knockout of neuregulin-1 gene in mice exacerbates doxorubicin-induced heart failure. *Am J Physiol Heart Circ Physiol*. 2005;289:H660-6.

91. Lemmens K, Doggen K and De Keulenaer GW. Activation of the neuregulin/ErbB system during physiological ventricular remodeling in pregnancy. *Am J Physiol Heart Circ Physiol*. 2011;300:H931-42.

92. Fang SJ, Wu XS, Han ZH, Zhang XX, Wang CM, Li XY, Lu LQ and Zhang JL. Neuregulin-1 preconditioning protects the heart against ischemia/reperfusion injury through a PI3K/Akt-dependent mechanism. *Chin Med J (Engl)*. 2010;123:3597-604.

93. Liu X, Gu X, Li Z, Li X, Li H, Chang J, Chen P, Jin J, Xi B, Chen D, Lai D, Graham RM and Zhou M. Neuregulin-1/erbB-activation improves cardiac function and survival in models of ischemic, dilated, and viral cardiomyopathy. *J Am Coll Cardiol*. 2006;48:1438-47.

94. García-Rivello H, Taranda J, Said M, Cabeza-Meckert P, Vila-Petroff M, Scaglione J, Ghio S, Chen J, Lai C and Laguens RP. Dilated cardiomyopathy in Erb-b4-deficient ventricular muscle. *American journal of physiology-heart and circulatory physiology*. 2005;289:H1153-H1160.

95. Zurek M, Johansson E, Palmer M, Albery T, Johansson K, Rydén-Markinhutha K and Wang QD. Neuregulin-1 Induces Cardiac Hypertrophy and Impairs Cardiac Performance in Post-Myocardial Infarction Rats. *Circulation*. 2020;142:1308-1311.

96. Baliga RR, Pimental DR, Zhao Y-Y, Simmons WW, Marchionni MA, Sawyer DB and Kelly RA. NRG-1-induced cardiomyocyte hypertrophy. Role of PI-3-kinase, p70S6K, and MEK-MAPK-RSK. *American Journal of Physiology-Heart and Circulatory Physiology*. 1999;277:H2026-H2037.

97. Tal-Or P, Di-Segni A, Lupowitz Z and Pinkas-Kramarski R. Neuregulin promotes autophagic cell death of prostate cancer cells. *Prostate*. 2003;55:147-57.

98. Schmukler E, Shai B, Ehrlich M and Pinkas-Kramarski R. Neuregulin promotes incomplete autophagy of prostate cancer cells that is independent of mTOR pathway inhibition. *PLoS One*. 2012;7:e36828.

99. Yin D, Lin D, Xie Y, Gong A, Jiang P and Wu J. Neuregulin-1β Alleviates Sepsis-Induced Skeletal Muscle Atrophy by Inhibiting Autophagy via AKT/mTOR Signaling Pathway In Rats. *Shock*. 2021.

100. An T, Huang Y, Zhou Q, Wei BQ, Zhang RC, Yin SJ, Zou CH, Zhang YH and Zhang J. Neuregulin-1 attenuates doxorubicin-induced autophagy in neonatal rat cardiomyocytes. *J Cardiovasc Pharmacol*. 2013;62:130-7.

101. Smith HW, Hirukawa A, Sanguin-Gendreau V, Nandi I, Dufour CR, Zuo D, Tandoc K, Leibovitch M, Singh S and Rennhack JP. An ErbB2/c-Src axis links bioenergetics with PRC2 translation to drive epigenetic reprogramming and mammary tumorigenesis. *Nature communications*. 2019;10:1-19.

102. Miao W, Luo Z, Kitsis RN and Walsh K. Intracoronary, adenovirus-mediated Akt gene transfer in heart limits infarct size following ischemia-reperfusion injury in vivo. *Journal of molecular and cellular cardiology*. 2000;32:2397-2402.

103. Suy S, Anderson WB, Dent P, Chang E and Kasid U. Association of Grb2 with Sos and Ras with Raf-1 upon gamma irradiation of breast cancer cells. *Oncogene*. 1997;15:53-61.

104. Wang Z. *ErbB Receptor Signaling: Methods and Protocols*: Springer; 2017.

105. Mutlak M and Kehat I. Extracellular signal-regulated kinases 1/2 as regulators of cardiac hypertrophy. *Frontiers in pharmacology*. 2015;6:149.

106. Mendoza MC, Er EE and Blenis J. The Ras-ERK and PI3K-mTOR pathways: cross-talk and compensation. *Trends in biochemical sciences*. 2011;36:320-328.

107. Giraud M-N, Fluck M, Zuppinger C and Suter TM. Expressional reprogramming of survival pathways in rat cardiocytes by neuregulin-1β. *Journal of applied physiology*. 2005;99:313-322.

108. Ueyama T, Kawashima S, Sakoda T, Rikitake Y, Ishida T, Kawai M, Yamashita T, Ishido S, Hotta H and Yokoyama M. Requirement of activation of the extracellular signal-regulated kinase cascade in myocardial cell hypertrophy. *Journal of molecular and cellular cardiology*. 2000;32:947-960.

109. Kuramochi Y, Guo X and Sawyer DB. Neuregulin activates erbB2-dependent src/FAK signaling and cytoskeletal remodeling in isolated adult rat cardiac myocytes. *J Mol Cell Cardiol*. 2006;41:228-35.

110. Bayer AL, Heidkamp MC, Patel N, Porter MJ, Engman SJ and Samarel AM. PYK2 expression and phosphorylation increases in pressure overload-induced left ventricular

hypertrophy. *American Journal of Physiology-Heart and Circulatory Physiology*. 2002;283:H695-H706.

111. Mansour H, de Tombe PP, Samarel AM and Russell B. Restoration of resting sarcomere length after uniaxial static strain is regulated by protein kinase Cepsilon and focal adhesion kinase. *Circ Res*. 2004;94:642-9.

112. Abu-Ghazaleh R, Kabir J, Jia H, Lobo M and Zachary I. Src mediates stimulation by vascular endothelial growth factor of the phosphorylation of focal adhesion kinase at tyrosine 861, and migration and anti-apoptosis in endothelial cells. *Biochem J*. 2001;360:255-64.

113. Chen K, Xu X, Kobayashi S, Timm D, Jepperson T and Liang Q. Caloric restriction mimetic 2-deoxyglucose antagonizes doxorubicin-induced cardiomyocyte death by multiple mechanisms. *Journal of biological chemistry*. 2011;286:21993-22006.

114. Kawaguchi T, Takemura G, Kanamori H, Takeyama T, Watanabe T, Morishita K, Ogino A, Tsujimoto A, Goto K and Maruyama R. Prior starvation mitigates acute doxorubicin cardiotoxicity through restoration of autophagy in affected cardiomyocytes. *Cardiovascular research*. 2012;96:456-465.

115. Shende P, Plaisance I, Morandi C, Pellieux C, Berthonneche C, Zorzato F, Krishnan J, Lerch R, Hall MN, Ruegg MA, Pedrazzini T and Brink M. Cardiac raptor ablation impairs adaptive hypertrophy, alters metabolic gene expression, and causes heart failure in mice. *Circulation*. 2011;123:1073-82.

116. Milano G, Raucci A, Scopece A, Daniele R, Guerrini U, Sironi L, Cardinale D, Capogrossi MC and Pompilio G. Doxorubicin and trastuzumab regimen induces biventricular failure in mice. *Journal of the American Society of Echocardiography*. 2014;27:568-579.

117. Nagiub M, Filippone S, Durrant D, Das A and Kukreja RC. Long-acting PDE5 inhibitor tadalafil prevents early doxorubicin-induced left ventricle diastolic dysfunction in juvenile mice: potential role of cytoskeletal proteins. *Can J Physiol Pharmacol*. 2017;95:295-304.

118. Matsumura N, Zordoky BN, Robertson IM, Hamza SM, Parajuli N, Soltys C-LM, Beker DL, Grant MK, Razzoli M and Bartolomucci A. Co-administration of resveratrol with doxorubicin in young mice attenuates detrimental late-occurring cardiovascular changes. *Cardiovascular research*. 2018;114:1350-1359.

119. Nicolay K and de Kruijff B. Effects of adriamycin on respiratory chain activities in mitochondria from rat liver, rat heart and bovine heart. Evidence for a preferential inhibition of complex III and IV. *Biochim Biophys Acta*. 1987;892:320-30.

120. Ennequin G, Capel F, Caillaud K, Chavanelle V, Etienne M, Teixeira A, Li X, Boisseau N and Sirvent P. Neuregulin 1 improves complex 2-mediated mitochondrial respiration in skeletal muscle of healthy and diabetic mice. *Scientific reports*. 2017;7:1-9.

121. Echave P, Machado-da-Silva G, Arkell RS, Duchen MR, Jacobson J, Mitter R and Lloyd AC. Extracellular growth factors and mitogens cooperate to drive mitochondrial biogenesis. *J Cell Sci*. 2009;122:4516-25.

122. Elenius K, Corfas G, Paul S, Choi CJ, Rio C, Plowman GD and Klagsbrun M. A Novel juxtamembrane domain isoform of HER4/ErbB4 isoform-specific tissue distribution and differential processing in response to phorbol ester. *Journal of Biological Chemistry*. 1997;272:26761-26768.

123. Junttila TT, Sundvall M, Määttä JA and Elenius K. Erbb4 and its isoforms: selective regulation of growth factor responses by naturally occurring receptor variants. *Trends in cardiovascular medicine*. 2000;10:304-310.

124. Veikkolainen V, Vaparanta K, Halkilahti K, Iljin K, Sundvall M and Elenius K. Function of ERBB4 is determined by alternative splicing. *Cell Cycle*. 2011;10:2647-57.

125. Icli B, Bharti A, Pentassuglia L, Peng X and Sawyer DB. ErbB4 localization to cardiac myocyte nuclei, and its role in myocyte DNA damage response. *Biochemical and biophysical research communications*. 2012;418:116-121.

126. Paatero I and Elenius K. ErbB4 and its isoforms: patentable drug targets? *Recent Pat DNA Gene Seq*. 2008;2:27-33.

127. Lemmens K, Doggen K and De Keulenaer GW. Role of neuregulin-1/ErbB signaling in cardiovascular physiology and disease: implications for therapy of heart failure. *Circulation*. 2007;116:954-60.

128. Wang Z, Chan HW, Gambarotta G, Smith NJ, Purdue BW, Pennisi DJ, Porrello ER, O'Brien SL, Reichelt ME, Thomas WG and Paravicini TM. Stimulation of the four isoforms of receptor tyrosine kinase ErbB4, but not ErbB1, confers cardiomyocyte hypertrophy. *J Cell Physiol*. 2021;236:8160-8170.

129. Tokarska-Schlattner M, Zaugg M, Zuppinger C, Wallimann T and Schlattner U. New insights into doxorubicin-induced cardiotoxicity: the critical role of cellular energetics. *J Mol Cell Cardiol*. 2006;41:389-405.

130. Ewer MS, Gibbs HR, Swafford J and Benjamin RS. Cardiotoxicity in patients receiving transtuzumab (Herceptin): primary toxicity, synergistic or sequential stress, or surveillance artifact? *Semin Oncol*. 1999;26:96-101.

131. Vasti C and Hertig CM. Neuregulin-1/erbB activities with focus on the susceptibility of the heart to anthracyclines. *World J Cardiol*. 2014;6:653-62.

132. Zhang Y, Kang YM, Tian C, Zeng Y, Jia LX, Ma X, Du J and Li HH. Overexpression of Nrdp1 in the heart exacerbates doxorubicin-induced cardiac dysfunction in mice. *PLoS One*. 2011;6:e21104.

133. Sishi BJ, Loos B, van Rooyen J and Engelbrecht A-M. Autophagy upregulation promotes survival and attenuates doxorubicin-induced cardiotoxicity. *Biochemical pharmacology*. 2013;85:124-134.

134. Horie T, Ono K, Nishi H, Nagao K, Kinoshita M, Watanabe S, Kuwabara Y, Nakashima Y, Takanabe-Mori R, Nishi E, Hasegawa K, Kita T and Kimura T. Acute doxorubicin cardiotoxicity is associated with miR-146a-induced inhibition of the neuregulin-ErbB pathway. *Cardiovasc Res*. 2010;87:656-64.

135. Pandya K and Smithies O. beta-MyHC and cardiac hypertrophy: size does matter. *Circ Res*. 2011;109:609-10.

136. Szablewski L. Glucose transporters in healthy heart and in cardiac disease. *Int J Cardiol*. 2017;230:70-75.

137. Galindo CL, Nguyen VT, Hill B, Easterday E, Cleator JH and Sawyer DB. Neuregulin (NRG-1beta) Is Pro-Myogenic and Anti-Cachectic in Respiratory Muscles of Post-Myocardial Infarcted Swine. *Biology (Basel)*. 2022;11.

138. Ricci DR, Orlick AE, Alderman EL, Ingels NB, Daughters GT and Stinson EB. Influence of heart rate on left ventricular ejection fraction in human beings. *The American Journal of Cardiology*. 1979;44:447-451.

139. Mosedale M, Button D, Jackson JP, Freeman KM, Brouwer KR, Caggiano AO, Eisen A, Iaci JF, Parry TJ and Stanulis R. Transient changes in hepatic physiology that alter bilirubin and bile acid transport may explain elevations in liver chemistries observed in clinical trials of GGF2 (cimaglermin alfa). *Toxicological Sciences*. 2018;161:401-411.

140. Ma Y, Zhang X, Bao H, Mi S, Cai W, Yan H, Wang Q, Wang Z, Yan J, Fan GC, Lindsey ML and Hu Z. Toll-like receptor (TLR) 2 and TLR4 differentially regulate doxorubicin induced cardiomyopathy in mice. *PLoS One*. 2012;7:e40763.

141. Li M, Sala V, De Santis MC, Cimino J, Cappello P, Pianca N, Di Bona A, Margaria JP, Martini M, Lazzarini E, Pirozzi F, Rossi L, Franco I, Bornbaum J, Heger J, Rohrbach S, Perino A, Tocchetti CG, Lima BHF, Teixeira MM, Porporato PE, Schulz R, Angelini A, Sandri M, Ameri P, Sciarretta S, Lima-Junior RCP, Mongillo M, Zaglia T, Morello F, Novelli F, Hirsch E and Ghigo A. Phosphoinositide 3-Kinase Gamma Inhibition Protects From Anthracycline Cardiotoxicity and Reduces Tumor Growth. *Circulation*. 2018;138:696-711.

142. Kobayashi S, Volden P, Timm D, Mao K, Xu X and Liang Q. Transcription factor GATA4 inhibits doxorubicin-induced autophagy and cardiomyocyte death. *Journal of Biological Chemistry*. 2010;285:793-804.

143. Smuder AJ, Kavazis AN, Min K and Powers SK. Doxorubicin-induced markers of myocardial autophagic signaling in sedentary and exercise trained animals. *Journal of applied physiology*. 2013;115:176-185.

144. Lu L, Wu W, Yan J, Li X, Yu H and Yu X. Adriamycin-induced autophagic cardiomyocyte death plays a pathogenic role in a rat model of heart failure. *Int J Cardiol*. 2009;134:82-90.

145. Gu X, Wang Z, Ye Z, Lei J, Li L, Su D and Zheng X. Resveratrol, an activator of SIRT1, upregulates AMPK and improves cardiac function in heart failure. *Genet Mol Res*. 2014;13:323-335.

146. Dutta D, Xu J, Dirain ML and Leeuwenburgh C. Calorie restriction combined with resveratrol induces autophagy and protects 26-month-old rat hearts from doxorubicin-induced toxicity. *Free Radical Biology and Medicine*. 2014;74:252-262.

147. Wang X, Wang XL, Chen HL, Wu D, Chen JX, Wang XX, Li RL, He JH, Mo L, Cen X, Wei YQ and Jiang W. Ghrelin inhibits doxorubicin cardiotoxicity by inhibiting excessive autophagy through AMPK and p38-MAPK. *Biochem Pharmacol*. 2014;88:334-50.

148. Li M, Russo M, Pirozzi F, Tocchetti CG and Ghigo A. Autophagy and cancer therapy cardiotoxicity: From molecular mechanisms to therapeutic opportunities. *Biochimica et Biophysica Acta (BBA)-Molecular Cell Research*. 2019.

149. Ennequin G, Caillaud K, Chavanelle V, Teixeira A, Etienne M, Li X, Boisseau N and Sirvent P. Neuregulin 1 treatment improves glucose tolerance in diabetic db/db mice, but not in healthy mice. *Archives of physiology and biochemistry*. 2018:1-6.

150. Tokarska-Schlattner M, Dolder M, Gerber I, Speer O, Wallimann T and Schlattner U. Reduced creatine-stimulated respiration in doxorubicin challenged mitochondria: particular sensitivity of the heart. *Biochim Biophys Acta*. 2007;1767:1276-84.

151. Yin J, Guo J, Zhang Q, Cui L, Zhang L, Zhang T, Zhao J, Li J, Middleton A and Carmichael PL. Doxorubicin-induced mitophagy and mitochondrial damage is associated with dysregulation of the PINK1/parkin pathway. *Toxicology in vitro*. 2018;51:1-10.

152. Heim P, Morandi C, Brouwer GR, Xu L, Montessuit C and Brink M. Neuregulin-1 triggers GLUT4 translocation and enhances glucose uptake independently of insulin receptor substrate and ErbB3 in neonatal rat cardiomyocytes. *Biochim Biophys Acta Mol Cell Res*. 2020;1867:118562.

153. Westermeier F, Bustamante M, Pavez M, García L, Chiong M, Ocaranza MP and Lavandero S. Novel players in cardioprotection: Insulin like growth factor-1, angiotensin-(1-7) and angiotensin-(1-9). *Pharmacol Res*. 2015;101:41-55.